Origin of the Neutrino Masses and Mixings, and their Radiative Corrections at Low Energy Scales

Konsam Sashikanta Singh

Department of Physics

Gauhati University

Thesis submitted to the

Gauhati University as a requirement for the degree of

Doctor of Philosophy

in Physics

Faculty of Science

April 2018

Certificate

This is to certify that the thesis titled ***"Origin of the Neutrino Masses and Mixings, and their Radiative Corrections at Low Energy Scales"*** *is the result of research work of* ***Mr. Konsam Sashikanta Singh****, carried out under my supervision, submitted to Gauhati University for the award of the degree of Doctor of Philosophy in the faculty of science. The research work reported in this thesis is original and candidate's own work. He has fulfilled all the requirements under the Ph.D regulations of Gauhati University. To the best of my knowledge, this thesis or part thereof has not been submitted in this or to any other universities for any degree or diploma, and also conforms to the standard of Ph.D. thesis under Gauhati University including the standard related to plagiarism.*

Prof. N. Nimai Singh

(Ph.D Supervisor)

Head
Department of Physics
Manipur University

Date: 14/9/2018

Declaration

I, **Konsam Sashikanta Singh**, hereby declare that except where specific references are made to the work of others, the contents of this thesis are original and have not been submitted in whole or in part for consideration for any other degree or qualification in this, or to any other universities. I confirm that the work submitted is my own, except the work which has formed part of jointly-authored publications, has been included. My contribution and those of the other authors to the works, have been explicitly mentioned. This thesis is my own work carried out under the guidance of Prof. N. Nimai Singh.

Signed: Konsam Sashikanta Singh

Date: 14 - 09 - 2018

Abstract

The study of neutrino physics is a very fundamental and interesting research area. From different neutrino experiments worldwide, we have gathered enough data that reveals some of its fundamental properties, but not enough to know all. Neutrino, at the very core, may hold the seeds to the observed matter-antimatter asymmetry of the universe. This possibility is strengthened by the recent experimental confirmation of the non-zero value of θ_{13}. It is also a proposed candidate for the Dark matter. It appears that neutrino is related to the basic working mechanism of the universe and understanding it may reveal some of the deepest secrets of the nature. It is in these regards that the study of neutrino has become a very important and fascinating research area in physics. All the properties of neutrinos are encoded in its nine parameters (three mixing angles, three masses, and three CP phases).

The main target of all the neutrino researchers (theorist and experimentalist) is to understand those nine parameters, and the question on how and why neutrinos are related to other areas of physics, like cosmology, as well. So far, we have succeeded in measuring the three mixing angles and two mass squared differences only. We are still unable to measure the three absolute masses, the three CP phases, and other related properties like the octant, seesaw scale etc. There is not a single definitive answer as to why the neutrinos behave/appear the way they are. An attempt to answer such challenging question demands one to go beyond the comfort zone of Standard Model (SM) of particle physics. In doing so, we use the concept of the MSSM (the minimal supersymmetric extension of the Standard Model). The idea of supersymmetry is very powerful and is assumed to be broken at some

specific energy scale, in order to account for the observed low energy physical world. At what scale the supersymmetry breaking occurs is an important yet unknown parameter. Moreover, the seesaw mechanism which provides the most satisfactory explanation for the observed smallness of neutrino mass, has no definite scale and are model dependent too.

Since, the research area of neutrino physics is huge and complicated as well, it is not at all possible to touch all the different areas of neutrinos in this thesis work. Instead, we make an attempt to study the radiative properties of the nine neutrino parameters using the concept of Renormalization Group method (only for the normal mass ordering). At the same time, the absence of a theoretical model demanding for a specific scale for both the supersymmetry breaking scale and the seesaw scale, inspire us to study the effects of their variations on the radiative properties of neutrinos.

Radiative study of the neutrino parameters requires a good knowledge of the RGEs for the three gauge couplings, third generation three Yukawa couplings both in the Standard Model (non-supersymmetric) and in the Minimal Supersymmetric Standard Model (supersymmetric regime). We also need to know the RGE of the quartic Higgs coupling in the SM. In this thesis, using the bottom-up approach, we first study the radiative properties of the gauge couplings and the Yukawa couplings as well as their unification scenarios by varying the supersymmetry (SUSY) breaking scale (m_s). We also study the inconsistencies between the predictions made by BM and TBM neutrino mixing patterns with the present neutrino oscillation data (independent of any RG methods). We then study the radiative properties of the nine neutrino parameters, using the top-down approach (from the seesaw scale down to the low energy scale), under varying m_s and seesaw scales (SS). We extend our analysis by incorporating a self-complementarity relation among the three neutrino mixing angles, at the seesaw scale. We also try to predict a possible range of m_s and seesaw scale scale by observing the stability of weak scale neutrino parameter values. We also study the stability of the mixing angles self-complementarity relation and the neutrino masses ratio under the

same conditions. In the last chapter we present the summary and discussion. We conclude this thesis by adding a brief discussions on some of the well known neutrino experiments.

This thesis is dedicated to

my loving parents

and to all those whose hard work and dedications have made this world a wonderful place with full of possibilities.

"If I have seen further than others, it is by standing upon the shoulders of giants".

Issac Newton

Acknowledgements

This thesis represents not only the work I have accomplished in the last six years at Gauhati University (GU), but also the the love, affection, motivation, and support from all the amazing people in my life. My experience at Physics Department, GU, has been nothing short of wonder. Since my first day as an M.Sc. student at GU, I feel like at home. I have been given many unique opportunities and I have taken advantage of them. This includes starting as a Master student, attending different schools, workshops, conferences, and finally joining as a Ph.D student in the Spring of 2012. Sometimes, when I look back at those last six years, I wonder whether I did any work at all, or I just managed to channel the energy, intellect, and support of everyone around me into a coherent curriculum vitae, attaching my name to it in the process. If GU allowed it, I would list everyone in this section as coauthors, but I guess my beloved teachers will be having a tough time in settling the issue. Today, I am at the stage of my Ph.D work due to all the unconditional love, motivation, and support from many people, whom I wish to acknowledge.

Firstly, I wish to convey my sincere gratitude to my advisor Prof. **Ngangkham Nimai Singh** for the continuous support of my Ph.D study and related research, for his patience, motivation, and immense knowledge. His guidance helped me in all the time of research and writing of this thesis. I could not have imagined having a better advisor and mentor for my Ph.D.

My sincere thanks to all my beloved teachers in our Physics Department for all their valuable support, suggestions, and guidance; and also for giving me the opportunity to be a

part of this department, for giving access to the laboratory and research facilities. Without their precious support, it would not have been possible to conduct this research.

I take this opportunity to thank Dr. Subhankar Roy and Dr. Chandan Duarah, for the collaborative work and the important discussions we have done. Also, a sincere thanks to Luxmi Machahari for her diligent proofreading of the entire thesis before handing it to my supervisor.

Besides those mentioned above, I would like to thank (i) all the members of the HEP lab Dr. Neelakshi, Dr. Tapashi, Dr. Baishali, Jugal, Ricky, Nilav, and Paramita, (ii) the research scholars of CMP lab Dr. Satyananda, Dr. Mintu Das and Mosumi Das, (iii) the research scholars of Astrophysics Murchana and Suniti.

I would also like to thank Dr. Monoranjan, Dr. Robindro, Dr. Shyam, Dr. Rajiv, Dr. Sanjiv, Dr. Kalyan, Dwep, Kamal Jn., Ram, Vivek, Kishore, Doimalu, Bijoy, Chinmoy for making my days in this university a memorable one.

I also like to thank all the non-teaching staffs of our department for their helps and support in all the official works.

I sincerely acknowledge UGC for its financial support (grant grant no. F.7-65/2007(BSR)).

There's no way I can ever list all of the wonderful people who got me this far. In case if I fail to mention anyone in this short acknowledgement, I sincerely apologize for my ignorance. I shall conclude this section by showing my appreciation toward my family members and, their supports have been unconditional all these years. They have given up many things for me to be at Gauhati University; they have cherished with me every great moment and supported me whenever I needed it.

Thank you, everyone.

Konsam Sashikanta Singh

Abbreviations

ANNIE	Accelerator Neutrino Neutron Interaction Experiment
ARIANNA	Antarctic Ross Ice-Shelf Antenna Neutrino Array
BMS	Beyond Standard Model
BNL	Brookhaven National Laboratory
BOREXINO	BORon EXperiment
CERN	European Centre for Nuclear research
CP	Charge and Parity
CC	Charge Current
CMSSM	Constrained Minimal Supersymmetric Standard Model
CPT	Charge, Parity, and Time Reversal
DONUT	Direct Observation of NU Tau
DUNE	Deep Underground Neutrino Experiment
GUT	Grand Unified Theory
IH	Inverted Hierarchy
IMB	Irvine Michigan Brookhaven
JCP	Jarlskog Invariant parameter
KamLAND	Kamioka Liquid Scintillator Antineutrino Detector
KATRIN	Karlsruhe Tritium Neutrino Experiment
LAGUNA	Large Apparatus studying Grand Unification and Neutrino Astrophysics
LBNE	Long Baseline Neutrino Experiment
LHC	Large Hadron Collider
LH	Left Handed
LEP	Large Electron–Positron Collider
MINOS	Main Injector Neutrino Oscillation Search
MSSM	Minimal Supersymmetric Standard Model
MSW	Mikheyev–Smirnov–Wolfenstein
NC	Neutral Current
NH	Normal Hierarchy
NMSSM	Next-to-Minimal Supersymmetric Standard Model
NOνA	NuMI Off-Axis ν_e Appearance
OPERA	Oscillation Project with Emulsion-tRacking Apparatus
PMNS	Pontecorvo–Maki–Nakagawa–Sakata
pMSSM	Phenomenological Minimal Supersymmetric Standard Model
QED	Quantum ElectroDynamics
RENO	Reactor Experiment for Neutrino Oscillation
RH	Right Handed
SLC	Stanford Linear Collider
SLAC	Stanford Linear Accelerator Center
SM	Standard Model
SNP	Solar Neutrino Problem
SNO	Sudury Neutrino Observatory
SS	See-Saw
SUSY	Supersymmetry
T2K	Tokai to Kamioka
UNO	Underground Nucleon decay and neutrino Observatory

Table of contents

List of figures

List of tables

Chapter 1

Introduction and Scope of the thesis

Among the discovery-based science, particle physics is one which probes to unravel the deep secrets of nature. Our understanding from the studies of the physical phenomena surrounding us, has made us aware of the fact that the universe we live in, is governed by universal principles which apply at time and distance scales far beyond our normal experience and perception. Particle physics is one such endeavor of scientific inquiry into these principles. It plays an essential role in the broader enterprise of the physical sciences. It inspires students, attracts young talented minds from around the world, and drives critical intellectual and technological advances in various fields.

The field of elementary particle physics is entering an era of unprecedented potential. The last run of LHC reached a ground breaking energy scale of 13 TeV with an integrated luminosity of over 20 fb^{-1} [4]. New experimental facilities, including accelerators, space-based experiments, underground laboratories, and critical precision measurements of various kinds, offer a wide varieties to explore the hidden nature of matter, energy, space, and time. The availability of technologies that can explore directly into the TeV scale, is especially exciting. Moreover, at TeV scale energies, formerly separated questions in cosmology and particle physics become connected, bridging the sciences of the very large and the very small.

S

One of the great scientific achievements of the 20th century was the development of the Standard Model (SM) of particle physics, which describes the relationships among the basic building blocks of nature and the characteristics of three of the four forces acting on those particles. The Standard Model is very much successful in explaining and predicting physics at the weak energy scale. However, in the high energy regime that physicists are able to access experimentally, the incompleteness of the Standard Model becomes apparent and the necessity for its extension or for a new theory becomes mandatory. The study of neutrino physics falls into this category. The phenomenon of neutrino oscillation leading to the non-zero neutrino masses, provides one of the solid evidences for the physics beyond Standard Model (BSM).

1.1 A brief sketch of Standard Model

After the great discovery of the long predicted Higgs boson at the LHC CERN in 2012 [5, 6], the SM of particle physics has now achieved the title of a full fledged theory of elementary particle at the electroweak scale (EW). It is a mathematical theory describing the three types of forces/interactions operating in nature viz; the strong, electromagnetic, and the weak interaction. These three forces describe the interaction between quarks and leptons, the fundamental SM particles. SM has no room for the fourth interaction, the gravitational interaction. It is in this sense SM is not a complete theory of nature. The four types of interaction operating in nature are shown in Table 1.1.

Interaction type	Carrier particle	mass (in GeV)	Spin
Strong force	Gluons	0	1
Electromagnetic force	Photons	0	1
Weak force	$W^{\pm}$, Z^0	$\sim 80,\ 91$	1
Gravitational force	graviton (hypothesized)	0	2

Table 1.1 Force carrier particles of Standard Model with their masses and spins.

Families	Generations			sensitive to	spin	Charge
	First	Second	Third			
Quarks	u	c	t	Strong, Electromagnetic, weak	$\frac{1}{2}$	$\frac{2}{3}$
	d	s	b		$\frac{1}{2}$	$-\frac{1}{3}$
Leptons	e	μ	τ	Electromagnetic, Weak	$\frac{1}{2}$	-1
	ν_e	ν_μ	ν_τ	Weak	$\frac{1}{2}$	0

Table 1.2 Matter particles of Standard Model with their interaction types, spins and charges.

There are two types of elementary fermions in Standard Model: leptons and quarks (see Table 1.2 for their complete family/generations). Any theory of elementary particles must be consistent with the two pillars of physics: special relativity and Quantum theory. The combination of quantum mechanics, electromagnetism and special relativity led Dirac to his famous equation now known as the Dirac equation. Quantization of these fields gives quantum field theory (QFT).

Like QED, the SM is also a theory of interacting fields. The construction of the Standard Model has been guided by the principles of symmetry. The mathematics of symmetry is provided by group theory. The connection between symmetries and physics is deep. For example, Noether's theorem states that for every continuous symmetry of nature, there is a corresponding conservation law. It follows from the presumed homogeneity of space and time that the Lagrangian of a closed system is invariant under uniform translations of the system in space and in time. Such transformations are therefore symmetry operations on the system.

SM is a gauge theory of microscopic interaction with the gauge group

$$G_{SM} = SU(3)_c \times SU(2)_L \times U(1)_Y, \tag{1.1}$$

which describes three out of the four fundamental interactions.

The particle spectrum of the SM and their transformation properties under the gauge groups eq. (1.1) are

$$\left.\begin{aligned} Q_i \equiv \begin{pmatrix} u_{Li} \\ d_{Li} \end{pmatrix} \sim \left(3,2,\tfrac{1}{6}\right) \quad U_i \equiv u_{Ri} \sim \left(\bar{3},1,\tfrac{2}{3}\right) \\ D_i \equiv d_{Ri} \sim \left(\bar{3},1,-\tfrac{1}{3}\right) \quad E_i \equiv e_{Ri} \sim \left(1,1,-1\right) \\ , \quad L_i \equiv \begin{pmatrix} \nu_{Li} \\ e_{Li} \end{pmatrix} \sim \left(1,2,-\tfrac{1}{2}\right) \end{aligned}\right\}, \tag{1.2}$$

The complete SM Lagrangian can be written as

$$\mathscr{L}_{SM} = \mathscr{L}_f + \mathscr{L}_k + \mathscr{L}_y + \mathscr{L}_S, \tag{1.3}$$

where, $\mathscr{L}_f$ is the kinetic term for all the fermions including their interactions with gauge bosons and is written as

$$\mathscr{L}_f = i\overline{\Psi}\gamma^\mu \mathscr{D}_\mu \Psi, \tag{1.4}$$

where,

$$\Psi = (Q_i,\, U_i,\, D_i,\, L_i,\, E_i) \text{ for all the fermion fields,} \tag{1.5}$$

$$\mathscr{D}_\mu = \partial_\mu - ig_s G^A_\mu \lambda^A - i\frac{g}{2} W^I_\mu \tau^I - ig' B_\mu Y, \tag{1.6}$$

where $A = 1,2,3,...,8$ with G^A_μ representing the $SU(3)_c$ gauge bosons, W^I_μ is the $SU(2)_L$ gauge bosons, B_μ is the $U(1)_Y$ gauge field, $I = 1,2,3$, and $g_s,\ g,\ g'$ are the gauge couplings.

$\mathscr{L}_k$ represent the kinetic terms for the gauge fields and self-interactions and is given by

$$\mathscr{L}_k = -\frac{1}{4} G^{\mu\nu A} G^A_{\mu\nu} - \frac{1}{4} W^{\mu\nu I} W^I_{\mu\nu} - \frac{1}{4} B^{\mu\nu} B_{\mu\nu}, \tag{1.7}$$

where

$$\left.\begin{aligned} G^A_{\mu\nu} &= \partial_\mu G^A_\nu - \partial_\nu G^A_\mu + g_s\, f_{ABC} G^B_\mu G^C_\nu \\ F^I_{\mu\nu} &= \partial_\mu W^I_\nu - \partial_\nu W^I_\mu + g_s\, f_{IJK} W^J_\mu W^K_\nu \\ B_{\mu\nu} &= \partial_\mu B_\nu - \partial_\nu B_\mu \end{aligned}\right\}, \tag{1.8}$$

where f_{ABC} and f_{IJK} represents the structure constants of the $SU(3)$ and $SU(2)$ groups, respectively.

$\mathscr{L}_y$ represent the Yukawa interaction between the fermions and the Higgs boson, and is given by

$$\mathscr{L}_y = h^u_{ij}\overline{Q}_i U_j \tilde{H} + h^d_{ij}\overline{Q}_i D_j H + h^e_{ij}\overline{L}_i E_j H + h.c, \tag{1.9}$$

where, $\tilde{H} = i\sigma^2 H^*$. This interaction is responsible for the generation of particle masses after the gauge symmetry breaking from $G_{SM} \to SU(3)_c \times U(1)_{em}$.

The scalar part of the Lagrangian is

$$\mathscr{L}_S = \left(\mathscr{D}_\mu H\right)^\dagger \mathscr{D}_\mu H - V(H), \tag{1.10}$$

where

$$V(H) = \mu^2 H^\dagger H + \lambda (H^\dagger H)^2. \tag{1.11}$$

The Higgs field attains a vacuum expectation value (vev) at the minimum of the potential when $\mu^2 < 0$. After that the fermions also attain their masses through their Yukawa couplings. At this point only neutrinos remain massless due to the absence of right handed neutrinos. Finally, the Standard Model is renormalizable and anomaly free. This feature is still to be maintained even in the case of Minimal Supersymmetric Standard Model (MSSM).

1.1.1 Limitations of Standard Model

The limitations of the Standard Model are evident. When physicists attempt to include gravity into the Standard Model, they run into severe mathematical inconsistencies. In addition to this, astronomical discoveries also pose another severe challenge to the SM as listed below:

- SM can account for only 4% of the total composition of the universe. There is no room for the remaining 96% (nearly 25% Dark matter and about 70% dark energy).
- The predominance of matter over antimatter in the universe also pose a serious problem for the Standard Model.
- Standard Model doesn't provide any idea on the possible cause for the inflation.
- Standard Model cannot account for the non-zero value of neutrino masses.

  etc.

Thus, at the very outset of the 21st century, particle physics experiments, astronomical observations, and theoretical developments in both high energy physics and cosmology are pointing towards exciting new phenomena that are just on the verge of being observed. Fusing quantum theory with general relativity, understanding dark matter and dark energy etc. will require new ideas and new experiments. The technologies needed to conduct these experiments are now becoming accessible. As a result, particle physics is on the brink of a scientific revolution as profound as the one Einstein and others ushered in the early 20th century. There is every possibility that the "Terascale" discoveries will have an equally important impact across the fields of science. Thus, despite the extraordinary success of the SM, it is evident that, a much deeper understanding of the nature will be achieved only when we continue to study the fundamental constituents of the universe at higher and higher energy scales with new ideas.

1.2 A brief introduction to Minimal Supersymmetric Standard Model

Minimal Supersymmetric Standard Model (MSSM) is the Supersymmetric extension of the Standard Model, meaning that the Lagrangian of the SM eq.(1.3) is not only gauge invariant but also supersymmetric invariant. The term 'Minimal' in MSSM refers to the minimum choice of the particle spectrum necessary for the model to work. Just like the SM, MSSM should be renormalizable and anomaly free.

While going from SM to MSSM, the ordinary quantum fields are upgraded to superfields or supermultiplets. Every SM matter field is replaced by a chiral superfield and every vector field by a vector superfield so the existing particle spectrum of MSSM is just the double of the SM particles content. A chiral superfield contains a Weyl fermion, a scalar and an auxillary scalar field, and are generally denoted by F. A vector superfield contains a spin 1 boson, a spin $\frac{1}{2}$ fermion, and an auxillary scalar field called D. Further, at least two Higgs superfields are required to complete the spectrum: one giving masses to the up-type quarks and the other to the down-type quarks and charged leptons. These are the minimal number of Higgs particles required for the model to be consistent with QFT point of view. The particle contents of MSSM are given below:

$$\left.\begin{aligned} Q_i \equiv \begin{pmatrix} u_{Li} & \tilde{u}_{Li} \\ d_{Li} & \tilde{d}_{Li} \end{pmatrix} \sim \left(3,2,\tfrac{1}{6}\right) \quad U_i^c \equiv (u_i^c\ \tilde{u}_i^c) \sim \left(\bar{3},1,-\tfrac{2}{3}\right) \\ D_i \equiv \left(d_i^c\ \tilde{d}_i^c\right) \sim \left(\bar{3},1,\tfrac{1}{3}\right) \quad E_i \equiv (e_i^c\ \tilde{e}_i^c) \sim \left(1,1,1\right) \\ L_i \equiv \begin{pmatrix} \nu_{Li} & \tilde{\nu}_{Li} \\ e_{Li} & \tilde{e}_{Li} \end{pmatrix} \sim \left(1,2,-\tfrac{1}{2}\right) \end{aligned}\right\}, \tag{1.12}$$

where 'i' stands for the three generation index. Q_i represents the left handed quark doublets containing both the up and down quarks for each generation. Similarly, L_i represents left

handed lepton doublet, U_i, D_i, E_i represent right handed up-quark, down-quark, and charged lepton singlets respectively. The numbers in the parenthesis represent the transformation properties of the particles under G_{SM} (eq.(1.3)).

The MSSM Lagrangian is under the strict constraint of R-parity which is defined as,

$$\left.\begin{aligned} R &= (-1)^{3L+B+2s} \\ \text{or equivalently} & \\ R &= (-1)^{3(L-B)+2s} \end{aligned}\right\} \tag{1.13}$$

where, B is the baryon number, L is the lepton number, and s is the spin. Further,

$$R = \begin{cases} 1 & \text{for all SM particles} \\ -1 & \text{for all sparticles} \end{cases} \tag{1.14}$$

Imposing R-parity has an advantage of providing a natural candidate for dark matter[1]. It also protects proton from decaying too fast, though there are other options to R-parity which can also make proton stable.

The complete MSSM Lagrangain w.r.t. the particle content of eq.(1.12) can be written as

$$\mathscr{L}_{MSSM} = \mathscr{L}^0_{MSSM} + \mathscr{L}_{soft}. \tag{1.15}$$

The first term on the left side of eq.(1.15) represents the MSSM Lagrangian without any SUSY breaking and is of the form

$$\mathscr{L}^0_{MSSM} = \mathscr{L}_{vector} + \mathscr{L}_{chiral} + \mathscr{L}_{ext\ int} + \mathscr{L}_W + \mathscr{L}^\dagger_W, \tag{1.16}$$

where

[1]It is because R-parity distinguishes a particle from its superpartner. R-parity constrains baryon and lepton number violating couplings of dimension four or rather only at the renormalizable level.

- $\mathscr{L}_{vector}$ represents the vector supermultiplet $\left(A^a_\mu,\ \lambda^a,\ D^a\right)$

$$\mathscr{L}_{vector} = \mathscr{L}_{gauge} = -\frac{1}{4}F^a_{\mu\nu}F^{\mu\nu a} + i\lambda^{\dagger a}\overline{\sigma}^\mu D_\mu \lambda^a + \frac{1}{2}D^a D^a. \tag{1.17}$$

- $\mathscr{L}_{chiral}$ represents the chiral supermultiplets

$$\mathscr{L}_{chiral} = D^\mu \psi^* D_\mu \psi + i\psi^\dagger \overline{\sigma} D_\mu \psi + F^* F, \tag{1.18}$$

and

$$\mathscr{L}_{ext\ int} = -\sqrt{2}g\left(\phi^* \lambda^{aT} t^a c\psi - \psi^\dagger c\lambda^{a*} t^a \psi\right) + gD^a \phi^* t^a \phi. \tag{1.19}$$

- $\mathscr{L}_W$ represents the Lagrangian of the superpotential and is expressed as

$$\mathscr{L}_W = F\frac{\partial W}{\partial \phi} - \frac{1}{2}\psi^T c\psi \frac{\partial^2 W}{\partial \phi^2}. \tag{1.20}$$

The constraint equation for F is

$$\left.\begin{array}{rcl} F^* & = & -\frac{\partial W}{\partial \phi} \\ V_F & = & \left|\frac{\partial W}{\partial \phi}\right|^2. \end{array}\right\} \tag{1.21}$$

Similarly, the constraint equation for D^a is

$$\left.\begin{array}{rcl} D^a & = & -g\phi^* t^a \phi \\ V_D & = & \frac{1}{2}g^2\left(\phi^* t^a \phi\right)^2. \end{array}\right\} \tag{1.22}$$

The superpotential term can be divided into two parts as shown below:

$$W = W_Y + W_\mu. \tag{1.23}$$

The superpotential term is the source of nonlinear fermion-scalar interactions. It is required to generate the Higgs Yukawa couplings so that it can give mass to the quarks and the leptons. The appropriate choice is

$$W_Y = y_d^{ij}\bar{d}^i H_{d\alpha}\varepsilon_{\alpha\beta}Q_\beta^j + y_e^{ij}\bar{e}^i H_{d\alpha}\varepsilon_{\alpha\beta}L_\beta^i - y_u^{ij}\bar{u}^i H_{u\alpha}\varepsilon_{\alpha\beta}Q_\beta^j. \tag{1.24}$$

Among several possible contributions to W, the pure Higgs term is one and is given by

$$W_\mu = -\mu H_{d\alpha}\varepsilon_{\alpha\beta}H_{\mu\beta}. \tag{1.25}$$

The last term on the RHS of eq.(1.15) represents the SUSY breaking part. This term is necessary because in nature we do not observe any SUSY or Sparticles, implying the possibility of SUSY breaking in the MSSM. In a general Lagrangian, SUSY can be broken spontaneously if the auxiliary fields, F or D terms, appearing in the definitions of the chiral and vector superfields attain a vacuum expectation value (vev). If the F fields get a vev, it is called F-breaking and if the D fields get a vev, it is called D-breaking.

However, there is a cop out way to this problem. If the SUSY is broken in the hidden sector, a sector consisting of superfield not charged under the SM gauge group, and that information is communicated to the visible sector or MSSM through a messenger sector (it can be made up of gravitational interaction or an ordinary gauge interactions). This communication of the SUSY breaking leads to a SUSY breaking term in the MSSM. Thus, SUSY is not broken spontaneously but explicitly by adding a SUSY breaking term in the Lagrangian. However, not all the supersymmetric terms can be added. We need to add only those terms which do not re-introduce quadratic divergences back into the theory. Such terms are called "soft" supersymmetry breaking terms, represented by $\mathscr{L}_{soft}$ (as in eq.(1.15)) and

are defined as

$$\begin{aligned}\mathscr{L}_{soft} &= -M_{\tilde{f}}^2\left|\tilde{f}\right|^2 - \frac{1}{2}m_i\lambda_i^{Ta}c\lambda_i^a - \Big(A_d y_d \tilde{\bar{d}} H_{d\alpha}\varepsilon_{\alpha\beta}\tilde{Q}_\beta + \\ &\quad A_e y_e \tilde{\bar{e}} H_{d\alpha}\varepsilon_{\alpha\beta}\tilde{L}_\beta - A_u y_u \tilde{\bar{u}} H_{u\alpha}\varepsilon_{\alpha\beta}\tilde{Q}_\beta - B_\mu H_{d\alpha}\varepsilon_{\alpha\beta}\Big) - h.c. \qquad (1.26)\end{aligned}$$

The $\mathscr{L}_{soft}$ of eq.(1.26) consists of the following terms: (i) Gaugino mass terms, (ii) Scalar mass terms,(iii) Trilinear scalar couplings, (iv) Bilinear scalar couplings.

The MSSM can be further classified as shown below:

- Constrained MSSM (CMSSM): It contains only five parameters viz. the universal scalar (soft) mass m_0, the universal gaugino (soft) mass $m_{1/2}$, the universal trilinear coupling A_0 (all at GUT scale), the ratio of the vacuum expectation values of the two Higgs doublets $\tan\beta$, and the sign of the Higgsino mass parameter. Here, the weak scale parameters are obtained by Renormalization Group running.

- Phenomenological MSSM (pMSSM): It is the low-scale models, which are not directly derived from some high-scale (GUT) theory. In this bottom-up approach no assumptions about the mechanism of SUSY breaking are made. The soft breaking terms introduce plenty of new parameters. In total this version of MSSM involves 105 new parameters (masses, mixing angles and phases).

- Next-to-MSSM or (M+1)MSSM: This version is the simplest possible extension of MSSM and is obtained by adding a new gauge-singlet chiral supermultiplet that is even under matter parity. It is done in order to solve the μ-problem.

1.3 Introduction to neutrino physics

We repeatedly hear the terms like elusive, ghost, mysterious, puzzling etc. whenever we talk about neutrinos. Neutrino is such an elementary particle that deserves such kind of peculiar

distinction. It is the second most abundant elementary particle in the universe, next to photon (other than Dark energy and Dark matter). It was first hypothesized by W. Pauli in 1930 in order to account for the conservation of energy in nuclear beta decay process. Its existence was experimentally confirmed by Clyde Cowan and Fred Reines in 1956 at Savannah River in South Carolina, USA [7][2]. However, what they discovered was an anti-neutrino, from a nuclear reactor emitted through the process of inverse β decay.

Soon after its discovery, R. Davis detected the problem of solar neutrino (SNP), where the expected solar neutrino flux was not observed. This finding led Bruno Pontecorvo, in 1957, to introduce the concept of neutrino oscillation for the first time [9, 10]. Three scientists Ziro Maki, Masami Nakagawa and Shoichi Sakata, in 1962, introduced the PMNS matrix [11] to explain Bruno's idea on neutrino oscillation. Russian researchers Stanislav Mikheyev and Alexei Smirnov further refined this idea by suggesting that the solar neutrinos, which are none other than electron neutrino (ν_e), are changing into other flavors like muon neutrino (ν_μ) and tau neutrino (ν_τ) [12]. A brief timeline summarizing the various important developmental stages and discoveries of neutrinos are listed in the Appendix A.1 .

One of the amazing discoveries of the 50's is that all neutrinos have their spin anti-parallel to their momentum, whereas for antineutrinos it is parallel. In other words, neutrinos are left-handed whereas its corresponding antiparticles are right-handed. This is at the very heart of the chiral nature of the weak interaction, and is also the source for the effects of parity violation observed in nature. The existence of two different spin states for the particle and antiparticle, makes neutrino the viable candidate for "Majorana particle" also (since they are their own antiparticle). While all other fermions are "Dirac particle" having four

[2]The extremely small interaction cross-section is what makes neutrino very hard to detect. The neutrino-neutron scattering cross-section as calculated by H. Bethe and R. Peierls, using Fermi's theory, turned out to be $\sigma(n+\nu \rightarrow e^- + p) \sim E_\nu\ (meV) \times 10^{-44}\ cm^2$ implying that a steel column of ~ 10 light year in thickness would be required for stopping a neutrino of 1 MeV [8]. For example, solar neutrinos from the sun's core come directly with little or no interaction at all telling us that the fusion reaction is the source of sun's energy. Whereas, light takes millions of years to reach the surface due to continuous scattering, and it also exhibit a black body spectrum.

states (particle-antiparticle each having two different spin states). Neutrino is also a possible candidate for Dirac particle.

There are varieties of neutrinos sources viz. (i) Earth's core and other nuclear decay processes, (ii) nuclear reactors and particle accelerators, (iii) sun, stars and, other galactic or extra-galactic activities like supernova explosion, gamma ray burst etc.

Parameters	best-fit	best-fit $\pm 1\sigma$	2σ range	3σ Range
$\Delta m^2_{21}[10^{-5}eV^2]$	7.56	7.56 ± 0.19	7.20-7.95	$7.05 - 8.14$
$\Delta m^2_{31}[10^{-3}eV^2]$ [NO]	2.55	2.55 ± 0.04	2.47-2.63	$2.43 - 2.67$
$\theta_{12}/^\circ$	34.5	$34.5^{+1.1}_{-1.0}$	32.5-36.8	31.5- 38.0
$\theta_{23}/^\circ$ [NO]	41.0	41.0 ± 1.1	39.1-43.7	38.3 - 52.80
$\theta_{13}/^\circ$ [NO]	8.44	$8.44^{+0.18}_{-0.15}$	8.1-8.7	7.90 - 8.90
$\delta/^\circ$ [NO]	252	252^{+56}_{-36}	153-351	0-360
$\theta_{23}/^\circ$ [IO]	50.5	50.5 ± 1.0	39.5-42.5	38.5 - 53.0
$\theta_{13}/^\circ$ [IO]	8.41	$8.41^{+0.16}_{--0.17}$	8.0-8.7	7.90 - 8.90
$\Delta m^2_{31}[10^{-3}eV^2]$ [IO]	2.49	2.49 ± 0.04	2.41-2.57	$2.37 - 2.61$
$\delta/^\circ$ [IO]	259	259^{+47}_{-41}	182-347	0-31 & 142-360

Table 1.3 The recent global fit of neutrino oscillation parameters for both the normal ordering (NO) and inverted ordering (IO) cases [1].

1.3.1 Number of light and heavy neutrino species or flavors

Light neutrino species

From theoretical as well as experimental sides, it is now widely accepted that neutrino comes in three different flavors[3] viz. electron neutrino (ν_e), muon neutrino (ν_μ), and tau neutrino (ν_τ). They are sensitive only to weak interaction which can further be subdivided into two viz:

(i) One that couples with Z^0 boson where its momentum changes, keeping its identity fixed, also called as neutral current interaction, NC in short.

[3]The possible number of light neutrino species, that have the usual EW interaction, can be obtained from the process: $Z^0 \to \nu_\alpha + \overline{\nu}_\alpha$ such that the no. of light neutrino species is $N_\nu = \frac{\Gamma_{invisible}}{\Gamma_{\nu\overline{\nu}}} = 2.994 \pm 0.012$ where, $\Gamma_{\nu\overline{\nu}} = 166.9$ MeV is the partial decay width and $\Gamma_{invisible} = 498 \pm 4.2$ MeV is the branching ratio into invisible final states that is directly proportional to the number of light neutrino species.

(ii) One that couples with $W^{\pm}$ bosons, transforming into one of the charged leptons ($e^{\pm}$, $\mu^{\pm}$, $\tau^{\pm}$), also called as charged current interaction or CC in short.

It is because of the CC interaction that we can define the concept of neutrino flavors.

Heavy neutrino species

At present, there is not a single experimental data which hints for the possibility for any kind of heavy neutrino. However, there are theoretical models which demand for the existence of heavy neutrino, also called as right-handed neutrino (RH) and sterile neutrino. The see-saw mechanism (SSM), well known for explaining the infinitesimally small mass of left-handed neutrinos, demands for three RH neutrinos with mass scale of the order of seesaw scale ($10^{10} - 10^{15}$) GeV. For the time being, we have no definitive idea about the seesaw scale (SS) and in addition there are three different types of SSM. Like the light left-handed neutrinos, the possible mass spectrum of right-handed neutrinos is still an unknown. In addition to these three RH neutrinos, there are also theoretical prediction for another type of neutrino, called the sterile neutrino. Again depending upon the model, sterile neutrino and RH neutrinos are sometime considered as same [13] and different as well. Both RH neutrinos and sterile neutrino are singlet particles w.r.t. the SM gauge group (eq.(1.1)).

1.3.2 Neutrino mass in Standard Model

In SM neutrinos are massless. Due to the absence of right-handed neutrinos in SM, no Yukawa interaction can be written that would give a tree level mass to the neutrinos, and as a consequence neutrinos remain massless. Any possible neutrino mass term which could be built with the particle content of the SM would violate the $U(1)_L$ subgroup of G_{SM} (eq. (1.1)) and therefore, cannot be induced by loop corrections. Also, it cannot be induced by non-perturbative corrections because $U(1)_L$ subgroup of G_{SM} is non-anomalous. This is the reason why neutrinos are strictly massless in the SM.

If they are massless then there can neither be any mixing nor any CP-violation in the leptonic sector. But, these theoretical predictions are in stark contradiction with the current experimental data (see Table 1.3). The present experimental data has already confirmed that neutrino oscillates, have a small non-vanishing masses, and mixing do occurs. Also, the mixing angle θ_{13} is now confirmed to be non-zero, thereby implying the possibility of CP violation.

In order to accommodate the experimental data, either an alternative approach to SM or a modification/extension of the SM becomes mandatory. This is the reason why neutrino physics is termed as physics beyond Standard Model (BSM). Two most accepted minimal extensions of SM to explain the experimental results are

(i) Introduce a right handed neutrino ν_R and then impose the total lepton number (L) conservation so that, after EW spontaneous symmetry breaking the Lagrangian is

$$\mathscr{L}_D = \mathscr{L}_{SM} - M_\nu \bar{\nu}_L \nu_R + h.c., \tag{1.27}$$

In this case the neutrinos are called a Dirac neutrinos and $\nu^c \neq \nu$.

(ii) Construct a mass term only with the SM left-handed neutrinos by allowing L violation such that

$$\mathscr{L}_M = \mathscr{L}_{SM} - \frac{1}{2} M_\nu \bar{\nu}_L \nu_L^c + h.c. \tag{1.28}$$

In this case the neutrinos are known as Majorana neutrinos and $\nu^c = \nu$

1.3.3 The phenomenon of neutrino oscillation

The phenomenon of neutrino oscillation stemmed from our attempt to understand the SNP. It is a clear indication for the non-zero value of neutrino masses. Super-Kamiokande first witnessed the existence of neutrino oscillation. It was further confirmed by the Sudbury

Neutrino observatory (SNO) in Canada, by showing the conversion of solar neutrino flavor into other flavor. This finding finally solved the SNP.

This phenomenon implies that neutrino flavor states are not mass eigenstates but superpositions of such states. More precisely, a neutrino with definite flavor, $|\nu_\alpha\rangle$ can be described in terms of the mass eigenstate $|\nu_i\rangle$ as

$$|\nu_\alpha\rangle = \sum_{i=1}^{3} U^*_{\alpha i} |\nu_i\rangle \tag{1.29}$$

where U is a unitary matrix called lepton mixing matrix in analogy with the quark mixing matrix. In general, U may be a complex matrix. The pictorial representation of neutrino oscillation is shown in Fig. 1.1. Neutrino oscillation can be divided into two depending upon the medium in which it is happening viz.

1. vacuum oscillation - where the oscillation happen solely in the vacuum,

2. matter oscillation - where oscillation happens inside a material medium (for example Earth).

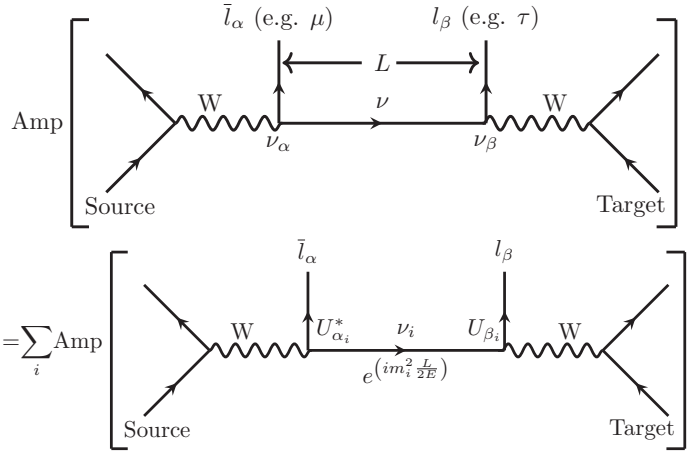

Fig. 1.1 The flavor changing process involving $\nu_\alpha \to \nu_\beta$ from source to detector.

1.3.3.1 Neutrino oscillation in vacuum

The phenomenon of neutrino oscillation can understood in more details by studying its probability of oscillation. In vacuum, eq. (1.29) allows us to calculate the probability of change in flavor and is given by

$$\begin{aligned}\mathscr{P}(\nu_\alpha \to \nu_\beta) &= \left|\mathscr{A}(\nu_\alpha \to \nu_\beta)\right|^2 \\ &= \delta_{\alpha\beta} - 4\sum_{i>j} Re\left(U^*_{\alpha_i} U_{\beta_i} U_{\alpha_j} U^*_{\beta_j}\right) \sin^2\left[\Delta m^2_{ij}\frac{L}{4E}\right] \\ &\quad +2\sum_{i>j} Im\left(U^*_{\alpha_i} U_{\beta_i} U_{\alpha_j} U^*_{\beta_j}\right) \sin^2\left[\Delta m^2_{ij}\frac{L}{2E}\right], \end{aligned} \tag{1.30}$$

where, $\Delta m^2_{ij} = m^2_i - m^2_j$, E is the neutrino energy and L is the distance from the source to the detector/target. The above eq.(1.30) holds for any number of neutrino mass eigenstates. The following important conclusions can be drawn,

1. Neutrino oscillation depends on the mass squared difference $\Delta m^2_{ij} = m^2_i - m^2_j$. Clearly, if the neutrinos are massless or are strictly degenerate, then eq.(1.30) reduces to

$$\mathscr{P}(\nu_\alpha \to \nu_\beta) = \delta_{\alpha\beta}, \tag{1.31}$$

   indicating no oscillation. In other words, for oscillation to happen neutrino must be massive (at least one of the three) and non-degenerate.

2. $\mathscr{P}$ is a function of $\dfrac{L}{E}$.

3. Assuming the CPT invariance, we have

$$\mathscr{P}(\overline{\nu}_\alpha \to \overline{\nu}_\beta) = \mathscr{P}(\nu_\beta \to \nu_\alpha). \tag{1.32}$$

Again, from eq.(1.30), we can produce

$$\mathscr{P}(\nu_\beta \to \nu_\alpha : U) = \mathscr{P}(\nu_\alpha \to \nu_\beta : U^*), \tag{1.33}$$

leading to the relation,

$$\mathscr{P}(\overline{\nu}_\alpha \to \overline{\nu}_\beta : U) = \mathscr{P}(\nu_\alpha \to \nu_\beta : U^*). \tag{1.34}$$

This implies the possibility of violation of CP symmetry during the oscillation process.

$$\mathscr{P}(\nu_\alpha \to \nu_\beta) - \mathscr{P}(\overline{\nu}_\alpha \to \overline{\nu}_\beta) = 4\sum_{i>j} Im\left(U^*_{\alpha_i} U_{\beta_i} U_{\alpha_j} U^*_{\beta_j}\right) \sin^2\left[\Delta m^2_{ij} \frac{L}{4E}\right]. \tag{1.35}$$

Discovery of

$$\mathscr{P}\left(\overline{\nu}_\alpha \to \overline{\nu}_\beta\right) \neq \mathscr{P}\left(\nu_\alpha \to \nu_\beta\right) \tag{1.36}$$

would imply the violation of CP invariance.

Eq. (1.30) remains valid even if we assume equal momenta for all the neutrinos [14]. The negligibly small mass of neutrino allows us to approximate the momenta for all typical energies by

$$p_k \simeq E - \frac{m_k^2}{2E}. \tag{1.37}$$

In order for the oscillation to be observable, the phase $\Delta m^2 \frac{L}{E}$ must be of the order of 1, implying that the characteristic oscillation length (L_{osc}) must be similar to the distance between the source and the detector (L). For $L \ll L_{osc}$, no oscillation will be observed as neutrinos have no enough time for oscillation to develop.

For three massive neutrinos, the matrix U can be parametrized in terms of three Euler angles (called mixing angles) and six phase parameters. If the neutrinos are Dirac in nature (meaning distinct particle and antiparticle), only one of the phases is physical and gives

rise to CP violation. If, however, neutrinos are Majorana type (particle and antiparticle are identical), additional CP violating phases are required.

1.3.3.2 Neutrino oscillation in Matter - MSW effect

The oscillation probability we discussed so far, concerns only the neutrinos propagating through vacuum. However, this is not the only possible case. In case of neutrino traveling in matter, like Earth or Sun, the $\mathscr{P}$ of eq. (1.30) gets modified. This variation in oscillation probability is due to the so-called Mikheev-Smirnov-Wolfenstein (MSW) effect [31, 32] and it arises solely due to the fact that the weak interactions of electron-neutrinos in matter differ from those of muon-neutrinos and tau-neutrinos. This effect can be enhanced (called resonant enhancement), depending upon the electron density and on the neutrino energy. More precisely, the coherent forward scattering of an ν_e from electrons in matter, caused by W-boson exchange, gives the ν_e an extra interaction potential energy given by $V = +\sqrt{2}G_F N_e$. Similarly, for an $\overline{\nu}_e$ the extra interaction potential energy is given by $\overline{V} = -\sqrt{2}G_F N_e$. These extra energies raise the effective mass of a ν_e in matter, and lower that of a $\overline{\nu}_e$. Now, let us consider the simple case of two neutrinos flavor mixing. The corresponding oscillation probability is given as

$$\mathscr{P}(\nu_e \to \nu_\mu) = \sin^2 2\theta_M \sin^2\left[\frac{\Delta m^2_M X}{4E}\right], \tag{1.38}$$

where the effective mixing angle θ_M and effective mass squared difference Δm^2_M are

$$\sin^2 2\theta_M \;\to\; \frac{\sin^2 2\theta}{\sin^2 2\theta + (\cos 2\theta - X)^2}, \tag{1.39}$$

$$\Delta m^2_M \;\to\; \Delta m^2 \sqrt{\sin^2 2\theta + \left(\cos 2\theta - \frac{2\sqrt{2}G_F N_e E}{\Delta m^2}\right)^2}. \tag{1.40}$$

Here, θ is the vacuum mixing angle and $X = \frac{2\sqrt{2}G_F N_e E}{\Delta m^2}$ is in terms of the electron density N_e, neutrino energy E, and Δm^2 is the mass squared difference. G_F is the Fermi constant. When $X = \cos 2\theta$, the amplitude of oscillation become unity and maximum resonant oscillation occur and total transition between flavors happens.

1.3.4 Parametrization of U

Let's consider the general case where U is an $n \times n$ matrix. Now, it can be represented as $U = e^{iH}$, where H is another $n \times n$ Hermitian matrix having n^2 independent real parameters. The number of parameters required to parametrize H is the same to that of the parameters used to parametrize an $n \times n$ orthogonal matrix, say O. Similarly, O can also be represented as $O = e^A$. The orthogonality condition ($O^T O = 1$) demands A to be antisymmetric. Hence, A has got $n(n-1)/2$ real diagonal elements. This indicates that U has

$$N_\theta = \frac{n(n-1)}{2} \tag{1.41}$$

number of angles. So, the number of phases required to characterize U is

$$N_\phi = n^2 - N_\phi \frac{n(n+1)}{2}. \tag{1.42}$$

Since $n = 3$, hence $N_\theta = 3$ angles and $N_\phi = 6$ phases are required to parametrize the lepton mixing matrix U. We present U as

$$U = \Psi_1 \, R_{23} \, R13 \, \Psi_2 \, R_{12} \, \Psi_3, \tag{1.43}$$

where, R_{ij} are the orthogonal matrices and Ψ_is are diagonal matrices containing the phases. R_{ij} and Ψ_i have the following forms:

$$R_{23} = \begin{pmatrix} 1 & 0 & 0 \\ 0 & c_{23} & s_{23} \\ 0 & -s_{23} & c_{23} \end{pmatrix}, R_{21} = \begin{pmatrix} c_{13} & 0 & s_{13} \\ 0 & 1 & 0 \\ -s_{13} & 0 & c_{13} \end{pmatrix}, R_{12} = \begin{pmatrix} c_{12} & s_{12} & 0 \\ s_{12} & c_{12} & 0 \\ 0 & 0 & 1 \end{pmatrix}, \tag{1.44}$$

$$\Psi_1 = \begin{pmatrix} e^{i\phi_1} & 0 & 0 \\ 0 & e^{i\phi_2} & 0 \\ 0 & 0 & e^{i\phi_3} \end{pmatrix}, \Psi_2 = \begin{pmatrix} 1 & 0 & 0 \\ 0 & e^{i\phi_4} & 0 \\ 0 & 0 & 1 \end{pmatrix}, \Psi_3 = \begin{pmatrix} e^{i\phi_5} & 0 & 0 \\ 0 & e^{i\phi_6} & 0 \\ 0 & 0 & 1 \end{pmatrix}, \tag{1.45}$$

where $c_{ij} = \cos\theta_{ij}$ and $s_{ij} = \sin\theta_{ij}$. These θ_{ij}s are the Euler's rotation angles.

After proper redefinition of the neutrino fields, the lepton mixing matrix U can be expressed

1. in terms of the three mixing angles and one phase as shown below (for Dirac neutrinos)

$$U = U\left(\theta_{12},\ \theta_{13},\ \theta_{23},\ \phi_4\right). \tag{1.46}$$

2. in terms of three mixing angles and three phases as shown below (for Majorna neutrinos)

$$U = U\left(\theta_{12},\ \theta_{13},\ \theta_{23},\ \phi_4,\ \phi_5,\ \phi_6\right). \tag{1.47}$$

Thus, altogether, we have nine neutrino parameters to account for all the neutrino related events. The determination of these parameters will ultimately decide whether neutrinos are Dirac of Majorana particle. Hence, an appropriate parametrization of the matrix U is an important part of neutrino physics.

1.3.4.1 Standard parametrization scheme for U

The Particle Data Group (PDG) [3] adopted a parametrization scheme of U called as the Standard parametrization. In this parametrization scheme U is defined as the product of three consecutive rotation matrices multiplied by a diagonal matrix containing phases and can be written as

$$U = R_{23}(\theta_{23} : 0)\, U_{13}(\theta_{13} : \delta)\, R_{12}(\theta_{12} : 0)P; \tag{1.48}$$

where,

$$U_{13} = \begin{pmatrix} c_{13} & 0 & s_{13}e^{-i\delta} \\ 0 & 1 & 0 \\ -s_{13}e^{i\delta} & 0 & c_{13} \end{pmatrix}, P = \begin{pmatrix} e^{i\alpha} & 0 & \\ 0 & e^{i\beta} & 0 \\ 0 & 0 & 1 \end{pmatrix}, \tag{1.49}$$

where, δ is the phase for Dirac type neutrinos while α and β are the phases for the Majorana type neutrinos. When neutrinos are Dirac type, then both α and β become zero. The lepton mixing matrix of eq.(1.48) can be rewritten as

$$U_{PMNS} = \begin{pmatrix} c_{12}c_{13} & s_{12}c_{13} & s_{13}e^{-i\delta} \\ -s_{12}c_{23} - c_{12}s_{23}s_{13}e^{i\delta} & c_{12}c_{23} - s_{12}s_{23}s_{13}e^{i\delta} & s_{23}c_{13} \\ s_{12}s_{23} - c_{12}c_{23}s_{13}e^{i\delta} & -c_{12}s_{23} - s_{12}c_{23}s_{13}e^{i\delta} & c_{23}c_{13} \end{pmatrix} \begin{pmatrix} e^{i\alpha} & 0 & \\ 0 & e^{i\beta} & 0 \\ 0 & 0 & 1 \end{pmatrix} \tag{1.50}$$

The angles $\theta_{12},\ \theta_{13}$ and, θ_{23} are known as the three mixing angles.

1.3.4.2 Symmetric Parametrization scheme for U

Other than the Standard Parametrization scheme, there is another parametrization scheme known as Symmetric parametrization scheme. It describes the mixing matrix U as

$$U = U_{23}(\theta_{23} : \omega_{23})\, U_{13}(\theta_{13} : \omega_{13})\, R_{12}(\theta_{12} : \omega_{12}); \tag{1.51}$$

where,

$$U_{23} = \begin{pmatrix} 1 & 0 & 0 \\ 0 & c_{23} & s_{23}e^{-i\omega_{23}} \\ 0 & -s_{23}e^{i\omega_{23}} & c_{23} \end{pmatrix} \tag{1.52}$$

$$U_{13} = \begin{pmatrix} c_{13} & 0 & s_{13}e^{-i\omega_{13}} \\ 0 & 1 & 0 \\ -s_{13}e^{-i\omega_{13}} & 0 & c_{13} \end{pmatrix} \tag{1.53}$$

$$U_{12} = \begin{pmatrix} c_{12} & s_{12}e^{-i\omega_{12}} & 0 \\ -s_{12}e^{i\omega_{12}} & c_{12} & 0 \\ 0 & 0 & 1 \end{pmatrix} \tag{1.54}$$

All the phases appearing in the matrix U are physical. The phases in the two parametrization schemes can be related as

$$\left.\begin{aligned} \delta &= \omega_{13} - \omega_{12} - \omega_{23}, \\ \alpha &= \omega_{12} + \omega_{23}, \\ \beta &= \omega_{23} \end{aligned}\right\} \tag{1.55}$$

Of the two parametrization scheme, the Standard parametrization scheme is more preferred. The neutrino mixing matrix contributes towards the final U only if, the charged lepton mass matrix is diagonal. The three neutrino generations can be represented as

$$\begin{pmatrix} \nu_{eL} \\ \nu_{\mu L} \\ \nu_{\tau L} \end{pmatrix} = \begin{pmatrix} U_{e1} & U_{e2} & U_{e3} \\ U_{\mu 1} & U_{\mu 2} & U_{\mu 3} \\ U_{\tau 1} & U_{\tau 2} & U_{\tau 3} \end{pmatrix} \begin{pmatrix} \nu_1 \\ \nu_2 \\ \nu_3 \end{pmatrix} \tag{1.56}$$

The above eq.(1.56) shows that the left handed flavor eigenstates are just the linear superposition of neutrino mass eigenstates (confirming the previous claim of eq. (1.29)). For example,

$$|\nu_{\mu L}\rangle = U_{\mu 1}|\nu_1\rangle + U_{\mu 2}|\nu_2\rangle + U_{\mu 3}|\nu_3\rangle \tag{1.57}$$

Neutrino observable parameters like, θ_{13}, θ_{12}, θ_{23}, and δ can be extracted out of the matrix U in the following ways:

$$\left.\begin{array}{rcl} \sin^2\theta_{13} & = & |U_{e3}|^2 \\ \sin^2\theta_{13} & = & \frac{|U_{e2}|^2}{1-|U_{e3}|^2} \\ \sin^2\theta_{23} & = & \frac{|U_{\mu 3}|^2}{1-|U_{e3}|^2} \\ \delta & = & -Arg\,[U_{e3}] \end{array}\right\}, \tag{1.58}$$

which are in accordance with the Standard parametrization.

There are different possibilities to measure the unknown parameters like the three mixing angles, three mass eigenvalues and three phases. The neutrino oscillation experiment deals with the neutrino mass squared differences, mixing angles and the Dirac CP phase. On the other hand, experiment like neutrinoless double beta decay ($\nu 0\beta\beta$) deals with the mass parameters and the Majorana phases.

1.3.5 Majorana CP phases α and β

We have already discussed the possibility of CP violation (see eq.(1.35)) in the oscillation processes involving ($\nu_\alpha \to \nu_\beta$) and ($\overline{\nu}_\alpha \to \overline{\nu}_\beta$). This phenomenon can be expressed more elegantly by using an invariant parameter called Jarlskog Invariant parameter (JCP) and is

expressed as

$$\begin{aligned} J_{CP} &= Im\left[U_{\alpha i}\, U_{\beta j}\, U^{*}_{\alpha j}\, U^{*}_{\beta i}\right] \\ &= c_{12}s_{12}c^{2}_{13}s_{13}c_{23}s_{23}\sin\delta \end{aligned} \tag{1.59}$$

The asymmetry between $\mathscr{P}(\nu_\alpha \to \nu_\beta)$ and $\mathscr{P}(\overline{\nu}_\alpha \to \overline{\nu}_\beta)$ can only account for the Dirac CP violating phases. The neutrinoless double beta decay, if observed, will be the proof of neutrinos Majorana nature, yet it cannot envisage the phases.

The recent experimental confirmation on the non-zero value of θ_{13} has already ignited the confidence of many to measure the Dirac phase in the upcoming experiments. Also, a non-zero value of Dirac phase is emerging (see Table.1.3). A more challenging task will be, to predict the Majorana phases α and β.

A systematic analysis encompassing the $\nu_\alpha \to \overline{\nu}_\beta$ and $\overline{\nu}_\alpha \to \nu_\beta$ processes can shed light on the Majorana phases. Concerning the certain asymmetry that may arise between the oscillation probabilities $\mathscr{P}(\nu_\alpha \to \overline{\nu}_\beta)$ and $\mathscr{P}(\overline{\nu}_\alpha \to \nu_\beta)$, certain Jarsklog like parameters ($\mathscr{V}^{ij}_{\alpha\beta}$) are defined as follows,

$$\mathscr{V}^{ij}_{\alpha\beta} = Im\left[U_{\alpha i}\, U_{\beta i}\, U^{*}_{\alpha j}\, U^{*}_{\beta j}\right]. \tag{1.60}$$

These parameters satisfy the following relations,

$$\mathscr{V}^{ij}_{\alpha\beta} = \mathscr{V}^{ij}_{\beta\alpha} = -\mathscr{V}^{ji}_{\alpha\beta} = -\mathscr{V}^{ji}_{\beta\alpha} \tag{1.61}$$

Some examples of $\mathscr{V}_{\alpha\beta}^{ij}$ are,

$$\left.\begin{aligned} \mathscr{V}_{ee}^{12} &= c_{12}^2 s_{12}^2 c_{13}^4 \sin 2(\alpha-\beta), \\ \mathscr{V}_{ee}^{13} &= c_{12}^2 s_{13}^2 c_{13}^2 \sin 2(\delta+\alpha), \\ \mathscr{V}_{ee}^{23} &= s_{12}^2 c_{13}^2 s_{13}^2 \sin 2(\delta-\beta), \\ &\ldots \end{aligned}\right\} \tag{1.62}$$

Details of the similar equations can be found in [15]. In the limit when $\delta = 0$, then, $J_{CP} = 0$. In general, $\mathscr{V}_{\alpha\beta}^{ij}$ are non-vanishing. In this limit there is no signature for CP violation in $\nu - \nu$ or $\overline{\nu} - \overline{\nu}$ oscillation, however there may be in the $\nu - \overline{\nu}$ oscillation process. Only when $\nu 0\beta\beta$ is confirmed, then we can plan for the determination of α and β in the future experiments involving neutrino and antineutrino oscillations.

1.3.5.1 Massive neutrino and the hierarchy problem

The discussion so far clearly implies that neutrinos have a non-zero masses and they are non-degenerate (at least one of them). This idea creates another problem well known as neutrino mass hierarchy problem. The problem is, which among the three is the heaviest and which one is the lightest, and based on this, there are three possible neutrino mass hierarchies viz. (i) Normal hierarchy ($m_3 \gg m_2 \geq m_1$), (ii) quasi-degenerate hierarchy ($m_3 \approx m_2 \approx m_1$), and (iii) Inverted hierarchy ($m_2 \simeq m_1 \gg m_3$).

1.3.6 Seesaw Mechanism

In addition to the mass hierarchy problem, there is no satisfactory explanation as to why the neutrino masses are infinitesimally small. At present, the most simplest and satisfactory explanation for the smallness of neutrino mass is provided by the seesaw mechanism. Our current understanding on neutrino physics has no means to discriminate whether neutrinos are Dirac or Majorana in nature.

The seesaw mechanism is based on the Dirac and Majorana mass terms. It is apparently the most natural and viable mechanism of neutrino mass generation. For simplicity, let us consider the case of a single neutrino family. In this case, the Lagrangian for the Dirac and the Majorana mass terms is defined as

$$\mathscr{L}^{D+M} = -\frac{1}{2} m_L \overline{\nu}_L (\nu_L)^c - m_D \overline{\nu}_L \nu_R - \frac{1}{2} m_R \overline{\nu}_R^c + h.c., \tag{1.63}$$

where m_L, m_D, and m_R are the left-handed Majorana, Dirac and right-handed Majorana mass terms respectively. The mass term of eq. (1.63) can be expressed in the matrix form as

$$\mathscr{L}^{D+M} = \frac{1}{2} \bar{n}_L M^{D+M} (n_L)^c + h.c., \tag{1.64}$$

where

$$\left.\begin{aligned} M^{D+M} &= \begin{pmatrix} m_L & m_D \\ m_D & m_R \end{pmatrix} \\ n_L &= \begin{pmatrix} \nu_L \\ (\nu_L)^c \end{pmatrix} \end{aligned}\right\} \tag{1.65}$$

For convenience we make

$$M^{D+M} = \frac{1}{2} Tr M^{D+M} + M, \tag{1.66}$$

where $TrM = 0$. We have

$$M = \begin{pmatrix} -\frac{1}{2} & m_D \\ m_D & \frac{1}{2}(m_R - m_L) \end{pmatrix}. \tag{1.67}$$

The matrix M can be easily diagonalized by an orthogonal transformation

$$M = O\bar{m}O^T, \tag{1.68}$$

where

$$O = \begin{pmatrix} \cos\theta & \sin\theta \\ -\sin\theta & \cos\theta \end{pmatrix} \tag{1.69}$$

is an orthogonal matrix and

$$\overline{m}_{1,2} = \pm\frac{1}{2}\sqrt{(m_r - m_L)^2 + 4m_D^2} \tag{1.70}$$

and the mixing angles are given by

$$\tan 2\theta = \frac{2m_D}{m_R - m_L}, \qquad \cos 2\theta = \frac{m_R - M_L}{\sqrt{(m_R - m_L)^2 + 4m_D^2}} \tag{1.71}$$

For the mass matrix M^{D+M} we can write

$$M^{D+M} = Om'O^T, \tag{1.72}$$

where

$$m'_{1,2} = \frac{1}{2}(m_R + M_L) \pm \frac{1}{2}\sqrt{(m_R - m_L)^2 + 4m_D^2} \tag{1.73}$$

The main assumptions of the seesaw mechanism are (i) $m_L = 0$, (ii) m_D is generated by the standard Higgs mechanism, (iii) m_R violate L at energy much higher than the EW scale, i.e.

$$m_R \equiv M_R \gg m_D \tag{1.74}$$

.

The masses of the Majorana particles follow from eq. (1.73) and eq.(1.74), and are given as

$$m_1 \simeq \frac{m_D^2}{M_R} \ll m_D, \qquad m_2 \simeq M_R \gg m_D. \tag{1.75}$$

Again from eq. (1.74) and eq. (1.71) we get,

$$\theta \simeq \frac{m_D}{M_R} \ll 1 \tag{1.76}$$

As far as the seesaw mechanism is concerned, the smallness of left-handed neutrino masses w.r.t. the masses of quarks and leptons, is connected with violation of the total lepton number at very high energy scale given by M_R. The suppression factor $\left(\frac{m_D}{M_R}\right)$ is characterized by the ratio of the EW scale and the scale of the violation of the lepton number. Notice that when we put

$$\left.\begin{aligned} m_D \simeq m_t \simeq 173.5 \text{ GeV}, \qquad & m_1 \simeq 5 \times 10^{-2} \text{ eV}, \\ \text{we get,} \qquad & M_R \simeq \tfrac{m_D^2}{m_1} \simeq 10^{15} \text{ GeV} \end{aligned}\right\} \tag{1.77}$$

Now, for the general case of three neutrinos, the seesaw matrix takes the form

$$M = \begin{pmatrix} 0 & m_D \\ m_D^T & M_R \end{pmatrix}, \tag{1.78}$$

where m_D and M_R are 3×3 matrices and $M_R = M_R^T$. Now, let us introduce the matrix m as

$$U^T M U = m, \tag{1.79}$$

where U is a unitary matrix. In analogy to our above discussion, we can choose the matrix U as

$$U = \begin{pmatrix} 1 & (m_D^T)^\dagger (M_R^{-1}) \\ -M_R^{-1} m_D^T & 1 \end{pmatrix} \tag{1.80}$$

From eq. (1.79) and eq. (1.80), it follows that up to the terms linear in $\left(\frac{m_D}{M_R}\right)$, the matrix m takes the form of block diagonal

$$m \simeq \begin{pmatrix} -m_D M_R^{-1} m_D^T & 0 \\ 0 & M_R \end{pmatrix}. \tag{1.81}$$

Thus the Majorana mass matrix is given by

$$m_\nu = -m_D M_R^{-1} m_D^T \tag{1.82}$$

M_R is the mass matrix for the heavy Majorana particles. The exact form of the matrices m_D and M_R helps in determining the values of neutrino masses and mixings as discussed in the above section. The structure eq. (1.82) with large M_R in denominator ensure the smallness of neutrino masses w.r.t. the masses of leptons and quarks.[4]

1.3.6.1 Types of seesaw mechanism

The seesaw model we discussed so far is the well known Type I seesaw. However, there are other different types of seesaw mechanism in order to explain the smallness of neutrino masses viz.

(i) **Type II seesaw mechanism:** Type II also provides another mechanism, for explaining the observed value of neutrino masses [16, 17]. In this mechanism, the vacuum

[4] another approach to explain the smallness of neutrino masses is based on the assumption that the total Lagrangian of the theory is the sum of the SM Lagrangian with massless neutrinos and non-renormalizable effective Lagrangian

expectation value of the neutral components of scalar gauge-SU(2) triplets is suppressed in such a way that the left-handed neutrinos (ν_L) acquires a vanishingly small Majorana mass term, arising from the Yukawa couplings with the neutral components and is given by

$$m_\nu^{II} \simeq Y_\nu \upsilon_\Delta, \tag{1.83}$$

where Y_ν is the Yukawa coupling, Δ is the $SU(2)_L$ Higgs triplet, and υ_Δ is the VEV of the neutral components of the Higgs triplet. υ_Δ is defined as $\frac{\mu v^2}{M_\Delta^2}$, where M_Δ is the mass of the Higgs triplet and μ is the scale at which the SM Higgs and triplet mixes.

The similarity between the Type I and Type II is that both require a very high mass scale, which is the mass scale of thee scalar triplet. This makes Type I and Type II extremely difficult to test.

(ii) **Type III seesaw mechanism** Type III is implemented recently in the context of the grand unified theories [18–20]. In this case one can generate the neutrino masses by adding two extra matter field in the adjoint representation of $SU(2)_L$ with zero hypercharge

$$m_\nu^{III} \simeq \frac{\Gamma_\nu^2 \upsilon^2}{M_\rho}, \tag{1.84}$$

where M_ρ is the mass of fermion triplets and Γ_ν is the Dirac Yukawa coupling. In the context of $SU(5)$ Type III can give rise to Type I, since the fields (for both) responsible for the seesaw lives in the adjoint representation of $SU(5)$.

(iii) **Linear and Inverse seesaw mechanism:** Unlike the standard seesaw models (Type - I, II, III), which are assumed at an energy scale close to the GUT scale, the linear and the inverse seesaw models try to realize the same at the electroweak scale by adding new particles to the SM particle contents. The low scale seesaw scenarios have two extra neutral lepton singlets per family, ν_R and S_t (right-handed and sterile neutrinos).

Under such assumption the mass matrix, in the basis $(\overline{\nu}_L, \overline{\nu^c}_R, S_t^c)$, takes the form

$$\mathscr{L}_m = \frac{1}{2}\left(\overline{\nu}_L, \overline{\nu^c}_R, S_t^c\right) \begin{pmatrix} 0 & m_D & 0 \\ m_D^T & 0 M_R & \\ 0 & M_R^T & 0 \end{pmatrix} \begin{pmatrix} \nu_L^c \\ \nu_R \\ S_t \end{pmatrix} + h.c. \tag{1.85}$$

This mass texture does not violate the lepton number and the neutrinos remain massless. However, in this model one can generate a small neutrino mass by adding a small mass parameter that violate the lepton number. This technique is possible without requiring an extremely large M_R value. This is the reason why it is known as *low scale seesaw*.

The model is called a linear seesaw if, in the eq. (1.85), the block $\left[\mathscr{M}^{(\nu)}\right]_{13} \equiv \varepsilon$. It is because the light neutrino masses are linear in m_D, such that $m_\nu \sim \varepsilon \dfrac{m_D}{M_R}$. However, if the block $\left[\mathscr{M}^{(\nu)}\right]_{33} \equiv \mu$ is the small mass parameter then the model is known as *inverse seesaw* and the corresponding light neutrino masses $m_\nu \sim \mu \dfrac{m_D^2}{M_R^2}$.

1.3.7 Current status of neutrino masses and mixings

Within the standard 3ν framework, the global fit of neutrino oscillation data provides the most accurate information on the neutrino parameters. The five known oscillation parameters ($\left|\Delta m_{21}^2\right|$, $\sin^2\theta_{12}$, $\left|\Delta m_{31}^2\right|$, $\sin^2\theta_{13}$, $\sin^2\theta_{23}$) have been determined with fractional accuracies as small as 2.4%, 5.8%, 1.8%, 4.7%, 9%, respectively. The most recent neutrino oscillation data are given in Table 1.3.

The status of the three unknown oscillation parameters is as follows. The ambiguity of the θ_{23} remains essentially unresolved. The best fit value of $\sin^2\theta_{23}$ is somewhat fragile, and by changing the data sets or by changing the hierarchy, it can flip the octant from the first to the second. For the CP-violating phase δ, the previous trend favoring $\sin\delta < 0$ still remains

(with a best fit at $\sin\delta \sim -0.9$), although all δ values are allowed at 3σ. Finally, there is no statistically significant indication in favor of the mass hierarchy (either NH or IH).

On changing the NOνA appearance data set, some differences appears but there is still no significant improvement on the octant ambiguity, while the indications on δ are strengthened, and some ranges with $\sin\delta > 0$ can be excluded at 3σ level. Concerning the mass hierarchy, the NH case appears to be slightly favored (at $\sim 90\%$ C.L.).

A study on the parameter covariances and the impact of different data sets allow us to appreciate the interplay among the various (known and unknown) parameters, as well as the synergy between oscillation searches in different kinds of experiments. The non-oscillation observables like the m_β, $m_{\beta\beta}$, $\sum m_i$ can help to probe the absolute neutrino masses. In this context, tight upper bounds on $\sum m_i$ from precision cosmology appear to favor the NH case.

1.3.8 Limits and constraints on neutrino masses

Currently, there is no experimental data which can predict the exact numerical values of the neutrino masses. What we have is just the upper bound on the total neutrino mass i.e., $\sum m_i$.[5] The most stringent bound on the combined neutrino masses comes from the cosmological observations. There are different ways to put constraint on $\sum m_i$, some of them are (i) Tritium beta decay ($^3H \rightarrow {}^3He + e^- + \bar{\nu}_e$): this reaction releases an energy of $Q = M_H - M_{h_e} - m_e = 18.58KeV$. Within the present and expected experimental accuracy, one can limit the combination $m_\beta = \sum m_i |U_{ei}|^2$. Currently, the bound on m_β is $< 2.2eV$ at 95%CL which is expected to be further constrained by increasing the sensitivity down to 0.2% (KATRIN), (ii) Relic neutrinos: The energy density of the neutrino in our universe can

[5] At present, there is no lower bound on the total neutrino masses $\sum m_i$. However, using the kinematical methods for determining the momentum and energy of neutrinos it is, in principle, possible to do a direct measurement of the neutrino masses. But, so far, we are successful only in determining an upper bound on the sum of three neutrino masses $\sum m_i$.

be estimated using the relation,

$$\omega_\nu = \frac{\rho_\nu}{\rho_c} = \frac{1}{h^2}\frac{\sum_i m_i}{93eV},$$

where ρ_c is the critical density of our universe and h is the Hubble constant $\simeq 0.65$ in units of $100Km/s/Mpc$ and $\omega_{tot}h^2 \leq 0.4$. A summary of the various experimental constraints on $\sum_i m_i$ at 95% CL are given in [3].

1.4 Grand Unification

Nowadays, looking beyond the SM has become a trend for the modern theoretical physicist, which is both exciting as well as frustrating. The idea of unification of the fundamental forces was first demonstrated by James Clerk Maxwell in 19$^{\text{th}}$ Century by unifying the electric and magnetic forces into electromagnetic force. This idea of unification was further extended by Steven Weinberg, Abdus Salam and Sheldon Lee Glashow. They proved that, at higher energies, the electromagnetic and weak force can be further unified into a single force called electroweak force (EW). The idea of Grand Unification is a continuation of this trend where the EW force and the strong nuclear force are hypothesized to be unified at an extremely high energy scale ($\sim 10^{16}$ GeV) called the GUT scale. GUT doesn't include the force of gravity. Unification of gravity with other three forces demands for more higher energy scale, called the Planck energy ($\sim 10^{19}$ GeV).

GUT can be of two types viz, non-SUSY GUT and SUSY GUTs. SUSY GUTs are an extension of non-SUSY GUTs [21–23]. This extended version becomes more favorable as it has a simpler and natural symmetry breaking pattern and not much rearrangements are required to fit the low energy data. In a SUSY GUT, low energy effective field theory (EFT) is assumed to satisfy $N = 1$ supersymmetry down to the EW scale in addition to the SM gauge symmetry. Simple non-SUSY $SU(5)$ model is ruled out mainly due to two reasons

viz; high accuracy measurement of $\sin^2\theta_W$ and by early bounds on the proton lifetime [24]. However, there are also papers which showed otherwise [25, 26]. When the SUSY breaking scale is increased the effect from the SUSY SM must get decoupled. This is a must for any theory beyond SM. However, we cannot increases the SUSY breaking scale randomly or else it will reintroduce the hierarchy problem. At present, the unification of the three gauge couplings within SUSY GUTs works extremely well, whereas the non-SUSY GUT misses the unification by about 12σ. However, a precise unification can be achieved with more fine tuning in the model.

SO(10) SUSY GUT models have the ability to accommodate the RH neutrinos automatically thereby favoring the SSM of neutrino mass [27, 28]. In the SUSY GUT inspired seesaw models neutrino masses are explained in the same way like other fermion masses. The non-zero value of θ_{13} was already predicted by these models [29, 30]. These models can also be very predictive since the idea of unified symmetry can precisely relate the Dirac neutrino mass matrix with the quark mass matrix and the charged lepton mass matrix.

1.5 Scope of the thesis

So far, we have highlighted only a brief idea about the successes and limitations of the SM. It is evident, that SM have no room for accommodating the non-zero neutrino masses and the resulting phenomena. In order to successfully explain the experimental/observational data of neutrinos, one has to go beyond the confines of SM. In the previous sections (Subsec. 1.3.2), we briefly discussed how to give masses to neutrinos in the SM by extending the particle content (of SM). In addition, we also discussed the Type I seesaw mechanism (Subsec. 1.3.6), which neatly explained the observed smallness of neutrino masses. However, this mechanism took place at an extremely high energy scale (close to the GUT scale), making it next to impossible for experimental verification. We also presented a brief ideas on the supersymmetric extension of the SM model (MSSM) (Sec. 1.2), which is a very promising

BSM physics. It is an attempt to understand the deeper working mechanism of our Universe. As already discussed, it has a good predictive power.

Both seesaw mechanism and Supersymmetric theories are successful in explaining things, which are otherwise very difficult. However, the lack of experimental evidences for both are disheartening. The non-existence of supersymmetry or any SUSY related particles (Sparticles), inspired one to consider that it got broken at some higher energy scale (SUSY breaking scale). Moreover, there is no hard-and-fast theoretical constraints on the scale where the phenomenon took place. It is this absence of a definitive scale, for both the seesaw mechanism and SUSY breaking, which motivated us to study the possible effects of their variations (over a certain range) on the couplings (gauge and Yukawa) and also on the various neutrino parameters during their radiative evolutions (using RG method). While doing so, we attempt to study some specific relations among certain neutrino parameters. We further, extend our study to narrow down the possible range of both m_s and SS scale in the light of the certain EW scale parameter values.

Evidently, a complete description of the neutrino physics is still lacking. So far, we have measured the three mixing angles and the two mass squared differences accurately. Other than these, we have no idea about the absolute neutrino mass eigenvalues and we have lesser idea about the phases etc. In this thesis, we make an attempt to explore the uncharted regime of neutrinos by studying its radiative properties while incorporating a varying m_s and SS scale (only for the normal mass ordering). Such analyses are made possible by the help of Renormalization Group (RG) method. Using this method, physics at a specific energy scale can be extrapolated to a different energy scale. This thesis is organized in the following ways,

- In Chapter 2, we study the radiative properties of the three gauge couplings, third generation three Yukawa couplings for both the Standard Model and the Minimal Supersymmetric Standard Model. Here, we adopt the bottom-up running approach.

We study how the gauge couplings unification point gets affected by the variation of SUSY breaking scale. The same analysis is done for the Yukawa couplings as well.

- In Chapter 3, we make an attempt to account for the observed deviations of the weak scale neutrino mixing angles from two well known flavor mixing patterns: Tri-Bi Maximal (TBM) and Bi-Maximal (BM) mixing patterns through the charged lepton correction. Here, we try to make a comparison between the two deviation matrices and also with the CKM matrix of the quark sector.

- In Chapter 4, we make an attempt to study the radiative properties of nine neutrino parameters using their respective RGEs in the top down approach (for the normal ordering/hierarchy). Here, we analyze the stability of neutrino parameters at EW scale values against the radiative evolution and under the combined effects of varying SUSY breaking scale and the SS scale. Inspired by the recent global neutrino oscillation data, we also study the possible existence of a self-complementarity relation among the neutrino mixing angles at the seesaw scale and hence its radiative stability under the same conditions as mentioned above. We further extend our analysis to include the radiative stabilities of the neutrino mass ratios also.

- Finally, in Chapter 5, we summarize our observations and discuss the results and also the shortcomings in our work. A short discussion on the possible extension of the present investigations and our area of interest are presented.

- In Appendix A, we present a brief timeline showing the various important stages of neutrino physics. We also highlight some of the well known neutrino experimental facilities that have been shutdown, that are still operational, and the one that are planned for the future. In the last section we discuss a brief note on some selected neutrino experiments.

Chapter 2

Unification of Yukawa and gauge couplings under varying SUSY breaking scale

2.1 Introduction

The idea that the three gauge couplings unify at a very high scale, close to Planck scale, is one of the main motivations of such theories. Besides, GUTs also provide answers and clues to many fundamental problems that plague the SM. However, the basic requirements for a model to be realistic are (i) gauge couplings unification, (ii) long enough proton lifetime, and (iii) fermion mass phenomenology has to be correct.

The simplest group with the minimal particles content that can embed the SM gauge group while preserving the L-R structure, is the SU(5) group, such that

$$SU(5) \supset SU(3)_c \times SU(2)_L \times U(Y)_Y. \tag{2.1}$$

It implies that the three gauge couplings unify above a particular energy scale, commonly known as the unification scale.

However, SU(5) GUT [31] needed to be extended as it does not satisfy the above three conditions. This can be remedied by multiple tweaking in the particle contents or by the introduction of a new symmetry called supersymmetry (SUSY). The most natural extension of the SU(5) GUT is the SUSY SU(5) GUT [32], which has wide predictive power [33, 34]. SUSY SU(5) model is very close to unifying the three gauge couplings and it can be made exact by including threshold corrections. But it still fails to satisfy the remaining two conditions which can be fulfilled by allowing non-renormlizable interactions. By introducing a more complex group called SO(10), the above three conditions can be satisfied without the requirement of any larger Higgs sectors or by the introduction of SUSY.

SUSY SU(5) GUT predicts the unification of the third generation Yukawa couplings at or below the unification scale, and provides a natural solution for the hierarchy problem and an alternative explanation of the EW symmetry breaking by the so called radiative breaking scenario [35, 36]. This theory also provides the prediction of proton decay [34] which is caused mainly by $D = 5$ operator [37–40]. The most stringent limit on proton lifetime is provided by the Super Kamiokande experiment [41–43], with the current lower experimental bound $\tau_p > 4 \times 10^{33}$ years [44]. Such restrictive value may serve as a criteria to discriminate certain GUT models. In order to suppress the fast $D = 5$ operator proton decay [45], we require to rise both the scale of unification and the mass of the color triplet multiplets. In such context, there is still enough scope for further investigations in this direction.

Here, our focus is on the unification of the gauge couplings as well as on the Yukawa couplings in two loops RGEs within the framework of Minimal Supersymmetric SU(5) GUT, using updated data consistent with the LHC result. We numerically solve the unification scale for three *gauge couplings* (g_1, g_2, g_3) as well as the third generation three *Yukawa couplings* (h_t, h_b, h_τ) with varying input values of SUSY breaking scale m_s [45], assuming a single

scale for all supersymmetric particles for simplicity of the calculation [46, 47]. There are hints that SUSY particles have a wide spectrum and are not confined to a single energy scale. This kind of assumption is valid as long as the m_z or $m_t \ll m_s$ [45]. We assume the scale m_s to be somewhere in between 500 GeV to 7 TeV. In the present calculation we also ignore the threshold effects of heavy particles which could be as large as a few percentage [45].

2.2 Evolution of gauge and Yukawa couplings with energy scales

The present experimental data from LHC [2, 3] necessary for our work, are given in Table 2.1.

mass in GeV	coupling constant
$m_z(m_z) = 91.19 \pm 0.0021$	$\alpha_{e.m}^{-1}(m_z) = 127.94 \pm 0.014$
$m_t(m_t) = 173.50 \pm 0.60$	$\alpha_s(m_z) = 0.118 \pm 0.007$
$m_b(m_b) = 4.18 \pm 0.030$	
$m_\tau(m_\tau) = 1.78 \pm 0.0016$	
Weinberg mixing angles =	$sin^2\theta_W(m_z) = 0.23 \pm 0.00012$

Table 2.1 Experimental input values for fermion masses, gauge couplings and Weinberg angle at electroweak scale m_z [2, 3].

In order to calculate the gauge coupling $\alpha_1(m_z)$ for $U(1)_Y$ and $\alpha_2(m_z)$ for $SU(2)_L$ for the Standard Model $SU(3)_C \times SU(2)_L \times U(1)_Y$, we start with the matching relation and definition of Weinberg mixing angle. Thus,

$$\frac{1}{\alpha_{em}(m_z)} = \frac{5}{3}\frac{1}{\alpha_1(m_z)} + \frac{1}{\alpha_2(m_z)}, \tag{2.2}$$

$$\sin^2\theta_W(m_z) = \frac{\alpha_{em}(m_z)}{\alpha_2(m_z)} \tag{2.3}$$

Substituting the observed values of coupling constants $\alpha_{em}(m_z)$, $\alpha_s(m_z)$ and $\sin^2\theta_W$ from Table 2.1 we obtain the numerical values of $\alpha_1(m_z)$ and $\alpha_2(m_z)$ with uncertainties arising from input value of $\alpha_s(m_z)$, $\alpha_1(m_z) = 1.7100^{+0.00012}_{-0.00017} \times 10^{-2}$ and $\alpha_2(m_z) = 3.3753^{-0.00215}_{+0.02150} \times 10^{-2}$ respectively. In term of the normalized coupling constant (g_i), α_i can be expressed as $g_i = \sqrt{4\pi\alpha_i}$, where $i = 1,2,3$ and it represents electromagnetic, weak and strong couplings respectively.

Here, we consider two possible scenarios for the unification of the couplings. In the first case, we consider the top quark mass m_t to be the starting energy scale for the evolution from which the supersymmetric effect on the couplings has been included. Since the observational data in Table 2.1 are given only at the z-pole mass scale, it is necessary to evolve them up to the top quark mass scale. The evolution equation of the coupling constants at one loop level [48] is given by,

$$\frac{d\alpha_i}{dt} = \frac{b_i}{2\pi}\alpha_i^2, \tag{2.4}$$

which can be simplified as

$$\frac{1}{\alpha_i(\mu)} = \frac{1}{\alpha_i(m_z)} - \frac{b_i}{2\pi} ln\left(\frac{\mu}{m_z}\right), \tag{2.5}$$

where, μ is the energy scale in the range ($m_z \leq \mu \leq m_t$). For non-SUSY case, the co-efficient for β function of the RGEs [49] [50] are,

$$b_i = \left(5.30, -0.50, -4.00\right)$$

.

The evolution of the third generation fermion masses (top, bottom and tau) are obtained by using the QED-QCD rescaling factor η as,

$$\left.\begin{array}{rcl} m_b(m_t) & = & \frac{m_b(m_b)}{\eta_b}, \\ m_\tau(m_t) & = & \frac{m_\tau(m_\tau)}{\eta_\tau} \end{array}\right\} \tag{2.6}$$

where, $\eta_b = 1.530$ and $\eta_\tau = 1.015$ [51, 52].

All the above physical parameters are evaluated in the modified minimal subtraction scheme ($\overline{MS}$), without any radiative corrections. The inclusion of radiative correction is achieved by using the method of dimensional regularization through dimensional reduction [53].

Estimation of Yukawa couplings for t, b and τ requires a careful determination of m_t, m_b and m_τ in the DR scheme [49]. However, the effect of running of m_τ on h_τ is very small and hence can be neglected. Furthermore, DR technique is used in order to reduce the large uncertainty in the value of α_s. Except m_b and α_s, all the other parameters are less affected by the radiative correction. So, we consider only m_b and α_s terms neglecting all the others. The equations relating the $\overline{MS}$ and $\overline{DR}$ scheme [53–56] for α_S and m_b $(for\ m_z \leq \mu \leq m_t)$ are given as

$$\frac{1}{\bar{\alpha}_s(\mu)^{DR}} = \frac{1}{\alpha_s(\mu)^{MS}} - \frac{1}{4}, \tag{2.7}$$

$$m_b^{\overline{DR}}(\mu) = m_b^{\overline{MS}}(\mu)\left(1 - \frac{1}{3\pi}\alpha_s(\mu) - \frac{29}{72\pi}\alpha_s(\mu)^2\right), \tag{2.8}$$

$$\begin{array}{rcl} m_b^{\overline{MS}}(\mu) & = & m_b^{\overline{MS}}(m_b)\dfrac{F_b(\mu)}{F_b(m_b)} \\ F_b(\mu) & = & \left(\dfrac{23\alpha_s(\mu)}{6\pi}\right)^{\frac{12}{23}}\left(1 + \dfrac{3731}{3174}\dfrac{\alpha_s(\mu)}{\pi} + 1.5007\left(\dfrac{\alpha_s(\mu)}{\pi}\right)^2\right). \end{array} \tag{2.9}$$

The values of α_1, α_2 and α_3 evaluated at top-quark mass scale using the above equations in $\overline{DR}$ scheme, are shown in Table 2.2.

	Lower limit	Central value	Upper limit
α_1	1.71×10^{-2}	1.71×10^{-2}	1.71×10^{-2}
α_2	3.77×10^{-2}	3.37×10^{-2}	3.37×10^{-2}
α_3^{DR}	0.11	0.11	0.12
g_1	0.46354	0.46356	0.46358
g_2	0.65148	0.65127	0.65107
g_3^{DR}	1.17	1.21	1.24

Table 2.2 Numerical values of gauge couplings at top quark mass scale m_t.

The values of m_b at various scales both in the $\overline{MS}$ and $\overline{DR}$ schemes are shown in Table 2.3.

	at	Lower limit	Central value	Upper limit
$\overline{MS}$	$m_b(m_b)$	4.15	4.18	4.21
	$m_b(m_z)$	2.76	2.86	2.96
	$m_b(m_t)$	2.69	2.78	2.87
$\overline{DR}$	$m_b(m_b)$	4.04	4.07	4.10
	$m_b(m_z)$	2.73	2.82	2.92
	$m_b(m_t)$	2.66	2.75	2.84

Table 2.3 m_b in $\overline{MS}$ and $\overline{DR}$ schemes.

2.3 Effect on the unification with m_t as the SUSY breaking scale ($m_s = m_t$)

With the numerical values of m_t, m_b^{DR} and m_τ at hand we can now determine the values of Yukawa couplings at top-quark mass scale using the following equations [52–57] from

Minimal Supersymmetric Standard Model (MSSM),

$$\left.\begin{array}{rcl} h_t & = & \frac{m_t(m_t)}{174 sin\beta} = \frac{m_t(m_t)\sqrt{1+tan^2\beta}}{174 tan\beta}, \\ h_b & = & \frac{m_b(m_b)}{174 \eta_b cos\beta} = \frac{m_b(m_t)\sqrt{1+tan^2\beta}}{174}, \\ h_\tau & = & \frac{m_\tau(m_\tau)}{174 \eta_\tau cos\beta} = \frac{m_\tau(m_t)\sqrt{1+tan^2\beta}}{174} \end{array}\right\} \tag{2.10}$$

Here h_t, h_b and h_τ are the third generation Yukawa couplings for top quark, bottom quark and tau lepton respectively. The vacuum expectation value without SUSY is $\frac{\upsilon}{\sqrt{2}} = 174$ GeV, $tan\beta = \frac{\upsilon_u}{\upsilon_d}$ is a free parameter in MSSM, where υ_u is the VEV for the up-type quarks $\upsilon_u = \upsilon sin\beta$ and υ_d for the down type quarks $\upsilon_d = \upsilon cos\beta$.

With the values of three gauge couplings in Table 2.2 as the input and Yukawa couplings in eq.(2.10), we estimate the nature of variation of gauge and Yukawa couplings from top quark mass scale m_t up to the point of unification using 2-loops RGEs [50] [52, 58, 59] defined as

$$\frac{dg_i}{dt} = \frac{b_i}{16\pi^2} g_i^3 + \left(\frac{1}{16\pi^2}\right)^2 \left[\sum_{j=1}^{3} b_{ij}\, g_i^3\, g_j^2 - \sum_{j=t,b,\tau} a_{ij}\, g_i^3\, h_j^2\right], \tag{2.11}$$

and for Yukawa couplings at 2-loop level, [20,21,22]

$$\left.\begin{aligned}
\frac{dh_t}{dt} &= \frac{h_t}{16\pi^2}\Bigg[\left(6h_t^2+h_b^2-\sum_{i=1}^{3}c_i\,g_i^2\right)+ \\
&\quad \frac{1}{16\pi^2}\Bigg(\sum_{i=1}\left(c_ib_i+\frac{c_i^2}{2}\right)g_i^4+g_1^2g_2^2+\frac{136}{45}g_1^2g_3^2+8g_2^2g_3^2+ \\
&\quad \left(\tfrac{6}{5}g_1^2+6g_2^2+16g_3^2\right)h_t^2+\tfrac{2}{5}g_1^2h_b^2-22h_t^4-5h_b^4-5h_t^2h_b^2-h_b^2h_\tau^2\Bigg)\Bigg] \\
\frac{dh_b}{dt} &= \frac{h_b}{16\pi^2}\Bigg[\left(6h_b^2+h_\tau^2+h_t^2-\sum_{i=1}^{3}c_i'\,g_i^2\right)+ \\
&\quad \frac{1}{16\pi^2}\Bigg(\sum_{i=1}\left(c_i'b_i+\frac{c_i'^2}{2}\right)g_i^4+g_1^2g_2^2+\tfrac{8}{9}g_1^2g_3^2+8g_2^2g_3^2+\left(\tfrac{2}{5}g_1^2+6g_2^2\right. \\
&\quad \left.+16g_3^2\right)h_b^2+\tfrac{4}{5}g_1^2h_t^2+\tfrac{6}{5}g_1^2h_\tau^2-22h_b^4-3h_\tau^4-5h_t^4-5h_b^2h_t^2-3h_b^2h_\tau^2\Bigg)\Bigg] \\
\frac{dh_\tau}{dt} &= \frac{h_\tau}{16\pi^2}\Bigg[\left(4h_\tau^2+3h_b^2-\sum_{i=1}^{3}c_i''\,g_i^2\right) \\
&\quad +\frac{1}{16\pi^2}\Bigg(\sum_{i=1}\left(c_i''b_i+\frac{c_i''^2}{2}\right)g_i^4+\tfrac{9}{5}g_1^2g_2^2+\left(\tfrac{6}{5}g_1^2+6g_2^2\right)h_\tau^2 \\
&\quad +\left(\tfrac{-2}{5}g_1^2+16g_3^2\right)h_b^2+9h_b^4-10h_\tau^4-3h_b^2h_t^2-9h_b^2h_\tau^2\Bigg)\Bigg]
\end{aligned}\right\} \quad (2.12)$$

where, $t = ln\mu$ and b_i, b_{ij}, a_{ij}, c_i, $c_i^{'}$, $c_i^{''}$ are β function coefficients in MSSM,

$$\left.\begin{aligned}
b_i &= \left(6.6, 1.0, -3.0\right) \quad b_{ij} = \begin{pmatrix} 7.96 & 5.40 & 17.60 \\ 1.80 & 25.00 & 24.00 \\ 2.20 & 9.00 & 14.00 \end{pmatrix} \\
a_{ij} &= \begin{pmatrix} 5.2 & 2.8 & 3.6 \\ 6.0 & 6.0 & 2.0 \\ 4.0 & 4.0 & 0.0 \end{pmatrix} \\
c_i &= \left(\tfrac{13}{15}, 3, \tfrac{16}{13}\right) c_i^{'} = \left(\tfrac{7}{15}, 3, \tfrac{16}{3}\right) c_i^{''} = \left(\tfrac{9}{5}, 3, 0\right)
\end{aligned}\right\} \quad (2.13)$$

With the central value of g_3^{DR}, there is an approximate gauge couplings unification around 2.59×10^{16} GeV and a Yukawa couplings unification at 1.99×10^{12} GeV as shown in Table

2.4. However, if we vary g_3^{DR} within the experimental bound $1.2084^{+0.0344}_{-0.0355}$, it is possible for both Gauge couplings and Yukawa couplings to have a sharp unification scale at their respective $\tan\beta$ values as shown in Table 2.5. Figure 2.1a and Figure 2.2a represent the exact unification point for the gauge and Yukawa couplings after RG evolution in the bottom-up approach.

At Experimental	$\tan\beta$	g_3	Unification points (in GeV)	
			Gauge	Yukawa
			U_{g_1,g_2,g_3}	U_{h_t,h_b,h_τ}
Central value	59.99	1.21	$\sim 2.59 \times 10^{16}$	1.99×10^{12}

Table 2.4 Approximate unification points for gauge couplings and Yukawa couplings for $g_3^{DR} = 1.2084$ and $m_s = m_t$.

At experimental	$\tan\beta$	g_3^{DR}	Unification points (Energy in GeV)	
			Gauge	Yukawa
			U_{g_1,g_2,g_3}	U_{h_t,h_b,h_τ}
Central Value	60.14	1.22	2.95×10^{16}	3.88×10^{11}

Table 2.5 Exact unification points for gauge couplings and Yukawa couplings for input values of g_3^{DR} in the range $1.2084^{+0.0344}_{-0.0355}$ and $m_s = m_t$.

2.4 Unification based on varying SUSY breaking scale for $m_s > m_t$

Following section 2, here we will consider the second case where SUSY breaking scale has been pushed higher up to 7 TeV. To be precise we consider some viable points viz., 500 GeV, 1 TeV, 2 TeV, 3 TeV, 5 TeV, 7 TeV assuming the supersymmetric effect to start somewhere in between.

The technique is almost similar with the previous section. The RGEs governing the evolution of the gauge couplings and the Yukawa couplings are the same as those given in

eq.(2.11) and eq.(2.12), with the only difference in the values of the energy scale and the coefficients of the beta function i.e., b_i and $c_i^{'}$s.

Because of the difference in the intermediate energy level, one more step is needed. In the previous section (section 2.3) we elevate the physical parameters from m_z scale up to m_t scale and then to unification scale using eq.(2.11), eq.(2.12), and eq.(2.13). Here in this case we will be doing the same but with one more step as shown below.

(i) Evolution from m_z scale up to m_t using eq.(2.10) and Table 2.2, for the energy range $m_z \leq \mu \leq m_t$

(ii) Evolution from m_t to m_s, where m_s =500 GeV, 1 TeV, 3 TeV, 5 TeV, 7 TeV using eq.(2.11), eq.(2.14), and eq.(2.15) with the beta function coefficients of eq.(2.16)

$$
\begin{aligned}
\frac{dh_t}{dt} &= \frac{h_t}{16\pi^2}\left(\tfrac{3}{2}h_t^2 - \tfrac{3}{2}h_b^2 + Y_2(S) - \textstyle\sum_{i=1}^{3} c_i\, g_i^2\right) + \\
&\quad \frac{h_t}{(16\pi^2)^2}\left[\tfrac{1187}{600}g_1^4 - \tfrac{23}{4}g_2^4 - 108g_3^4 - \tfrac{9}{20}g_1^2g_2^2 + \tfrac{19}{15}g_1^2g_3^2 + 9g_2^2g_3^2\right. \\
&\quad + \left(\tfrac{223}{80}g_1^2 + \tfrac{135}{16}g_2^2 + 16g_3^2\right)h_t^2 - \left(\tfrac{43}{80}g_1^2 - \tfrac{9}{16}g_2^2 + 16g_3^2\right)h_b^2 \\
&\quad + \tfrac{5}{2}Y_4(S) - 2\lambda\left(3h_t^2 + h_b^2\right) + \tfrac{3}{2}h_t^4 - \tfrac{5}{4}h_t^2h_b^2 + \tfrac{11}{4}h_b^4 \\
&\quad \left. + Y_2(S)\left(\tfrac{5}{4}h_b^2 - \tfrac{9}{4}h_t^2\right) - \chi_4(S) + \tfrac{3}{2}\lambda^2\right], \\
\frac{dh_b}{dt} &= \frac{h_b}{16\pi^2}\left(\tfrac{3}{2}h_b^2 - \tfrac{3}{2}h_t^2 + Y_2(S) - \textstyle\sum_{i=1}^{3} c_i'\, g_i^2\right) + \\
&\quad \frac{h_b}{(16\pi^2)^2}\left[-\tfrac{127}{600}g_1^4 - \tfrac{23}{4}g_2^4 - 108g_3^4 - \tfrac{27}{20}g_1^2g_2^2 + \tfrac{31}{15}g_1^2g_3^2 + 9g_2^2g_3^2\right. \\
&\quad - \left(\tfrac{79}{80}g_1^2 - \tfrac{9}{16}g_2^2 + 16g_3^2\right)h_t^2 + \left(\tfrac{187}{80}g_1^2 + \tfrac{135}{16}g_2^2 + 16g_3^2\right)h_b^2 \\
&\quad + \tfrac{5}{2}Y_4(S) - 2\lambda\left(h_t^2 + 3h_b^2\right) + \tfrac{3}{2}h_b^4 - \tfrac{5}{4}h_t^2h_b^2 + \tfrac{11}{4}h_t^4 \\
&\quad \left. + Y_2(S)\left(\tfrac{5}{4}h_t^2 - \tfrac{9}{4}h_b^2\right) - \chi_4(S) + \tfrac{3}{2}\lambda^2\right], \\
\frac{dh_\tau}{dt} &= \frac{h_\tau}{16\pi^2}\left(\tfrac{3}{2}h_\tau^2 + Y_2(S) - \textstyle\sum_{i=1}^{3} c_i''\, g_i^2\right) + \\
&\quad \frac{h_\tau}{(16\pi^2)^2}\left[\tfrac{1371}{200}g_1^4 - \tfrac{23}{4}g_2^4 - \tfrac{27}{20}g_1^2g_2^2 + \left(\tfrac{387}{80}g_1^2 + \tfrac{135}{16}g_2^2\right)h_\tau^2\right. \\
&\quad \left. + \tfrac{5}{2}Y_4(S) - 6\lambda h_t^2 + \tfrac{3}{2}h_\tau^4 - \tfrac{9}{4}Y_2(S)h_\tau^2 - \chi_4(S) + \tfrac{3}{2}\lambda^2\right], \\
\frac{d\lambda}{dt} &= \frac{1}{16\pi^2}\left[\tfrac{9}{4}\left(\tfrac{3}{25}g_1^4 + \tfrac{2}{5}g_1^2g_2^2 + g_2^4\right) - \left(\tfrac{9}{5}g_1^2 + 9g_2^2\right)\lambda + 4Y_2(S)\lambda - \right. \\
&\quad \left. 4H(S) + 12\lambda^2\right] \\
&\quad + \frac{1}{(16\pi^2)^2}\left[-78\lambda^3 + 18\left(\tfrac{3}{5}g_1^2 + 3g_2^2\right)\lambda^2 + \left(-\tfrac{73}{8}g_2^4 + \tfrac{117}{20}g_1^2g_2^2 + \right.\right. \\
&\quad \left.\tfrac{1887}{200}g_1^4\right)\lambda + \tfrac{305}{8}g_2^6 - \tfrac{867}{120}g_1^2g_2^4 - \tfrac{1677}{200}g_1^4g_2^2 - \tfrac{3411}{1000}g_1^6 - 64g_3^2\left(h_t^4 + h_b^4\right) \\
&\quad - \tfrac{8}{5}g_1^2\left(2h_t^4 - h_b^4 + 3h_\tau^4\right) - \tfrac{3}{2}g_2^4Y_2(S) + 10\lambda Y_4(S) + \tfrac{3}{5}g_1^2\left(-\tfrac{57}{10}g_1^2 + \right. \\
&\quad 21g_2^2\left.\right)h_t^2 + \left(\tfrac{3}{2}g_1^2 + 9g_2^2\right)h_b^2 + \left(-\tfrac{15}{2}g_1^2 + 11g_2^2\right)h_\tau^2 - 24\lambda^2Y_2(S) - \\
&\quad \left.\lambda H(S) + 6\lambda h_t^2h_b^2 + 20\left(3h_t^6 + 3h_b^6 + h_\tau^6\right) - 12\left(h_t^4h_b^2 + h_t^2h_b^4\right)\right]
\end{aligned}
\tag{2.14}
$$

where

$$\left.\begin{aligned} Y_2(S) &= 3h_t^2 + 3h_b^2 + h_\tau^2, \\ Y_4(S) &= \tfrac{1}{3}\left[3\sum c_i g_i^2 h_t^2 + 3\sum c_i^{'} g_i^2 h_b^2 + 3\sum c_i^{''} g_i^2 h_\tau^2\right], \\ \chi_4(S) &= \tfrac{9}{4}\left[3h_t^4 + 3h_b^4 + h_\tau^4 - \tfrac{2}{3}h_t^2 h_b^2\right] \\ H(S) &= 3h_t^4 + 3h_t^4 + h_\tau^4, \\ \lambda &= \tfrac{m_h^2}{\upsilon^2}, \end{aligned}\right\} \tag{2.15}$$

where λ is the Higgs self-coupling (m_h = Higgs mass) and υ=Vacuum expectation value.

With the values of beta function coefficients for non-SUSY case [50] [51]

$$\left.\begin{aligned} b_i &= \Big(4.100, -3.167, -7.000\Big), \quad g_{ij} = \begin{pmatrix} 3.98 & 2.70 & 8.8 \\ 0.90 & 5.83 & 12.0 \\ 1.10 & 4.50 & -26.0 \end{pmatrix}, \\ a_{ij} &= \begin{pmatrix} 0.85 & 0.5 & 0.5 \\ 1.50 & 1.5 & 0.5 \\ 2.00 & 2.0 & 0.0 \end{pmatrix} \\ c_i &= \Big(0.85, 2.25, 8.00\Big), \quad c_i^{'} = \Big(0.25, 2.25, 8.00\Big), \\ c_i^{''} &= \Big(2.25, 2.25, 0.00\Big) \end{aligned}\right\}, \tag{2.16}$$

for the energy range $m_t \leq \mu \leq m_s$

(iii) Evolution from m_s to m_{GUT} where, m_s =500 GeV, 1 TeV, 3 TeV, 5 TeV, 7 TeV, using eq.(2.11), eq.(2.12), and eq.(2.13).

Here, we obtain a similar result with that of Section 2.3. At the central value of g_3^{DR}, there is an approximate gauge couplings unification but a sharp Yukawa couplings unification (Table 2.6). However, if we vary g_3^{DR} within the experimental bounds, it is possible for

both gauge couplings and Yukawa couplings to have a sharp single unification scale at their respective energy scale and $\tan\beta$ values as shown in Table 2.7, Fig.2.1b and Fig.2.2b.

SUSY breaking scale (m_s)	$\tan\beta$	Unification points (Energy in GeV)	
		Gauge	Yukawa
		U_{g_1,g_2,g_3}	U_{h_t,h_b,h_τ}
500 GeV	60.91	3.74×10^{16}	1.93×10^{11}
1 TeV	61.46	4.11×10^{16}	8.61×10^{10}
3 TeV	62.42	4.84×10^{16}	2.57×10^{10}
5 TeV	62.81	5.18×10^{16}	1.63×10^{10}
7 TeV	63.05	5.40×10^{16}	1.26×10^{10}

Table 2.6 Approximate gauge unification points and Yukawa unification points for central value of $g_3^{DR} = 1.2084$

SUSY breaking scale (m_s)	$\tan\beta$	g_3^{DR}	Unification points (Energy in GeV)	
			Gauge	Yukawa
			U_{g_1,g_2,g_3}	U_{h_t,h_b,h_τ}
175 GeV	60.16	1.22	2.97×10^{16}	1.71×10^{11}
500 GeV	61.06	1.21	3.75×10^{16}	1.14×10^{11}
1 TeV	61.62	1.21	4.11×10^{16}	8.21×10^{10}
3 TeV	62.54	1.19	4.82×10^{16}	4.60×10^{10}
5 TeV	62.97	1.19	5.15×10^{16}	3.65×10^{10}
7 TeV	63.25	1.19	5.37×10^{16}	3.18×10^{10}

Table 2.7 Exact Unification points for gauge couplings and Yukawa couplings for input values of g_3^{DR} in the range $1.2084^{+0.0344}_{-0.0355}$.

2.5 Results and Discussion

To summarize, we have studied the unification scenario in supersymmetric SU(5) grand unified theory [60, 61] using the recent data and the two-loop renormalization group equations [33, 34]. From our study we have found that (in Section 2.3, where $m_s = m_t$) with the central value of g_3^{DR} there is an approximate gauge couplings unification and a sharp Yukawa couplings unification as given in Table 2.4. However, if we vary g_3^{DR} within the

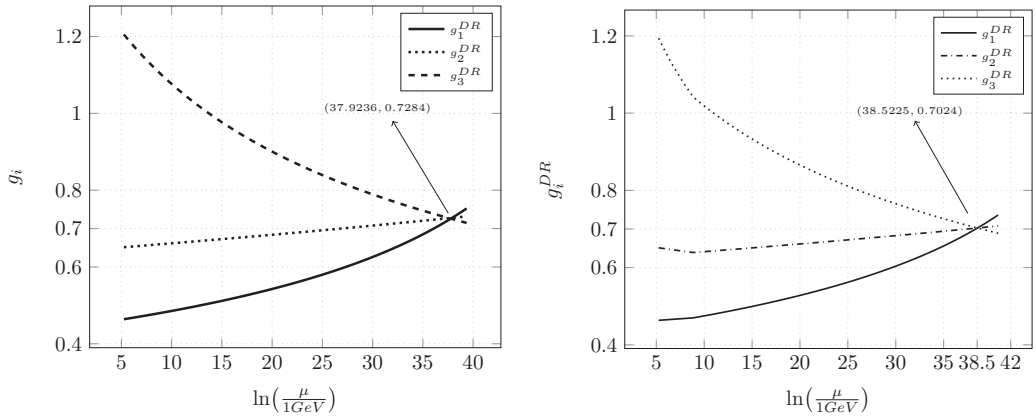

(a) (b)

Fig. 2.1 Radiative evolution of gauge couplings and their unification when (a) $m_s = m_t$ and (b) $m_s > m_t$ TeV. In (b) we take $m_s = 7$ TeV.

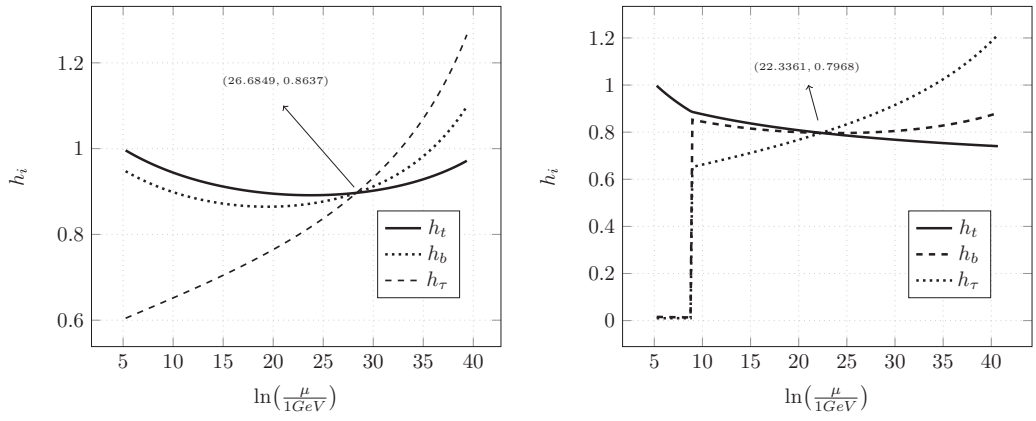

(a) (b)

Fig. 2.2 Radiative evolution of third generation three Yukawa couplings and their unification when (a) $m_s = m_t$ and (b) $m_s > m_t$ TeV. In (b) we take $m_s = 7$ TeV.

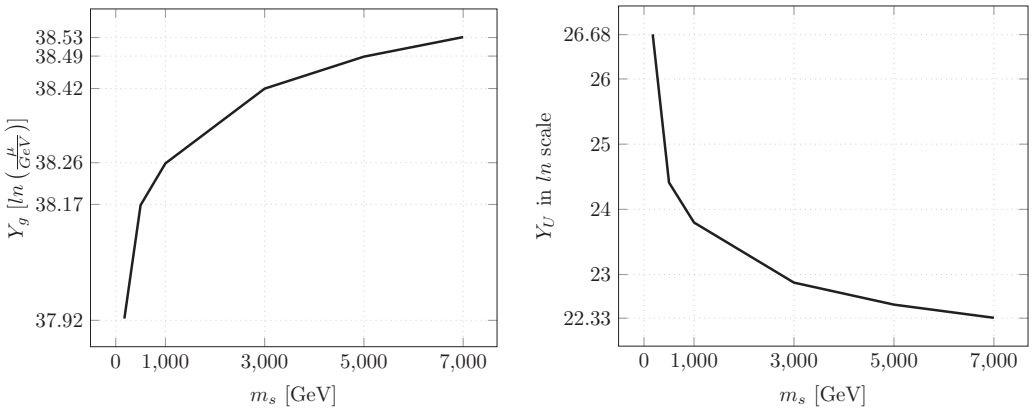

(a) (b)

Fig. 2.3 Variation of the unification points for (a) the three gauge couplings and (b) the third generation three Yukawa couplings with the variation of m_s scale. Here, the value of m_s are fixed at 500 GeV, 1 TeV, 3 TeV, 5 TeV, and 7 TeV.

experimental bounds ($1.2084^{+0.0344}_{-0.0355}$), it is possible to obtain a sharp unification scale for both the gauge couplings as well as for Yukawa couplings at their respective m_s and $\tan\beta$ values as shown in Fig.2.1a and Fig.2.2a in Table 2.5 (gauge unification at 2.9518×10^{16} GeV and Yukawa unification at 3.8828×10^{11} GeV). A similar result is found in section 4 where there are approximate (Table 2.6) and sharp unification scale for gauge couplings and Yukawa couplings at central value of g_3^{DR} (Table 2.7). But with the variation of g_3^{DR} within the experimental range $1.2084^{+0.0344}_{-0.0355}$, we obtain a single unification scale for the gauge couplings at 5.4175×10^{16} GeV and for Yukawa couplings at 5.0175×10^{9} GeV (Fig.2.1b and Fig.2.2b and Table 2.7). Here we have shown only the graph for $m_s = 7$ TeV, case as all the other graphs for different m_s have the similar pattern with the only difference in their unification scale. When we note down the unification points for both the gauge couplings as well as the Yukawa couplings for different values of m_s, a pattern emerged as shown in (Fig.2.3). For gauge couplings, the unification point increases with the increase in the SUSY breaking scale m_s (Fig.2.3a). But for Yukawa couplings, the unification points vary in the reverse order compared to the gauge couplings i.e., unification points decrease with the

increase in m_s Fig.2.3b. Finally, the present analysis addresses an important question on how the gauge and Yukawa couplings unification scales vary with the varying SUSY breaking scale.

The present analysis is based on an extremely simplifying assumption of a single scale for all SUSY particles. There are strong hints that this is not the case and the SUSY spectrum is more spread than being at a single scale [60]. Such simplifying assumption make the present analysis possible at the cost of exact numerical accuracy. We also neglect the threshold corrections [61] from various factors like (i) threshold correction from the two loop contribution in the running of coupling constants (ii) light threshold correction from all superpartners in the SUSY sector and (iii) threshold correction from particles of mass of the unification scale. The first assumption is valid so long as $m_s \gg m_t$ or m_z [29]. These two assumptions when properly taken into account will affect the result by a few percent.

This chapters serves as the backbone for the radiative studies of all the Standard Model particles e.g. neutrino parameters. A proper radiative analysis of neutrino parameters (which is one of the main theme of this thesis), demands a clear understanding of the various couplings (we consider only those couplings which give appreciable contributions). It will become clear in the following chapter (Chapter 4), that radiative evolution of all of the neutrino parameters depends upon the three gauge couplings as well as the third generation three Yukawa couplings.

Chapter 3

Parametrization of lepton mixing matrix in terms of deviations from bi-maximal and tri-bimaximl mixing

3.1 Introduction

Over the last five years contributions from reactor [62–65], accelerator [66, 67] and solar [68] neutrino experiments have provided precise values of three mixing angles and two mass squared differences under a three-neutrino mixing scenario. Global analysis [69–71] of 3ν oscillation data available from various experiments, provides us an overall view on mixing parameters.

As neutrino experiments have been trying for more and more precision measurements of neutrino mixing parameters, meanwhile theorists have been trying to realize the flavor mixing pattern of leptons. Bimaximal mixing (BM) [72] and Tri-bimaximal mixing (TBM) [73] have been playing an attractive role in the search of flavor mixing pattern over a decade. Both these mixing schemes are $\mu - \tau$ symmetric [74–76] and predict maximal atmospheric mixing and zero reactor angle. They differ in their predictions of solar angle in such that

BM mixing predicts maximal value of solar angle while TBM mixing leads to a value which equals $\arcsin(\frac{1}{\sqrt{3}})$. Out of these two mixing schemes, predictions of TBM mixing are more closer to global data [69–71] compared to the other. With the confirmation of non zero θ_{13} the deviation of lepton mixing from exact BM or TBM pattern is clear. It is therefore useful to study the deviations of lepton mixing from exact BM or TBM pattern. Deviations from BM or TBM mixing is in fact a natural idea frequently discussed in the literature [77–87].

In this chapter, we introduce three parameters which account for deviations of the three mixing angles, namely solar, atmospheric and reactor angle from their exact BM or TBM values. We then parametrize the lepton mixing matrix in terms of these three deviation parameters. Parametrization of lepton mixing matrix in terms of deviation parameters is also discussed in Ref. [88]. Our parametrization set up is however different from that. We mainly implicate the parametrization set up in predicting possible structure of charged lepton mixing matrix which in turn can generate the lepton mixing matrix from BM or TBM neutrino mixing via charged lepton correction. Charged lepton correction [89–98] is a very common tool to deviate special mixing schemes like BM or TBM mixing. Corrections to special mixing schemes can also be accounted in mass matrix formalism. We also analyse numerically the charged lepton mixing matrices with an interest to compare them with the CKM matrix [99, 100] of quark sector. In Grand Unified Theory (GUT) based models [101–104] CKM like charged lepton corrections to special mixing schemes are naturally considered. Such models also incorporates Quark-Lepton Complementarity (QLC) [105–108].

3.2 Parametrization of lepton mixing matrix

In general, lepton mixing matrix, known as PMNS matrix, is parametrized in terms of three mixing angles, namely θ_{12}, θ_{23} and θ_{13} which are commonly known as solar, atmospheric and reactor angle; and three CP violating phases- one Dirac CP phase δ and two Majorana phases α and β. In the standard Particle Data Group (PDG) parametrization [3] it looks like

$$U_{PMNS} = \begin{pmatrix} c_{12}c_{13} & s_{12}c_{13} & s_{13}e^{-i\delta} \\ -s_{12}c_{23} - c_{12}s_{23}s_{13}e^{i\delta} & c_{12}c_{23} - s_{12}s_{23}s_{13}e^{i\delta} & s_{23}c_{13} \\ s_{12}s_{23} - c_{12}c_{23}s_{13}e^{i\delta} & -c_{12}s_{23} - s_{12}c_{23}s_{13}e^{i\delta} & c_{23}c_{13} \end{pmatrix} .P, \tag{3.1}$$

where $c_{ij} = \cos\theta_{ij}$, $s_{ij} = \sin\theta_{ij}$ $(i, j = 1, 2)$ and $P = diag(1, e^{i\alpha}, e^{i\beta})$ contains the Majorana CP phases. In the present work we however drop Majorana phase matrix P assuming that neutrinos obey Dirac nature.

Both BM and TBM matrices predict $\theta_{13}^{bm/tb} = 0$ and $\theta_{23}^{bm/tb} = 45^\circ$ (suffices bm and tb represent BM and TBM respectively). However, their predictions for solar angle are different and are given by $\theta_{12}^{bm} = 45^\circ$ and $\theta_{12}^{tb} = \arcsin(\frac{1}{\sqrt{3}})$. Putting these predictions in eq. (3.1), BM and TBM matrices can be obtained as

$$U_{BM} = \begin{pmatrix} \frac{1}{\sqrt{2}} & \frac{1}{\sqrt{2}} & 0 \\ -\frac{1}{2} & \frac{1}{2} & \frac{1}{\sqrt{2}} \\ \frac{1}{2} & -\frac{1}{2} & \frac{1}{\sqrt{2}} \end{pmatrix}, \tag{3.2}$$

$$U_{TBM} = \begin{pmatrix} \sqrt{\frac{2}{3}} & \frac{1}{\sqrt{3}} & 0 \\ -\sqrt{\frac{1}{6}} & \frac{1}{\sqrt{3}} & \frac{1}{\sqrt{2}} \\ \sqrt{\frac{1}{6}} & -\frac{1}{\sqrt{3}} & \frac{1}{\sqrt{2}} \end{pmatrix}. \tag{3.3}$$

We now introduce three parameters which account for the deviations of three mixing angles from their corresponding BM or TBM values as follows :

$$\left.\begin{aligned} \theta_{12} &= \theta_{12}^{bm/tb} + \delta\theta_{12}^{bm/tb}, \\ \theta_{23} &= \theta_{23}^{bm/tb} + \delta\theta_{23}^{bm/tb}, \\ \theta_{13} &= \theta_{13}^{bm/tb} + \delta\theta_{13}^{bm/tb}, \end{aligned}\right\} \tag{3.4}$$

where the deviation parameters $\delta\theta_{12}^{bm/tb}$ and $\delta\theta_{23}^{bm/tb}$ can take positive as well as negative values whereas $\delta\theta_{13}^{bm/tb}$ takes only positive values. We present the best fit and 3σ values of mixing angles and Dirac CP phase in Table 1.3 [1]. Based on these global data we calculate the values of deviation parameters and are presented in Table 3.1.

For BM mixing we have from eq. (3.4)

$$\left.\begin{aligned} \theta_{12} &= 45^\circ + \delta\theta_{12}^{bm}, \\ \theta_{23} &= 45^\circ + \delta\theta_{23}^{bm}, \\ \theta_{13} &= \delta\theta_{13}^{bm}. \end{aligned}\right\} \tag{3.5}$$

Substituting these values in eq. (3.1) we have PMNS matrix as

$$U_{PMNS} = \begin{pmatrix} \frac{1}{\sqrt{2}}p\tilde{r} & \frac{1}{\sqrt{2}}\tilde{p}\tilde{r} & re^{-i\delta} \\ -\frac{1}{2}\left(\tilde{p}\tilde{q} + pqre^{i\delta}\right) & \frac{1}{2}\left(p\tilde{q} - \tilde{p}qre^{i\delta}\right) & \frac{1}{\sqrt{2}}q\tilde{r} \\ \frac{1}{2}\left(\tilde{p}q - p\tilde{q}re^{i\delta}\right) & -\frac{1}{2}\left(pq + \tilde{p}\tilde{q}re^{i\delta}\right) & \frac{1}{\sqrt{2}}\tilde{q}\tilde{r} \end{pmatrix}, \tag{3.6}$$

where,

$$\left.\begin{aligned} p &= \cos\delta\theta_{12}^{bm} - \sin\delta\theta_{12}^{bm}, \\ \tilde{p} &= \cos\delta\theta_{12}^{bm} + \sin\delta\theta_{12}^{bm}, \\ q &= \cos\delta\theta_{23}^{bm} + \sin\delta\theta_{23}^{bm}, \\ \tilde{q} &= \cos\delta\theta_{23}^{bm} - \sin\delta\theta_{23}^{bm}, \\ r &= \sin\delta\theta_{13}^{bm}, \\ \tilde{r} &= \cos\delta\theta_{13}^{bm}. \end{aligned}\right\} \tag{3.7}$$

For TBM mixing we have from eq. (3.4)

$$\left.\begin{aligned} \theta_{12} &= 35.26^\circ + \delta\theta_{12}^{tb}, \\ \theta_{23} &= 45^\circ + \delta\theta_{23}^{tb}, \\ \theta_{13} &= \delta\theta_{13}^{tb}. \end{aligned}\right\} \tag{3.8}$$

Mixing Scheme	Model	Parameter	Best fit	3 σ
BM	NH	$\delta\theta_{12}$	-10.4°	13.2° - (-7.2°)
		$\delta\theta_{23}$	3.9°	-6.2° - 8.3°
		$\delta\theta_{13}$	8.6°	7.9° - 9.3°
	IH	$\delta\theta_{12}$	-10.4°	13.2° - (-7.2°)
		$\delta\theta_{23}$	4.2°	-5.6° - 8.1°
		$\delta\theta_{13}$	8.7°	8.0° - 9.4°
TBM	NH	$\delta\theta_{12}$	-0.66°	-3.46° - 2.53°
		$\delta\theta_{23}$	3.9°	-6.2° - 8.3°
		$\delta\theta_{13}$	8.6°	7.9° - 9.3°
	IH	$\delta\theta_{12}$	-0.66°	-3.46° - 2.53°
		$\delta\theta_{23}$	4.2°	-5.6° - 8.1°
		$\delta\theta_{13}$	8.7°	8.0° - 9.4°

Table 3.1 Calculated values of the various neutrinos deviation parameters from the present global data (as in Table 1.3) [1].

Substituting these values in eq. (3.1) we have PMNS matrix as

$$U_{PMNS} = \begin{pmatrix} \frac{\sqrt{2}}{\sqrt{3}} p'\tilde{r}' & \frac{1}{\sqrt{3}} \tilde{p}'\tilde{r}' & r' e^{-i\delta} \\ -\frac{1}{\sqrt{6}} \left(\tilde{p}'\tilde{q}' + \sqrt{2} p' q' r' e^{i\delta} \right) & \frac{1}{\sqrt{3}} \left(p'\tilde{q}' - \frac{1}{\sqrt{2}} \tilde{p}' q' r' e^{i\delta} \right) & \frac{1}{\sqrt{2}} q'\tilde{r}' \\ \frac{1}{\sqrt{6}} \left(\tilde{p}' q' - \sqrt{2} p'\tilde{q}' r' e^{i\delta} \right) & -\frac{1}{\sqrt{3}} \left(p' q' + \frac{1}{\sqrt{2}} \tilde{p}'\tilde{q}' r' e^{i\delta} \right) & \frac{1}{\sqrt{2}} \tilde{q}'\tilde{r}' \end{pmatrix}, \quad (3.9)$$

where

$$\left.\begin{aligned} p' &= \cos\delta\theta_{12}^{tb} - \tfrac{1}{\sqrt{2}} \sin\delta\theta_{12}^{tb}, \\ \tilde{p}' &= \cos\delta\theta_{12}^{tb} + \sqrt{2}\sin\delta\theta_{12}^{tb}, \\ q' &= \cos\delta\theta_{23}^{tb} + \sin\delta\theta_{23}^{tb}, \\ \tilde{q}' &= \cos\delta\theta_{23}^{tb} - \sin\delta\theta_{23}^{tb}, \\ r' &= \sin\delta\theta_{13}^{tb}, \\ \tilde{r}' &= \cos\delta\theta_{13}^{tb}. \end{aligned}\right\} \quad (3.10)$$

We want to emphasize that parametrization of lepton mixing matrix in terms of deviation parameters has also been discussed by King [88]. There also exists some interest in

parametrizing the lepton mixing matrix in terms of Wolfenstein parameter λ [109–111], where λ accounts for the deviations of mixing angles from their values predicted by special mixing schemes.

3.3 An implication of the model : charged lepton mixing matrix

Deviations from BM or TBM mixing can be accounted in terms of charged lepton corrections [89–98]. In the basis where both charged lepton mass matrix (m_l) and left handed Majorana mass matrix (m_ν) are non diagonal, lepton mixing matrix is given by the product of two mixing matrices as

$$U_{PMNS} = U_{lL}^{\dagger} U_\nu, \tag{3.11}$$

where, U_{lL} diagonalizes the charged lepton mass matrix m_l and U_ν diagonalize the neutrino mass m_ν. In the basis where charged lepton mass matrix is itself diagonal, PMNS matrix is directly given by U_ν, U_{lL} being identity matrix. The general idea of charged lepton correction is to work in the basis where both m_l and m_ν are non diagonal and then considering U_ν to be a special mixing matrix like BM or TBM a small perturbation to it is accounted from U_{lL} leading to the desired PMNS matrix. Following this set up charged lepton corrections to special mixing patterns like BM, TBM, Hexagonal mixing etc. are done. For example charged lepton corrections to BM mixing are found in Refs. [112–114] and those to TBM mixing are discussed in Refs. [113–115]. With the same idea, in our work, we first find out U_{lL} which can deviate BM neutrino mixing matrix and yield the lepton mixing matrix in eq. (3.6). In that case U_ν in eq. (3.11) is given by U_{BM} and corresponding U_{lL} is then given by

$$U_{lL}^{bm} = \begin{pmatrix} a & -\frac{1}{\sqrt{2}}(b+z_1) & \frac{1}{\sqrt{2}}(c-z_2) \\ \frac{1}{\sqrt{2}}(d+z_3) & \frac{1}{2}(e+z_4) & \frac{1}{2}(f-z_5) \\ -\frac{1}{\sqrt{2}}(d-z_3) & \frac{1}{2}(e-z_4) & \frac{1}{2}(f+z_5) \end{pmatrix}, \tag{3.12}$$

where,

$$\left.\begin{aligned} a &= \cos\delta\theta_{12}^{bm}\tilde{r}, \\ b &= \sin\delta\theta_{12}^{bm}\tilde{q}, \\ c &= \sin\delta\theta_{12}^{bm}q, \\ d &= \sin\delta\theta_{12}^{bm}\tilde{r}, \\ e &= q\tilde{r}, \\ f &= \tilde{q}\tilde{r}, \\ z_1 &= \cos\delta\theta_{12}^{bm}qre^{-i\delta}, \\ z_2 &= \cos\delta\theta_{12}^{bm}\tilde{q}re^{-i\delta}, \\ z_3 &= re^{i\delta}, \\ z_4 &= \cos\delta\theta_{12}^{bm}\tilde{q} - \sin\delta\theta_{12}^{bm}qre^{-i\delta}, \\ z_5 &= \cos\delta\theta_{12}^{bm}q - \sin\delta\theta_{12}^{bm}\tilde{q}re^{-i\delta}. \end{aligned}\right\} \tag{3.13}$$

The parameters a-f and z_1-z_5 are used to express the matrix in eq. (3.11) in convenient way.

For TBM mixing case U_ν in eq. (3.11) is given by U_{TBM} and corresponding U_{lL} is then given by

$$U_{lL}^{tb} = \begin{pmatrix} a' & -\frac{1}{\sqrt{2}}(b'+z_1') & \frac{1}{\sqrt{2}}(c'-z_2') \\ \frac{1}{\sqrt{2}}(d'+z_3') & \frac{1}{2}(e'+z_4') & \frac{1}{2}(f'-z_5') \\ -\frac{1}{\sqrt{2}}(d'-z_3') & \frac{1}{2}(e'-z_4') & \frac{1}{2}(f'+z_5') \end{pmatrix}, \tag{3.14}$$

where the parameters a'-f' and z_1'-z_5' are given by eq. (3.13) with the substitutions of $\delta\theta_{12}^{bm}$, q, $\tilde{q}$, r and $\tilde{r}$ by $\delta\theta_{12}^{tb}$, q', $\tilde{q}'$, r' and $\tilde{r}'$ respectively.

We note that both charged lepton mixing matrices U_{lL}^{bm} and U_{lL}^{tb} have similar structure due to $\mu-\tau$ symmetry of BM and TBM mixing matrices. We estimate the numerical values (in

modulus) of the elements of these mixing matrices for best fit values of deviation parameters and are presented in eqs. (3.15) and (3.16).

$$U_{lL}^{bm} = \begin{pmatrix} 0.972512 & 0.183349 & 0.143535 \\ 0.185651 & 0.980189 & 0.062209 \\ 0.140544 & 0.074912 & 0.980319 \end{pmatrix}. \tag{3.15}$$

$$U_{lL}^{tb} = \begin{pmatrix} 0.988657 & 0.114991 & 0.096260 \\ 0.108234 & 0.991394 & 0.072972 \\ 0.103806 & 0.062329 & 0.992184 \end{pmatrix}. \tag{3.16}$$

Naturally, there exists naive interest in searching connection between quark sector and lepton sector. Grand unified theories (GUTs) generally provide the framework for quark-lepton unification. Quark-lepton-complementarity (QLC), which signifies interesting phenomenological relations between the lepton and quark mixing angles supports the idea of grand unification. Derivation of QLC relations assumes the deviation of lepton mixing from exact BM pattern to be described by quark mixing matrix. In GUT based models [80, 115, 101–104] charged lepton corrections to special neutrino mixing schemes are considered as CKM like. From such points of view we make comparison of the charged lepton mixing matrices in eqs. (3.15) and (3.16) with the CKM matrix. For convenience, we present the best fit values (in modulus) of the elements of CKM matrix in eq. (3.17) [116].

$$V_{CKM} = \begin{pmatrix} 0.97428 & 0.2253 & 0.00347 \\ 0.2252 & 0.97345 & 0.0410 \\ 0.00862 & 0.0403 & 0.999152 \end{pmatrix}. \tag{3.17}$$

Wee see that both the mixing matrices are close to CKM matrix. Like CKM matrix the diagonal elements in these mixing matrices are close to unity and non diagonal elements exhibit an approximate symmetric nature. One significant point, we note, is that the corner

elements, namely $(U_{lL})_{13}$ and $(U_{lL})_{31}$ in both the mixing matrices are relatively larger compared to those of V_{CKM} matrix.

3.4 Summary and discussion

BM and TBM are two special neutrino mixing schemes. To accommodate non zero θ_{13} and deviations of solar mixing and atmospheric mixing from maximality these special mixing schemes should be modified. We have three parameters, viz. $\delta\theta_{12}^{bm/tb}$, $\delta\theta_{23}^{bm/tb}$ and $\delta\theta_{13}^{bm/tb}$, which account the deviations of lepton mixing angles from their BM or TBM values. Numerical values of these deviation parameters can be obtained from global 3ν oscillation data. We then parametrize PMNS matrix in terms of these parameters. Such parametrization of lepton mixing matrix may help authors in phenomenological works which incorporate deviation of special mixing schemes. We implicate our parametrization set up in predicting possible structure of charged lepton mixing matrices which can generate the desired lepton mixing matrix from BM or TBM mixing matrices. We have found that charged lepton mixing matrices U_{lL}'s in both cases (BM and TBM) exhibit similar structures. Numerical analysis shows that these mixing matrices (U_{lL}^{bm} and U_{lL}^{tbm}), necessary to deviate BM mixing and TBM mixing in obtaining mixing parameters consistent with global data, are close to the CKM matrix of quark sector. This result is in agreement with the assumption, generally made in GUT based model, that charged lepton correction to neutrino mixing can be considered as CKM like.

In this Chapter, our primary focus is on how to deviate the BM and TBM mixing patterns, using the contributions from the charged lepton sector, so that their predictions are consistent with the present oscillation data. We do not use RG method here, as we confined ourselves only at the EW scale. However, in the next chapter (Chapter 4) we will be working in a model independent way and try to generate the same EW scale neutrino parameter values, using the RG method in the top down approach, without considering any special mixing

scheme or any possible contributions coming from the charged lepton sector (since there is no experimental evidence/hint for mixing among the charged leptons).

Chapter 4

Radiative stability of neutrino parameters and self-complementarity relation with varying SUSY breaking scale

4.1 Introduction

The physics of neutrino is going through a revolutionary period. From various recent experiments, a small but nonzero value of the reactor angle, θ_{13} is confirmed[1, 117]. In addition to this, the Dirac CP phase, δ is also observed [118, 119]. Recent experiments on neutrino oscillation, $0\nu\beta\beta$, and the cosmological observations have revealed precise and important results on the observational parameters like the three mixing angles (θ_{13}, θ_{12}, θ_{23}), two mass-squared differences (Δm^2_{21},Δm^2_{31}) and possible upper bound on the sum of neutrino masses (Σm_i) etc. [120–122]. But still we are unable to understand the absolute value of neutrino masses, nature of neutrino mass hierarchy, or its type: Dirac/Majorana etc. The

realization that neutrinos are massive in contrast to its old popular assumption that it is massless (according to SM) is one of the strong signatures that the SM of particle physics has to be extended beyond its present horizon.

Most of the current studies on physics beyond the SM (BSM) relies on the possible existence of supersymmetry (SUSY). But there are other models of BSM physics which does not incorporate the idea of SUSY [123, 124]. It is hypothesized that SUSY existed at the early stage of big bang. But with the expansion of our Universe SUSY gets broken and reduced to our present day SM. At what scale that breaking occurs is still an unknown but an important parameter. The general idea is that there are two possible energy scales for the SUSY breaking (m_s): low and high. The low m_s scale [125, 126] is expected to be about a few TeV or so as suggested by the grand unified theory (GUT), whereas the high SUSY breaking scale is expected to be somewhere around 10^{12} GeV [127].

One significant finding from the recent LHC experiment which sounds little disappointing towards the possibility of SUSY is that the experiment which was operated at an energy scale of 13 TeV, has not provided any evidence of the existence of SUSY particles so far [128, 129]. In SUSY inspired neutrino physics it is predicted that SUSY plays an important role over the neutrino masses and other observational parameters [130–132]. The gauge coupling and Yukawa coupling constants suffer different radiative contributions from the MSSM and SM sectors. Similar to this, we expect that the neutrino observational parameters are also subjected to such kind of effects.

One of the reasons why the variation in m_s is expected to bring changes to various observational parameters is owing to the changes in the effective range of both MSSM and SM. When we increase the m_s scale, the effective range of SM increases, whereas that for MSSM decreases and vice versa. It will change the amount of radiative correction that each parameter receives from the SM and MSSM, respectively. In Chapter 2, we show the variation of the unification point of the gauge couplings with varying m_s scale. Such behavior

is likely to be seen for the neutrino oscillation parameters too. In this regard, it is important to study the possible effects of varying m_s on the radiative evolution of the neutrinos and hence, to determine (or narrow down) the possible range of m_s scale.

The possible reason behind the suppression of SUSY motivated effects at the LHC experiments may be due to the low luminosity of the beam. By the end of 2012, LHC's integrated luminosity, running at a centre-of-mass energy $\sqrt{s} = 8$ TeV, is already over 20 fb^{-1} [4]. The present integrated luminosity of the LHC for $\sqrt{s} = 13$ TeV is 35.9 fb^{-1} for CMS [133] and 36.1 fb^{-1} for ATLAS [134]. Some predicted the required integrated luminosity for observing SUSY related events to be 3000 fb^{-1} [135, 136], which is approximately 85 times greater than the present luminosity. Nevertheless, this still gives us a hope for the possible existence of $m_s < 13$ TeV. If a seesaw mechanism (SSM) is the only cause behind the generation of small neutrino masses, then it appears that the right handed neutrino mass scale must lie somewhere within the range of $(10^{10} - 10^{16})$ GeV [137, 138]. In our analysis, we shall vary the seesaw scale (SS) scale starting from 10^{10}-10^{15} GeV.

One sees that the numerical range of three mixing angles within 1σ[1] appears as in the following:

$$\theta_{13} = 8.44^{0+0.16}_{-0.17}, \theta_{12} = 34.5^{0+1.1}_{1.0} \text{ and } \theta_{23} = 41.0^{0+1.1}_{-1.1}. \tag{4.1}$$

We see that there may lie a self complementarity (SC) among these parameters in terms of the following relation

$$\theta_{23} = q \times (\theta_{13} + \theta_{12}), \tag{4.2}$$

where the parameter, q, is either unity or $\mathcal{O}(1)$. The self-complementarity relation (SC) is an important phenomenological relation [139, 140] similar to the quark-lepton complementarity relations [106, 141, 142]. The possible existence of such relations among

the parameters are expected to be the signatures of a certain flavor symmetry working in the background. The present analysis attempts not to deal with the possible origin of such a kind of a SC relation, rather it insists on the existence of such a relation even at higher energy scale. Our work starts with an assumption that this SC relation holds good at the SS scale. Through our analysis, we will show that this relation remains invariant against the radiative evolution for varying the m_s and SS scale. We emphasize that similar to the works in the literature which focus only on the renormalization group invariant parameters [143–147], the SC relation can also serve as an RGE invariant relation.

The present investigation is a continuation of Chapter 2, where we studied the radiative evolution of the three gauge, third generation Yukawa and quartic Higgs couplings following a bottom-up approach, with varying SUSY breaking scale m_s. It was observed that the unification scales for both the gauge couplings and Yukawa couplings vary but in the opposite trend and tend to attain a fixed value with increasing m_s. There, we vary m_s starting from 500 GeV to 7 TeV. However, in the present work, we follow the top down approach starting from the seesaw scale (SS) up to the electroweak scale. We fix, $\tan\beta = 58.6$, which is relevant in the context of our previous work [148].

4.2 RGEs for neutrino parameters

Renormalization group approach is a tool for studying physics at a different energy scale, which are otherwise impossible to reach with the current technology, and then to compare it with the available low energy data. Radiative analysis of neutrino parameters requires the RGEs of gauge couplings, Yukawa couplings, and the quartic Higgs couplings. The radiative properties of these couplings have been studied extensively in different models, and these three gauge couplings are expected to be unified at an energy scale approximately at 2×10^{16} GeV [149–154]. The RGEs for the gauge couplings, Yukawa couplings, and quartic Higgs coupling are given in the Chapter 2. We use 2-loops RGEs for both the SM and MSSM.

The RGE analysis of the neutrino parameters can be done in two possible ways viz: i) by a run and diagonalize method: where, the whole neutrino mass matrix is allowed to evolve using their appropriate RGEs, and then the corresponding neutrino parameters can be achieved at the desirable energy scale (μ) by diagonalizing the neutrino mass matrix, ii) by using the RGEs of the corresponding neutrino parameters separately as defined by the eqs. (4.3) to (4.13). In both the cases, the RGEs of all the neutrino parameters and the RGEs of various coupling parameters are required to be solved simultaneously. In this work, we adopt the later stand.

The input parameters for the gauge, Yukawa, and quartic Higgs couplings at the SS, given in Table 4.1, are taken form Chapter 2. In the present analysis, we choose our starting energy scale to be the SS scale. We consider a different possible SS scale starting from 10^{10} GeV to 10^{15} GeV, and we run down all the observational neutrino parameters from SS scale up to the electroweak scale ($m_Z = 91.18$ GeV) via m_s, which also varies in our analysis.

The radiative properties of neutrinos has been studied extensively in various models [154–163]. The standard two loops RGEs for the neutrino masses, mixings, and CP phases are shown below. For the three neutrino mixing angles [154] ,the RGEs are,

$$\dot{\theta}_{12} = -\frac{Cy_\tau^2}{32\pi^2}\sin 2\theta_{12}s_{23}^2\frac{|m_1e^{i\psi_1}+m_2e^{i\psi_2}|^2}{\Delta m_{21}^2}, \tag{4.3}$$

$$\dot{\theta}_{13} = -\frac{Cy_\tau^2}{32\pi^2}\sin 2\theta_{23}\frac{m_3}{\Delta m_{31}^2(1+\xi)} \tag{4.4}$$

$$\times\left[m_1\cos(\psi_1-\delta)-(1+\xi)m_2\cos(\psi_2-\delta)-\xi m_3\cos\delta\right], \tag{4.5}$$

$$\dot{\theta}_{23} = -\frac{Cy_\tau^2}{32\pi^2}\sin 2\theta_{23}\frac{1}{\Delta m_{31}^2}\left[c_{12}^2|m_2e^{i\psi_2}+m_3|^2+s_{12}^2\frac{|m_1e^{1\psi_2}+m_3|^2}{(1+\xi)}\right],$$

where, $\Delta m_{21}^2 = m_2^2 - m_1^2$ and $\Delta m_{31}^2 = m_3^2 - m_1^2$, $\xi = \frac{\Delta m_{21}^2}{\Delta m_{31}^2}$.

The RGEs for the three phases are

(for Dirac phase)

$$\dot{\delta} = \frac{Cy_\tau^2}{32\pi^2}\frac{\delta^{(-1)}}{\theta_{13}} + \frac{Cy_\tau^2}{8\pi^2}\delta^0, \tag{4.6}$$

where

$$\begin{aligned}
\delta^{(-1)} &= \sin 2\theta_{12}\sin 2\theta_{23}\frac{m_3}{\Delta m_{31}^2(1+\xi)}\times \\
&\quad [m_1\sin(\psi_1-\delta) - (1+\xi)m_2\sin(\psi_2-\delta) + \xi m_3\sin\delta], \qquad (4.7)\\
\delta^{(0)} &= \frac{m_1 m_2 s_{23}^2\sin(\psi_1-\psi_2)}{\Delta m_{21}^2} \\
&\quad + m_3 s_{12}^2\left[\frac{m_1\cos 2\theta_{23}\sin\psi_1}{\Delta m_{31}^2(1+\xi)} + \frac{m_2 c_{23}^2\sin(2\delta-\psi_2)}{\Delta m_{31}^2}\right] \qquad (4.8)\\
&\quad + m_3 c_{12}^2\left[\frac{m_1 c_{23}^2\sin(2\delta-\psi_1)}{\Delta m_{31}^2(1+\xi)} + \frac{m_2\cos 2\theta_{23}^2\sin(\psi_2)}{\Delta m_{31}^2}\right],
\end{aligned}$$

(for Majorana phases)

$$\begin{aligned}
\dot{\psi}_1 &= \frac{Cy_\tau^2}{4\pi^2}\left\{m_3\cos 2\theta_{23}\frac{m_1 s_{12}^2\sin\psi_1 + (1+\xi)m_2 c_{12}^2\sin\psi_2}{\Delta m_{31}^2(1+\xi)}\right. \qquad (4.9)\\
&\quad \left. + \frac{m_1 m_2 c_{12}^2 s_{23}^2\sin(\psi_1-\psi_2)}{\Delta m_{21}^2}\right\}, \\
\dot{\psi}_2 &= \frac{Cy_\tau^2}{4\pi^2}\left\{m_3\cos 2\theta_{23}\frac{m_1 s_{12}^2\sin\psi_1 + (1+\xi)m_2 c_{12}^2\sin\psi_2}{\Delta m_{31}^2(1+\xi)}\right. \qquad (4.10)\\
&\quad \left. + \frac{m_1 m_2 s_{12}^2 s_{23}^2\sin(\psi_1-\psi_2)}{\Delta m_{21}^2}\right\}.
\end{aligned}$$

The RGEs for the neutrino mass eigenvalues are

$$\begin{aligned}
\dot{m}_1 &= \frac{1}{16\pi^2}\left[\alpha + Cy_\tau^2\left(2s_{12}^2 s_{23}^2 + F_1\right)\right]m_1, \qquad (4.11)\\
\dot{m}_2 &= \frac{1}{16\pi^2}\left[\alpha + Cy_\tau^2\left(2c_{12}^2 s_{23}^2 + F_2\right)\right]m_2, \qquad (4.12)\\
\dot{m}_3 &= \frac{1}{16\pi^2}\left[\alpha + 2Cy_\tau^2 c_{13}^2 c_{23}^2\right]m_3, \qquad (4.13)
\end{aligned}$$

Gauge couplings	Yukawa couplings	Quartic-Higgs couplings
g_1 - 0.6032	y_t - 0.76809	λ - 0.58
g_2 - 0.6826	y_b - 0.80488	-
g_3 - 0.7557	y_τ - 0.91448	-

Table 4.1 Input values for gauge, Yukawa and quartic Higgs couplings are extracted from Chapter 2.

where

$$\left.\begin{aligned} F_1 &= -s_{13}\sin 2\theta_{12}\sin 2\theta_{23}\cos\delta + 2s_{13}^2 c_{12}^2 c_{23}^2, \\ F_2 &= s_{13}\sin 2\theta_{12}\sin 2\theta_{23}\cos\delta + 2s_{13}^2 s_{12}^2 s_{23}^2, \end{aligned}\right\} \tag{4.14}$$

$$\left.\begin{aligned} \alpha &= -\tfrac{6}{5}g_1^2 - 6g_2^2 + 6y_t^2 \\ C &= 1 \end{aligned}\right\} \text{ for MSSM} \tag{4.15}$$

$$\left.\begin{aligned} \alpha &= -3g_2^2 + 2y_\tau^2 + 6y_t^2 + 6y_b^2 \\ C &= \tfrac{-3}{2} \end{aligned}\right\} \text{ for SM} \tag{4.16}$$

With all the necessary mathematical frameworks in hand, we can now study the radiative nature of neutrino masses, mixings, and CP phases using the top-down running approach together with the MSSM unification conditions.

In the first step, all the parameters are allowed to run down from the SS to the SUSY breaking scale using their respective MSSM RGEs and from the SUSY breaking scale further down to the EW scale using their SM RGEs. At the transition point from MSSM to SM, we apply appropriate matching conditions as shown below,

$$g_i\left(M_{SUSY}^{-}\right) = g_i\left(M_{SUSY}^{+}\right), \tag{4.17}$$

$$\lambda_t\left(M_{SUSY}^{-}\right) = \lambda_t\left(M_{SUSY}^{+}\right)\sin\beta, \tag{4.18}$$

$$\lambda_b\left(M_{SUSY}^{-}\right) = \lambda_b\left(M_{SUSY}^{+}\right)\cos\beta, \tag{4.19}$$

$$\lambda_\tau\left(M_{SUSY}^{-}\right) = \lambda_\tau\left(M_{SUSY}^{+}\right)\cos\beta, \tag{4.20}$$

where $\tan\beta = v_u/v_d$ such that $v_u = v\sin\beta$, $v_d = v\cos\beta$ and $v = 246$ GeV is the vacuum expectation value (VEV) of the Higgs field. In our analysis, we choose a single SUSY spectrum for simplicity and study the radiative stability of the neutrino parameters at the weak scale for varying m_s.

4.3 Radiative effects on the neutrino oscillation parameters and the CP phases

The radiative effects on the neutrino parameters for a strict normal or inverted hierarchy is small. If the neutrinos masses have a quasidegenerate spectrum, then the RG evolution between the lowest SS and the EW energy scale can have sizable effects [164–167] on the neutrino oscillation parameters. The RG effects may even account for the difference between the mixings in the quark and the lepton sectors [168].

In MSSM, both the atmospheric (θ_{23}) and solar mixing angle (θ_{12}) increase with the decrease in energy as predicted by eq.(4.3) and eq.(4.4). Out of the three mixing angles, the solar mixing angle is prone to the largest RG effects because of the presence of a small Δm^2_{31} in the denominator, whereas θ_{13} is subjected to the smallest RG effect.

In the top-down approach, all the three mass eigenvalues behave in a similar fashion, and they all decrease with the decrease in energy scale. Because of the comparatively larger

value of α with respect to y_t, y_b, and y_τ, the RG running effect on the mass eigenvalues is less. But, due to the same factor α, there is appreciable running in the RGEs of the mass eigenvalues in the SM case. The running of the mass eigenvalues in the MSSM is defined by a common scaling factor, except for the case of a large $\tan\beta$ where it deviates considerably.

For nearly degenerate neutrino masses and a large $\tan\beta$, the radiative influence of CP phases over other parameters becomes important. All of the phases (both Majorana and Dirac) undergo radiative corrections. For different sets of the input phases, the RG effects on the neutrino oscillation parameters may differ. In the context, when the two Majorana phases are equal[154], the evolutions of the parameters are highly suppressed since the leading terms in the RGEs of the phases become zero [See eq.(4.10) and eq. (4.11)].

4.4 Numerical analysis and the Results

The RGEs are differential equations and demand the input values for the parameters to be sought out, at the very outset. In our case, the starting point is the SS scale, and finally, we end up at the EW scale. From the SS scale upto the m_s scale, the RGEs follow a certain pattern [eq. (4.15)] and reverts to another form in the region from m_s upto the EW scale [eq. (4.16)]. Both the SS scale and m_s are unknown to us. Our present analysis although tries to visualize the effect on the neutrino observational parameters for varying m_s, yet gives emphasis on the choice of the SS scale also. We fix the m_s values in between 1 TeV to 13 TeV. In addition, the SS scale is also assigned certain fixed values between 10^{10} GeV to 10^{15} GeV.

The parameters, g_1, g_2, g_3, y_t, y_b, y_τ, and λ are specified as per Table 4.1. In the present analysis, we have got nine free parameters: m_1, m_2, m_3, θ_{13}, θ_{23}, θ_{12}, δ, ψ_1, and ψ_2. As stated earlier, the present study presumes the existence of the SC relation [see eq. (4.2)] at the SS scale. By virtue of this relation, we assign initial input values only to θ_{13} and θ_{12}. Further simplifications are made regarding the initial choice of ψ_1 and ψ_2, which are constrained

to be equal,$(\psi_1)_0 = (\psi_2)_0$, for all subsequent calculations [the notations $(...)_0$ represent the initial input value of the parameter within the bracket]. In that way, we assign input values only to six neutrino observational parameters. To simplify, we summarize our strategy in the following way,

(Step 1) We vary the initial values of the six neutrino parameters at a fixed m_s scale. To ensure that the initial choice of the parameters beget the numerical values at the EW scale which are consistent within a 3σ range, we follow a simple mechanism. To illustrate, let us fix m_s at 5 TeV, SS scale at 10^{14} GeV, and assume, $(m_2)_0 = 2.34 \times 10^{-2}$ eV and $(\delta)_0 = 90^\circ$. The remaining parameters, $(\theta_{13})_0$, $(\theta_{23})_0$, $(m_1)_0$, $(m_3)_0$, and $(\psi_1)_0$ are assigned with certain numerical values, so that the final output at the EW scale lies within 3σ. Next, we vary the parameter, $(\psi_1)_0$ and see how the remaining parameters, like, $(\theta_{ij})_0$, and $(m_i)_0$ are to be adjusted in order to keep the outcome within the 3σ range. For details, see Table 4.2, Fig. 4.1a, and Fig. 4.1b. We see that, except $(m_3)_0$ which varies a little, the other input parameters are almost stable against changing $(\psi_1)_0$. The motivation behind performing this step is to ensure that the final numerical values in concern with the neutrino observational parameters, are not too sensitive to the initial input of the Majorana phase. This observation helps us to choose an arbitrary value for $(\psi_1)_0$. We take $(\psi_1)_0 = 45^\circ$ for all subsequent calculations.

4.4.1 For varying m_s and SS scale

(Step 2) The SUSY breaking scale m_s, is attributed to the following numerical values like, $1, 3, 5, ...13$ TeV, and in accordance with that, we categorize seven sets of input values as, $A1$, $A3$, $A5$...$A13$, respectively. For example, the set A_5 corresponds to the set of input $(\theta_{ij})_0$, $(m_i)_0$, $(\delta)_0$ and $(\psi_1)_0$, at $m_s = 5$ TeV. For all the above mentioned sets, we fix $(\delta)_0 = 90^\circ$. Similarly, we assign sets, $B1$, $B3$, $B5$...$B13$ with $(\delta)_0 = 270^\circ$. This is to be noted that both kinds of sets Aj and Bj are the input values of the neutrino

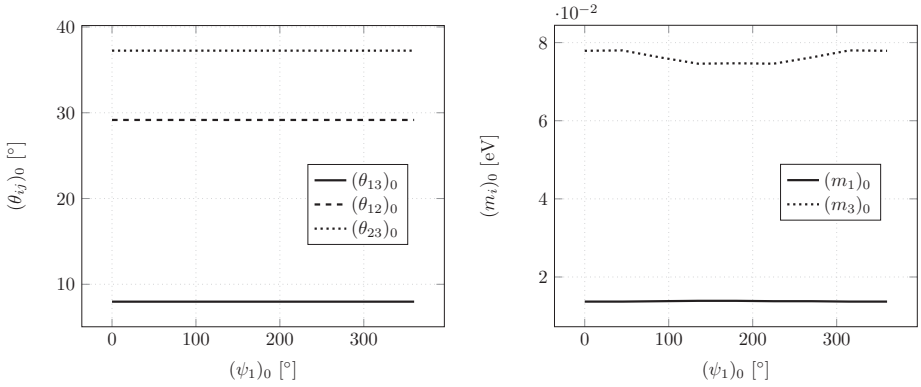

(a) (b)

Fig. 4.1 (a) The variation of the $(\theta_{ij})_0$ against $(\psi_i)_0$ is shown. (b)The stability of $(m_i)_0$ against $(\psi_i)_0$ is studied. In our calculations, we assume the Majorana parameters to be equal. The m_s and SS scale are fixed at 5 TeV and 10^{14} GeV respectively. The other initial input, $(\delta)_0 = 90^\circ$ and $(m_2)_0 = 2.34 \times 10^{-2}$ GeV. The purpose of this study is to achieve the numerical values of the parameters at EW scale within 1σ.

parameters, at the SS scale of 10^{14} GeV. There is another $\mathcal{O}(1)$ parameter, q which appears in eq. (4.2) is tuned between 0.95 to 0.97. For details, see Table 4.3.

(Step 3) In this step, keeping a certain input set, say $A5$ fixed, we vary the m_s scale between 1 TeV to 13 TeV, and check the stability of the neutrino observational parameters at the EW scale. The details are shown in the Tables 4.4- 4.11.

(Step 4) We repeat step 3, for different values of theee SS scale, such as 10^{10}, 10^{11}...10^{15} GeV.

We will now discuss the results of our analysis.

4.4.2 For varying m_s at fixed SS scale

We keep track of the numerical values of the neutrino observational parameters at the EW scale. From Tables 4.4-4.11, one sees that, except Δm^2_{21}, other parameters like θ_{13}, θ_{12}, θ_{23}, and Δm^2_{31} show stability at the face of the changing m_s. For all the three mixing angles, the fluctuations are consistent within 3σ bound [1].But for Δm^2_{31}, the fluctuations sometimes cross the 3σ bound. Although the input entries corresponding to different neutrino parameters

are almost the same for all the sets Aj and Bj, yet the solar mass squared difference at the EW scale is found quite sensitive towards both: the initial input as well as to the m_s scale. To illustrate, one can see that for the input data set, say $A5$, which results in $\Delta m^2_{21} = 7.57 \times 10^{-5}$ eV^2 and this is consistent within 1σ bound, for m_s being set at 5 TeV. If m_s is changed a little, say to 3 TeV and 7 TeV, we see that for the same input data set $A5$, the Δm^2_{21} becomes, 9.16×10^{-5} eV^2 and 6.67×10^{-5} eV^2 respectively. This output lies strictly outside the 3σ region. However, if we achieve an acceptable Δm^2_{21}, against a higher m_s scale, we can expect a little stability. To exemplify, if for $A11$, we achieve, $\Delta m^2_{21} = 7.54 \times 10^{-5}$ eV^2 (within 1σ bound), against $m_s = 11$ TeV, then changing the m_s to either 9 or 13 TeV, will not take this parameter outside 3σ. In addition, both solar and atmospheric mass squared difference decreases, with the increase in m_s scale. The CP violating phases also vary a little, if m_s were changed. With the increase of the latter, δ decreases, whereas the two Majorana phases increase [See Fig. 4.2].

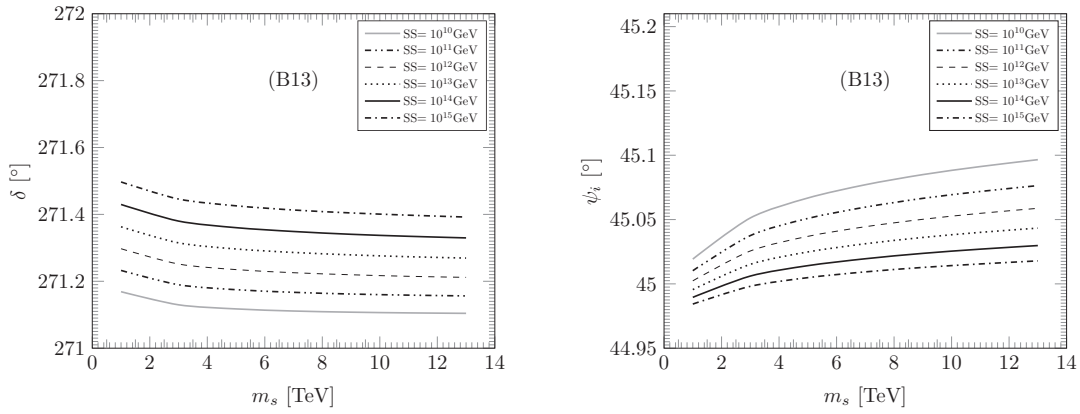

Fig. 4.2 The fluctuations of (a) the Dirac phase (δ) and (b) the Majorana phase (ψ_i) after RG evolution, at the EW scale, against changing m_s, and the SS scale are studied. m_s values are fixed at 1 Tev, 3 TeV, 5 Tev, 7 TeV, 9 Tev, 11 Tev, 13 TeV, and different SS scales are assumed at 10^{10} GeV, 10^{11} GeV, 10^{12} GeV, 10^{13} GeV, 10^{14} GeV, and 10^{15} GeV. Here, we consider only one input data set B13 as in Table 4.3.

The discussion concerned so far is true only for the SS scale: 10^{14} GeV. We try to see how a changing SS scale, along with m_s, can affect the physical parameters at the EW scale as per the step(4) mentioned above. We note down the following. To exemplify, let us choose the input data set $B5$, which is capable of producing, observable parameters at the EW scale consistent within 3σ, with m_s being fixed at 5 TeV, and the SS scale at 10^{14} GeV. With the SS scale fixed, first we vary m_s, and we get a certain plot, which shows how the numerical value of that observable parameter at the EW scale changes against m_s. We redo the same to get another plot, but at a different SS scale, for same input data set. We observe the ascent or descent of the plots against the different SS scale.

(a) Among the three mixing angles, θ_{13} at EW scale decreases if the SS scale is increased, whereas θ_{12} and θ_{23} increase. For a wide ranges of the m_s and SS scale, the output values stay within the 3σ bound. However, for different input data sets concerned, the exclusion of certain m_s values or SS scales are also possible, depending upon the 3σ bound of the concerned mixing angles. For example, consider the case of θ_{12} at the EW scale, against a fixed input data set $B5$. If we believe the SS scale to be 10^{10} GeV, then, from the plots, it is evident that the SUSY breaking scale should not be more than 7 TeV [See Fig. 4.3a]. For the other two mixing angles, (θ_{13}) and (θ_{23}), see Fig. 4.4 and Fig. 4.5 respectively.

(b) With all the conditions being the same as before, the δ increases if the SS scale is increased, whereas the reverse is true for the Majorana phases. [See Fig. 4.2a and Fig. 4.2b].

(c) We observe certain interesting results in concern with Δm^2_{21} and Δm^2_{31}. The mass squared differences are found highly sensitive to the initial data set, m_s, and the SS scale. The Δm^2_{31} remains more or less stable against m_s, but crosses 3σ bound if the SS scale is varied. On the contrary, the Δm^2_{21} fluctuates more with m_s but less with SS

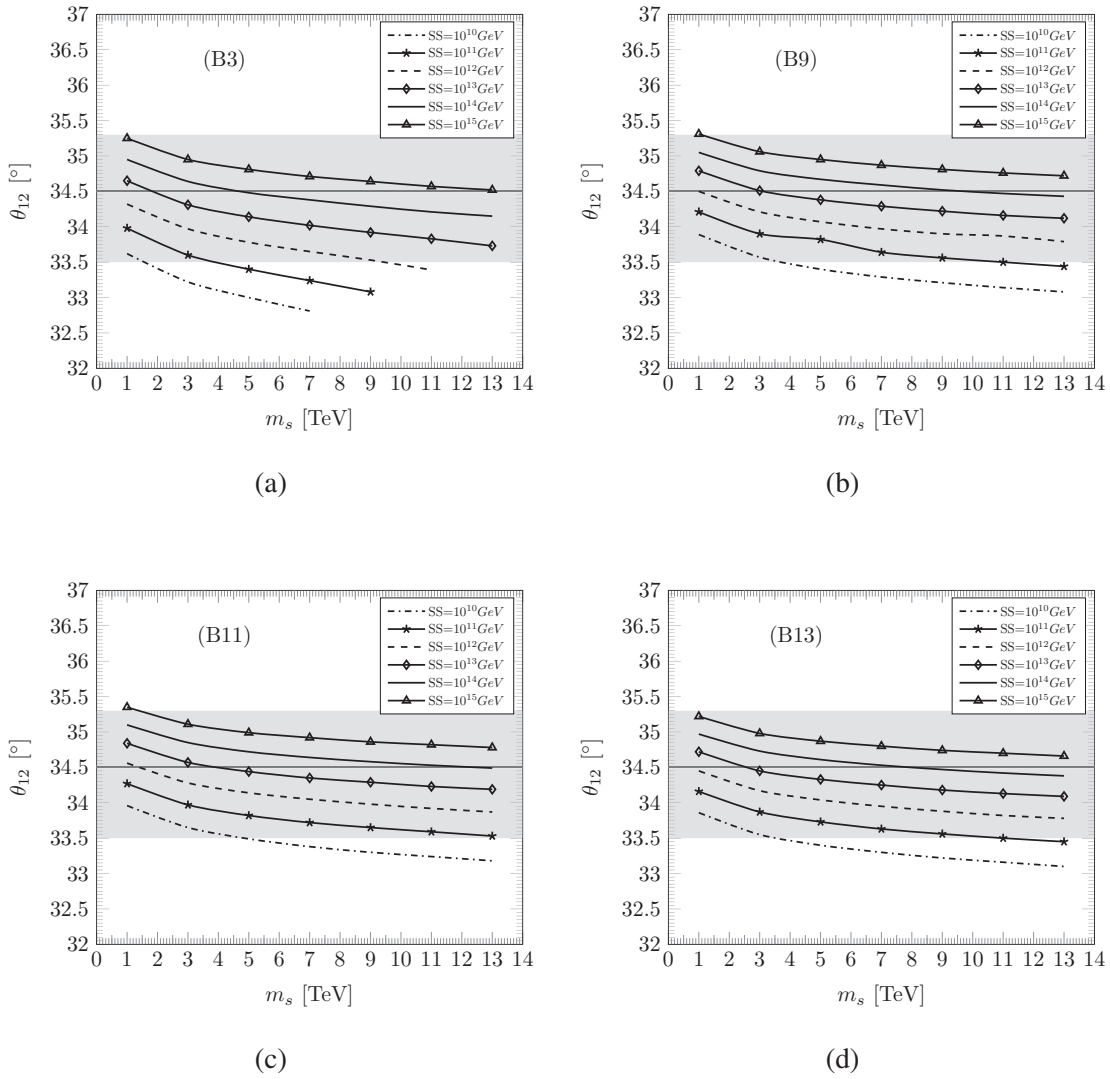

Fig. 4.3 The fluctuations of the numerical values of θ_{12}, at the EW scale is studied, against changing m_s , and SS scale. The shaded region (horizontal) represents the experimental 3σ range [1] and the horizontal bold line inside the shaded region indicates the best-fit value. The four figures (a), (b), (c), and (d) are for the different input data sets B3, B9, B11, and B13 respectively (as given in Table 4.3). The SS scales are fixed at 10^{10} GeV, 10^{13} GeV, 10^{14} GeV, and 10^{15} GeV.

scale. It is interesting to note that against a fixed input data set (say, B5), with respect to 3σ range of Δm^2_{21}, one can even find a bound over the m_s scale. This bound shifts to the right, i.e. towards a higher m_s region as we take the input numerals as per the initial data sets from $B1$ to $B13$ (see Fig. 4.6 and Fig. 4.7).

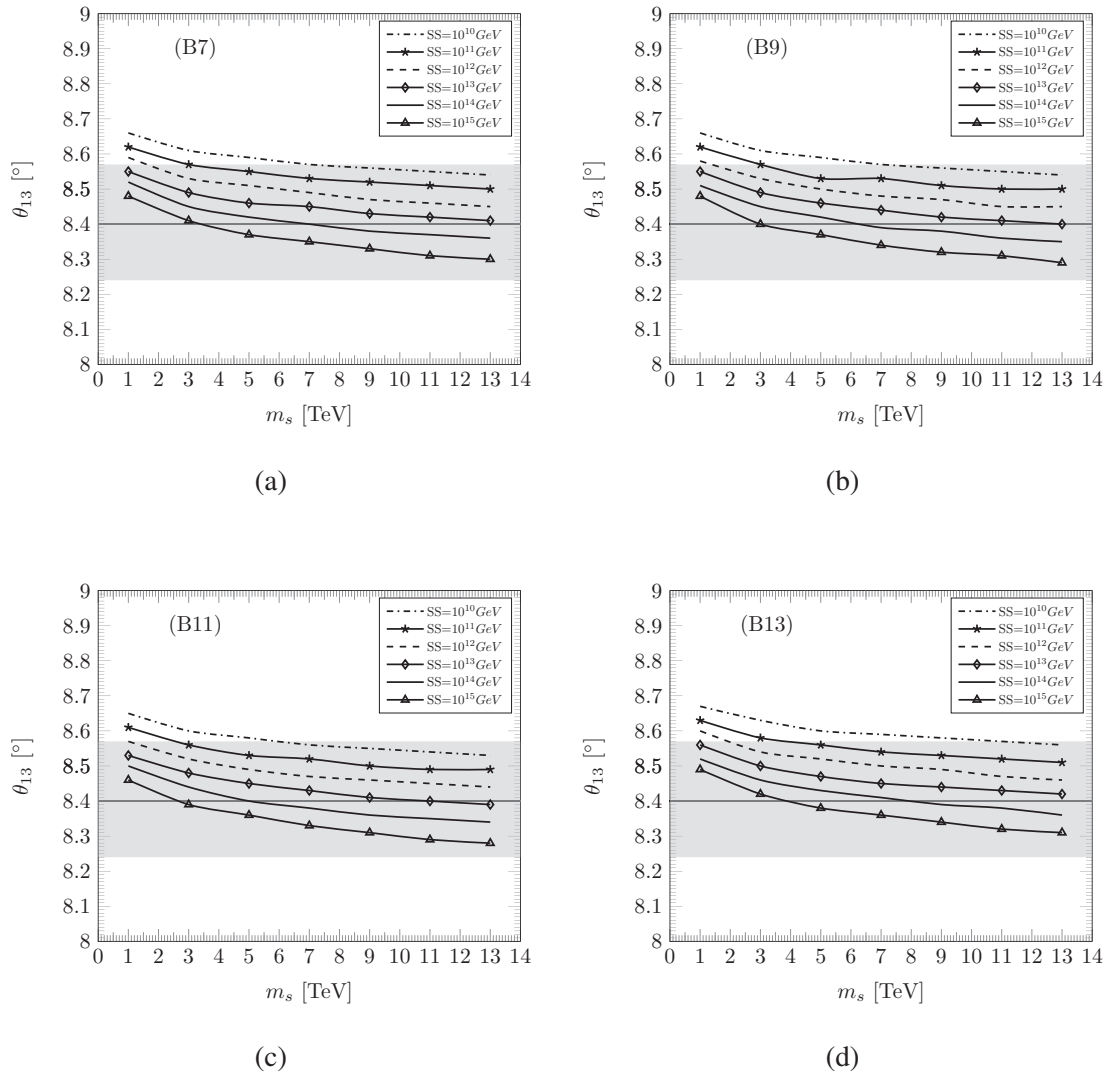

Fig. 4.4 The fluctuations of the numerical values of θ_{13}, at the EW scale is studied, against changing m_s , and SS scale. The shaded region (horizontal) represents the experimental 3σ range [1] and the horizontal bold line inside the shaded region indicates the best-fit value. The four figures (a), (b), (c), and (d) are for the different input data sets B3, B5, B7, B9, B11, and B13 respectively (as given in Table 4.3). The SS scales are fixed at 10^{12} GeV, 10^{13} GeV, 10^{14} GeV, and 10^{15} GeV.

4.4.3 The SC relation and the mass ratios

In addition to the physical observables, we try to see how the certain parameters/ relation evolve against the varying energy scale. Although the neutrino oscillation experiments hints

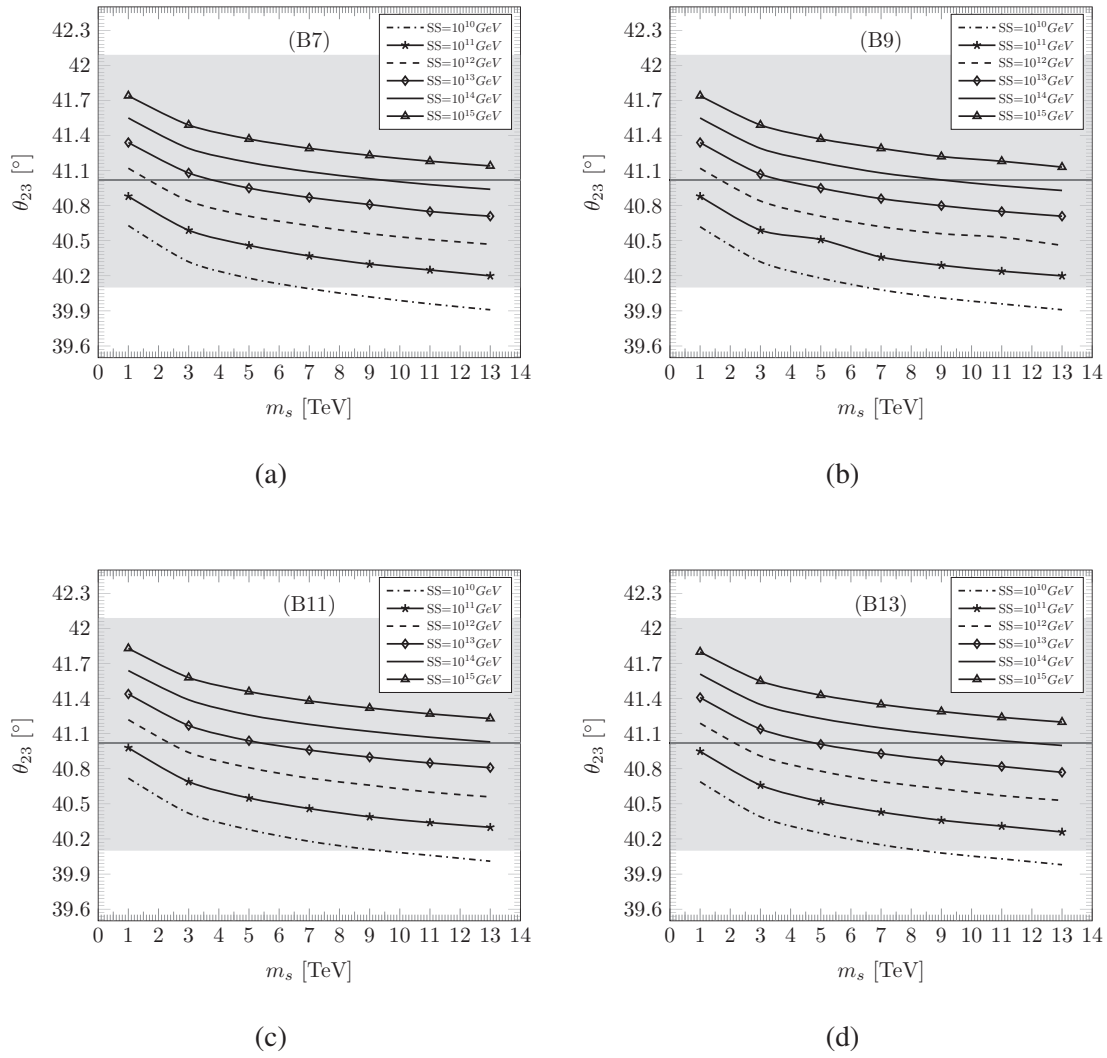

Fig. 4.5 The fluctuations of the numerical values of θ_{23}, at the EW scale is studied, against changing m_s , and SS scale. The shaded region (horizontal) represents the experimental 3σ range [1] and the horizontal bold line inside the shaded region indicates the best-fit value. The four figures (a), (b), (c), and (d) are for the different input data sets B3, B5, B7, B9, B11, and B13 respectively (as given in Table 4.3). The SS scales are fixed at 10^{12} GeV, 10^{13} GeV, 10^{14} GeV, and 10^{15} GeV.

not for individual neutrino masses, yet the study of individual parameters and how they evolve carry physical insight. This study is relevant from the model building point of view.

(a) As stated earlier, we have assumed that at the SS scale, the three mixing angles are connected via a complementarity relation [See eq. (4.2)]. We see that for a fixed m_s and a chosen SS scale, with all the input parameters fixed to a certain data set (say, B5), the

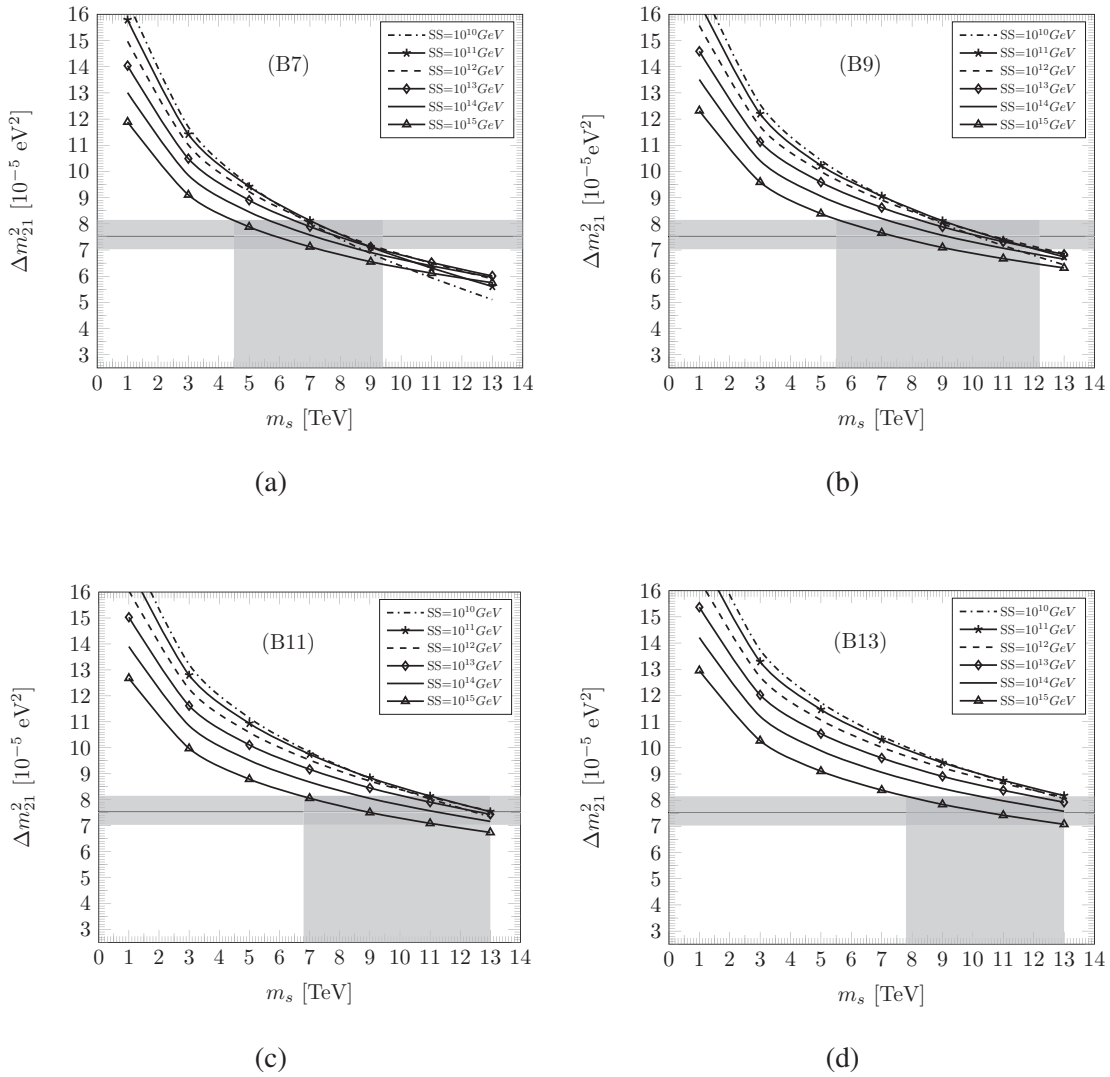

Fig. 4.6 The fluctuations of the numerical values of Δm^2_{21}, at the EW scale is studied, against changing m_s, and the SS scale. The shaded region (horizontal) represents the experimental 3σ range [1], and the horizontal bold line inside the shaded region indicates the best-fit value. The vertical shaded region corresponds to the allowed m_s region, for which the plots for different SS scale lie within the 3σ bound. The four figures (a), (b), (c), and (d) are for the different input data sets B3, B5, B7, B9, B11, and B13 respectively (as given in Table 4.3). The SS scales are fixed at 10^{12} GeV, 10^{13} GeV, 10^{14} GeV, and 10^{15} GeV.

angles evolve (except θ_{13} which is almost stable), but the SC relation connecting the mixing angles, remains almost invariant against the radiative evolution. This stability is achievable, even if we vary the SS scale or m_s. We have shown the radiative evolution of the angles along with the SC relation for both varying m_s (with a fixed SS scale) and

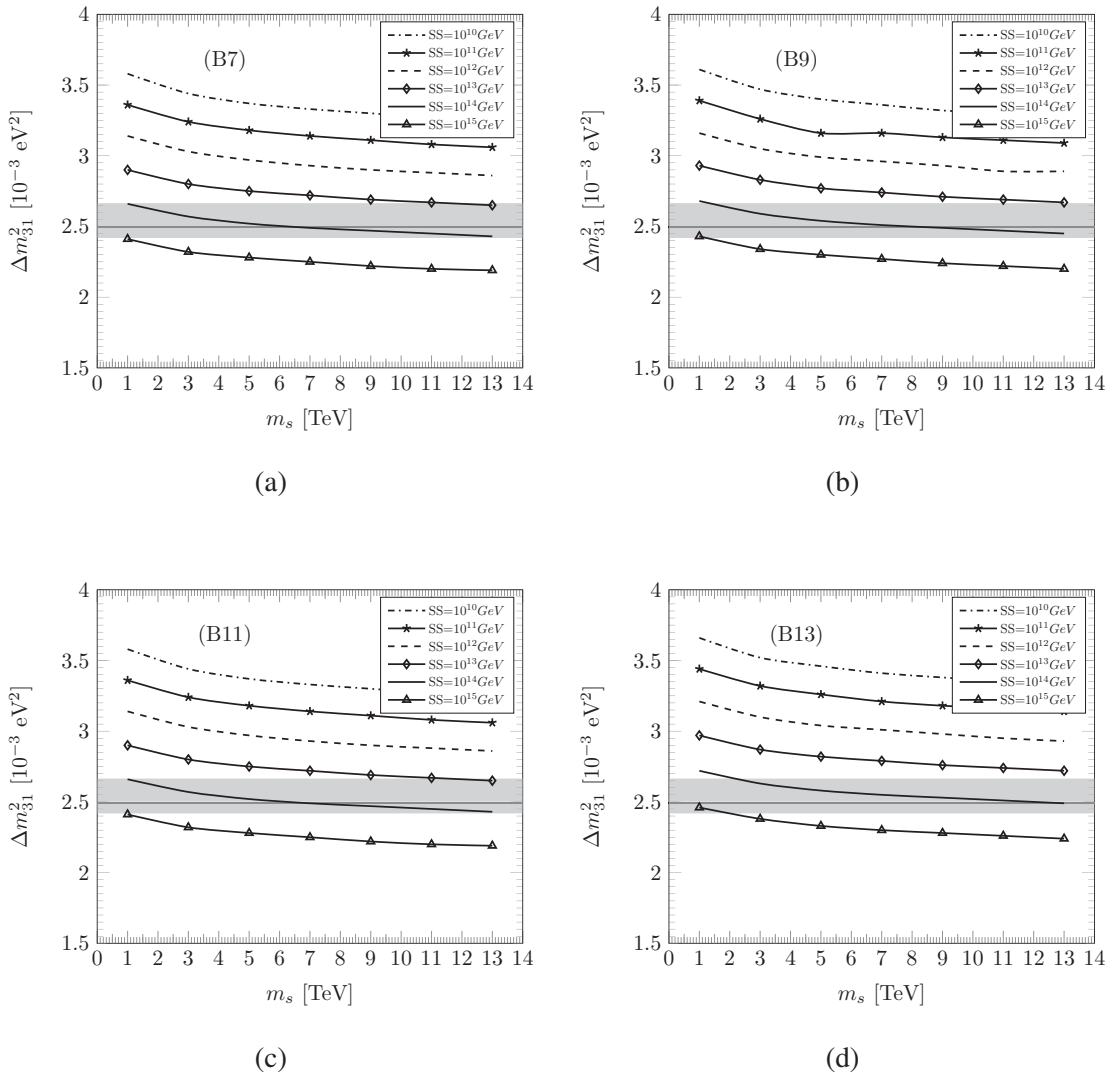

Fig. 4.7 The fluctuations of the numerical values of Δm^2_{31}, at the EW scale is studied, against changing m_s, and the SS scale. The shaded region (horizontal) represents the experimental 3σ range [1], and the horizontal bold line inside the shaded region indicates the best-fit value. The vertical shaded region corresponds to the allowed m_s region, for which the plots for different SS scale lie within the 3σ bound. The four figures (a), (b), (c), and (d) are for the different input data sets B3, B5, B7, B9, B11, and B13 respectively (as given in Table 4.3). The SS scales are fixed at 10^{12} GeV, 10^{13} GeV, 10^{14} GeV, and 10^{15} GeV.

varying SS scale (with a fixed m_s). For details, see Fig. 4.8-Fig. 4.9. The SC relation is a phenomenologically motivated relation like the QLC relation [169] that connects the quark and lepton sectors. A relation of this kind bears the signature of a certain hidden symmetry. As pointed out in our analysis, that which reflects the invariance

of the former against radiative evolution may turn out as fruitful information for the model builders.

(b) Like the mixing angles, we try to see how the mass parameters respond to radiative evolution. Instead of concentrating on individual neutrino masses, we focus on the three mass ratios as such: m_2/m_1, m_3/m_1, and m_3/m_2. This is inspired by the phenomenology of the quark sector. Where, we see that the mass ratio between the down and strange quarks is naturally related to the quark mixing angle (Cabibbo angle) which plays an important role in describing the mixing among the quarks [170, 171]. To exemplify, we fix the m_s at 5 TeV and the input data set at $B5$. Following this, we see how the three neutrino mass ratios vary against the changing SS scale. The details are shown in Fig. 4.10. One sees that the ratio m_3/m_1 or m_3/m_2 though remains invariant in the SUSY region, changes after crossing the m_s scale. But, interestingly, the ratio m_2/m_1 remains almost invariant and tries to maintain a constant numerical value as such: $m_2/m_1 \sim 2$. A summarized version of the different types of effect each neutrino parameters receive due to the variation of m_s and SS are given in Table 4.12.

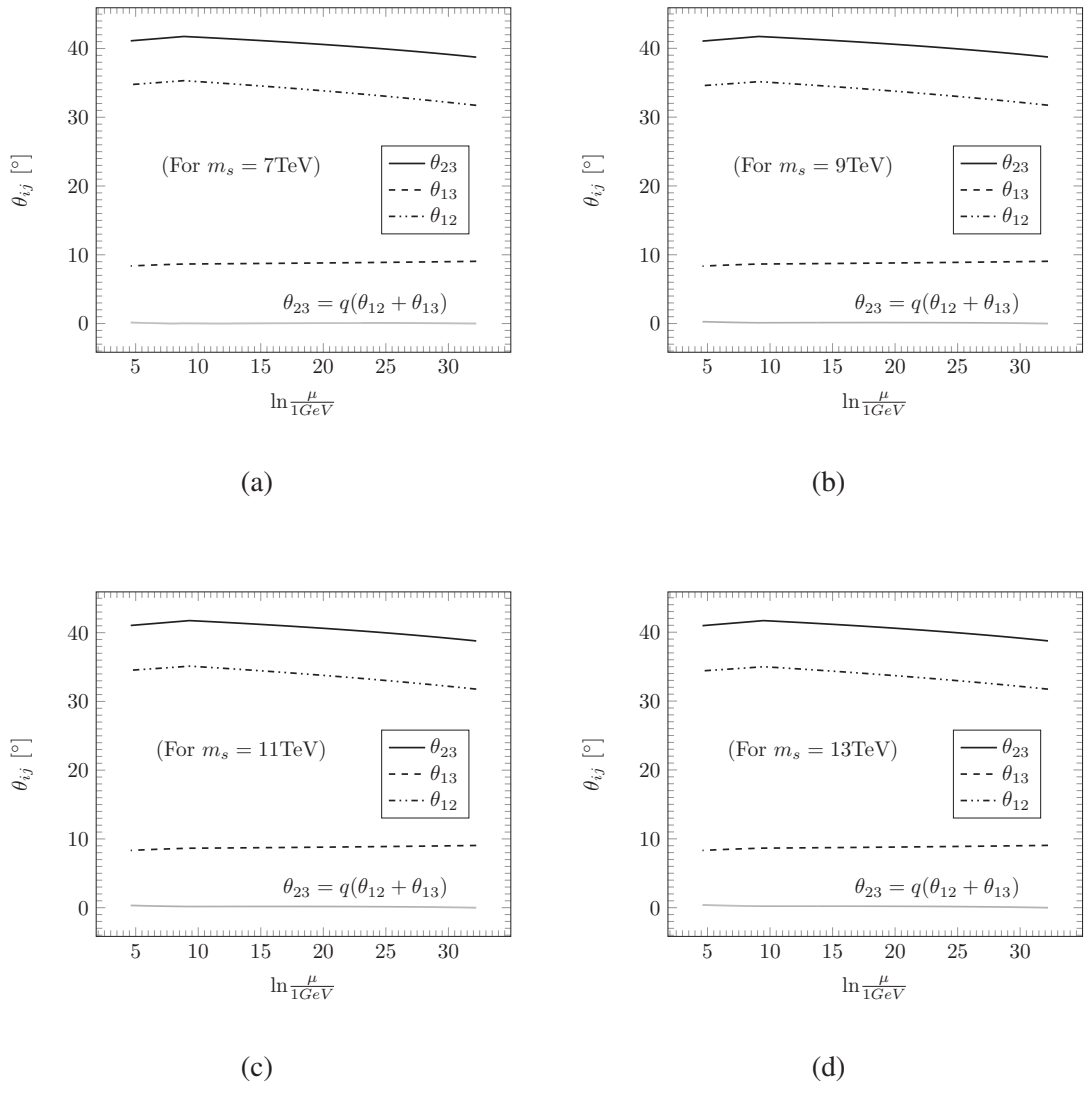

Fig. 4.8 Radiative evolution of the three neutrino mixing angles and its self-complementarity relation from the seesaw scale to the EW scale for different choices of m_s are studied. The four figures (a), (b), (c), and (d) are for the different input data sets B3, B5, B7, B9, B11, and B13 respectively (as given in Table 4.3). Here we consider only one SS scale (10^{14} GeV).

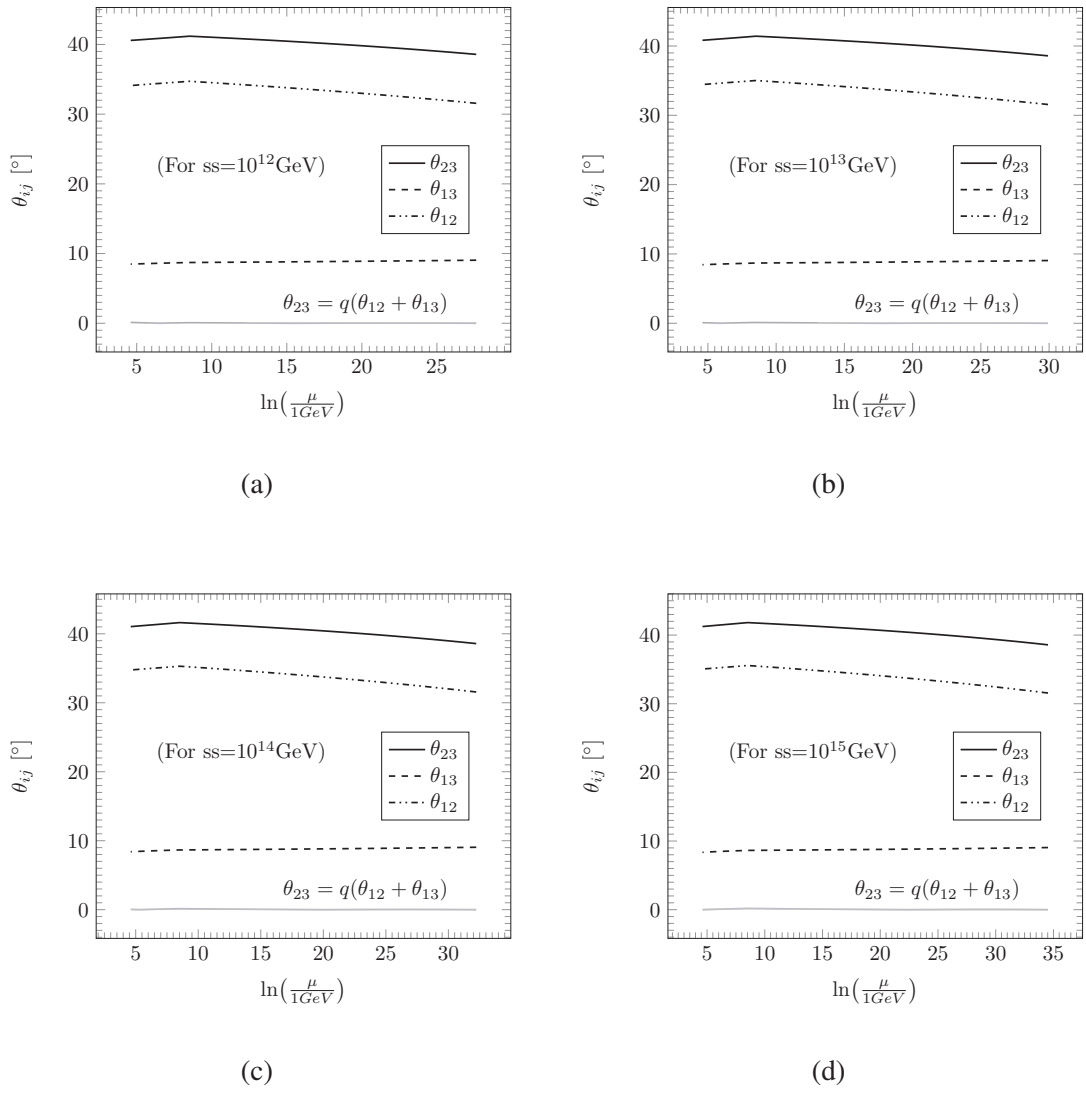

Fig. 4.9 Radiative evolution of the three neutrino mixing angles and its self-complementarity relation from the seesaw scale to the EW scale for a fixed data set B5, $m_s = 5$ TeV (as given in Table 4.3) are studied for different seesaw scales. The four figures (a), (b), (c), and (d) corresponds to the different choices of SS at 10^{12} GeV, 10^{13} GeV, 10^{14} GeV, and 10^{15} GeV respectively.

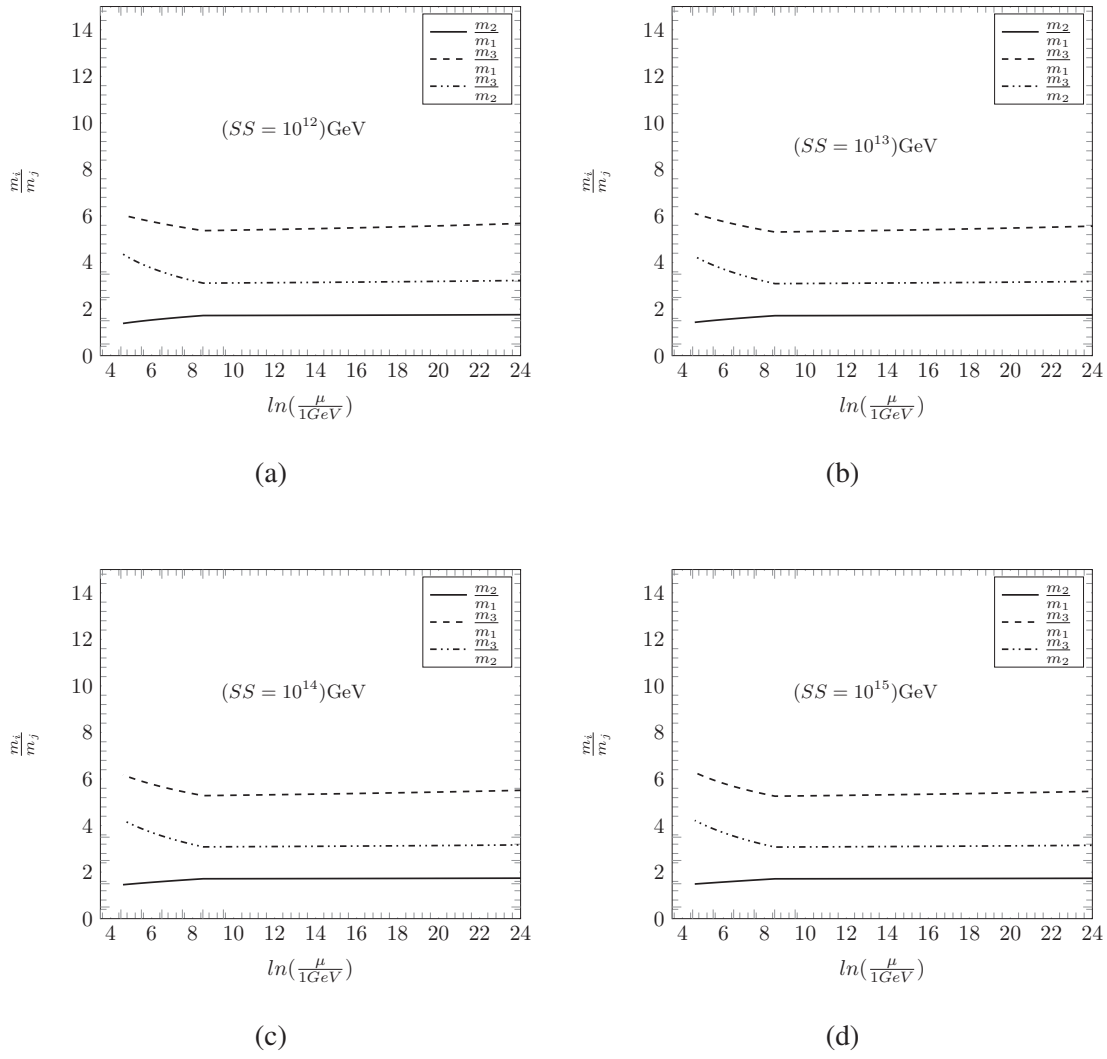

Fig. 4.10 Radiative evolution of the three neutrino mass ratios from the seesaw scale to the EW scale for a fix input data set B5, fix $m_s = 5$ TeV (as given in Table 4.3) for different seesaw scales are studied. The four figures (a), (b), (c), and (d) corresponds to the different choices of SS at 10^{12} GeV, 10^{13} GeV, 10^{14} GeV, and 10^{15} GeV respectively.

$(\psi_1)_0/^\circ \rightarrow$	0.0	45	90	135	180	225	270	315	360
$(\theta_{23})_0/^\circ \rightarrow$	37.240	37.240	37.240	37.240	37.240	37.240	37.240	37.240	37.240
$(\theta_{12})_0/^\circ \rightarrow$	29.160	29.160	29.160	29.160	29.160	29.160	29.160	29.160	29.160
$(\theta_{13})_0/^\circ \rightarrow$	7.974	7.974	7.974	7.974	7.974	7.974	7.974	7.974	7.974
$(m_1)_0 \times 10^{-2} eV \rightarrow$	1.370	1.375	1.380	1.390	1.395	1.389	1.380	1.375	1.370
$(m_3)_0 \times 10^{-2} eV \rightarrow$	7.791	7.802	7.626	7.460	7.470	7.469	7.522	7.801	7.779

Table 4.2 The initial values of the neutrino parameters ($(\theta_{ij})_0$ and $(m_i)_0$) against varying Majorana phase ($(\psi_1)_0$, $(\psi_2)_0$,with, $(\psi_1)_0 = (\psi_2)_0$). The m_s and the SS scale are fixed at 5 TeV and 10^{14} GeV respectively. We choose, the initial value of the Dirac phase, $(\delta)_0 = 90^\circ$, and $(m_2)_0 = 2.340 \times 10^{-2} eV$. The purpose of this study is to achieve the numerical values of the parameters within 3σ range at EW scale.

Input ν Parameters	Different possible sets of neutrino parameters input values at the seesaw scale													
	↓	↓	↓	↓	↓	↓	↓	↓	↓	↓	↓	↓	↓	↓
	$A1$	$A3$	$A5$	$A7$	$A9$	$A11$	$A13$	$B1$	$B3$	$B5$	$B7$	$B9$	$B11$	$B13$
$(m_1)_0$	1.51	1.36	1.32	1.29	1.27	1.25	1.23	1.51	1.38	1.33	1.30	1.27	1.25	1.24
$(m_2)_0$	2.34	2.34	2.34	2.34	2.34	2.34	2.34	2.34	2.34	2.34	2.34	2.34	2.34	2.34
$(m_3)_0$	7.61	7.74	7.79	7.81	7.86	7.92	7.92	7.46	7.56	7.58	7.63	7.65	7.68	7.72
$(\theta_{12})_0/^\circ$	30.36	31.05	31.45	31.46	31.51	31.62	31.79	30.36	31.22	31.79	31.79	31.79	31.79	31.79
$(\theta_{13})_0/^\circ$	8.42	8.53	8.53	8.53	8.53	8.53	8.53	8.93	9.05	9.05	9.05	9.05	9.05	9.05
$(\theta_{23})_0/^\circ$	37.12	37.61	37.99	37.99	38.04	38.15	38.31	38.12	38.26	38.80	38.80	38.80	38.80	38.80
q	0.96	0.95	0.95	0.95	0.95	0.95	0.95	0.97	0.95	0.95	0.95	0.95	0.95	0.95
$(\psi_1)_0/^\circ$	45.0	45.0	45.0	45.0	45.0	45.0	45.0	45.0	45.0	45.0	45.0	45.0	45.0	45.0
$(\delta)_0/^\circ$	90.0	90.0	90.0	90.0	90.0	90.0	90.0	270.0	270.0	270.0	270.0	270.0	270.0	270.0

Table 4.3 The Table for different sets of input parameters to be used for subsequent analysis.The $(\theta_{23})_0$ is connected to $(\theta_{13})_0$ and $(\theta_{12})_0$ via the S.C relation as presumed in eq. (4.2). We choose only the $(\theta_{13})_0$ and $(\theta_{12})_0$ as input. The Majorana phase, $(\psi_1)_0$ is fixed at 45°. The sets $A1$, $A3$,...$A13$ represent the collection of initial inputs to be attributed to the parameters at the SS scale, for the m_s scale being fixed at 1, 3...13 TeV respectively, with $(\delta)_0 = 90^\circ$. The SS scale is fixed at 10^{14} GeV. The sets $B1$, $B2$,... $B13$ are similar to the sets $A1$, $A3$...$A13$ respectively, except for the former, $(\delta)_0 = 270^0$. The numerical entries are so adjusted for a specific m_s scale (say, $A5$ at 5 TeV) that after running the RGEs, the parameters at EW scale lie within the 3σ range.

m_s in TeV	Δm^2_{21} ($\times 10^{-5} eV^2$) at EW scale													
	$A1$	$A3$	$A5$	$A7$	$A9$	$A11$	$A13$	$B1$	$B3$	$B5$	$B7$	$B9$	$B11$	$B13$
1.0	**7.56**	11.1	13.0	12.9	13.5	13.8	14.2	**7.5**	11.1	12.3	13.0	13.5	13.8	14.2
3.0	1.79	**7.56**	9.16	9.82	10.8	10.8	11.2	1.88	**7.57**	9.05	9.63	10.4	10.8	11.2
5.0	×	5.94	**7.57**	8.42	9.06	9.47	9.84	×	5.95	**7.58**	8.43	9.06	9.50	9.88
7.00	×	4.87	6.64	**7.55**	8.21	8.64	9.01	×	4.87	6.64	**7.55**	8.20	8.66	9.06
9.0	×	4.01	5.93	6.89	**7.57**	8.01	8.40	×	4.00	5.93	6.88	**7.56**	8.03	8.44
11.0	×	3.30	5.39	6.38	7.08	**7.54**	7.92	×	3.27	5.37	6.36	7.07	**7.56**	7.97
13.0	×	2.64	4.92	5.95	6.67	7.13	**7.53**	×	2.61	4.89	5.29	6.65	7.15	**7.55**

Table 4.4 The fluctuations of Δm^2_{21} after RG evolution, at the EW scale have been studied, against changing m_s, at constant SS scale. The Aj or Bj correspond to the set of initial entries at constant m_s as mentioned in Table 4.3. The diagonal entries marked in Bold text reflect the output values of, Δm^2_{21} within 3σ for which the initial entries of Aj or Bj were tuned at constant m_s. On keeping a input data set (say, $A5$) fixed, if the m_s scale is varied, one sees that, against the radiative correction, the value of Δm^2_{21}, at EW scale fluctuates. If m_s is lesser, the fluctuation is more. The output values which lies within 3σ are underlined. The irrelevant output are omitted with '$\times$' sign.

m_s in TeV	Δm^2_{31} ($\times 10^{-3} eV^2$) at EW scale for different sets of inputs													
	$A1$	$A3$	$A5$	$A7$	$A9$	$A11$	$A13$	$B1$	$B3$	$B5$	$B7$	$B9$	$B11$	$B13$
1.0	**2.51**	2.65	2.86	2.70	2.74	2.80	2.80	**2.49**	2.59	2.62	2.66	2.68	2.71	2.74
3.0	2.40	**2.53**	2.62	2.57	2.62	2.67	2.67	2.40	**2.50**	2.53	2.53	2.59	2.62	2.64
5.0	×	2.48	**2.51**	2.51	2.56	2.61	2.61	×	2.45	**2.49**	2.52	2.54	2.57	2.60
7.0	×	2.44	2.47	**2.48**	2.52	2.57	2.57	×	2.42	2.45	**2.49**	2.51	2.54	2.56
9.0	×	2.41	2.44	2.44	**2.49**	2.54	2.54	×	2.40	2.43	2.47	**2.48**	2.51	2.53
11.0	×	2.39	2.41	2.42	2.46	**2.51**	2.51	×	2.38	2.41	2.45	2.46	**2.49**	2.52
13.0	×	2.37	2.39	2.40	2.44	2.49	**2.44**	×	2.36	2.39	2.43	2.45	2.47	**2.49**

Table 4.5 The fluctuations of Δm^2_{31} after RG evolution, at the EW scale have been studied, against changing m_s, at constant SS scale. The Aj or Bj correspond to the set of initial entries at constant m_s as mentioned in Table 4.3. The diagonal entries marked in Bold text reflect the output values of, Δm^2_{31} within 3σ for which the initial entries of Aj or Bj were tuned at constant m_s. On keeping a input data set (say, $A5$) fixed, if the m_s scale is varied, one sees that, against the radiative correction, the value of Δm^2_{31}, at EW scale fluctuates. If m_s is lesser, the fluctuation is more. The output values which lies within 3σ are underlined. The irrelevant results in view of 3σ bound are omitted with '$\times$' symbol.

m_s in TeV	$\theta_{23}/^\circ$ at EW scale													
	$A1$	$A3$	$A5$	$A7$	$A9$	$A11$	$A13$	$B1$	$B3$	$B5$	$B7$	$B9$	$B11$	$B13$
1.0	**41.0**	41.4	41.6	41.8	41.8	41.9	42.1	**41.0**	41.1	41.6	41.6	41.6	41.6	41.6
3.0	40.6	**41.1**	41.4	41.5	41.5	41.6	41.8	40.7	**40.8**	41.3	41.3	41.3	41.3	41.3
5.0	×	41.0	**41.3**	41.3	41.4	41.5	41.6	×	40.7	**41.2**	41.2	41.2	41.2	41.2
7.0	×	40.9	41.2	**41.2**	41.3	41.4	41.5	×	40.6	41.1	**41.1**	41.1	41.1	41.1
9.0	×	40.8	41.2	41.2	**41.2**	41.3	41.4	×	40.5	41.1	41.1	**41.1**	41.0	41.0
11.0	×	40.8	41.1	41.1	41.1	**41.2**	41.4	×	40.5	41.0	41.0	41.0	**41.0**	41.0
13.0	×	40.7	41.1	41.0	41.1	41.2	**41.3**	×	40.4	41.0	41.0	41.0	41.0	**41.0**

Table 4.6 The fluctuations of atmospheric angle after RG evolution, at the EW scale have been studied, against changing m_s, at constant SS scale. The Aj or Bj represent the set of initial entries at constant m_s as mentioned in Table 4.3. The diagonal entries marked in Bold text reflect the output values of, θ_{23} within 3σ for which the initial entries of Aj or Bj are adjusted at constant m_s. On keeping a input data set (say, $A5$) fixed, if the m_s scale is varied, one sees that, against the radiative correction, the value of θ_{23}, at EW scale fluctuates, but a little and output values lie within 3σ range. The irrelevant results in view of 3σ bound are omitted with '$\times$' symbol.

m_s in TeV	$\theta_{12}/^\circ$ at EW scale													
	$A1$	$A3$	$A5$	$A7$	$A9$	$A11$	$A13$	$B1$	$B3$	$B5$	$B7$	$B9$	$B11$	$B13$
1.0	**34.6**	34.8	34.8	34.8	34.8	34.8	35.0	**34.8**	35.0	35.3	35.1	35.1	35.1	35.0
3.0	34.1	**34.4**	34.6	34.6	34.5	34.6	34.7	34.3	**34.7**	35.0	34.9	34.9	34.8	34.7
5.0	×	34.3	**34.5**	34.4	34.4	34.5	34.6	×	34.5	**34.9**	34.7	34.7	34.7	34.6
7.0	×	34.2	34.4	**34.3**	34.3	34.4	34.5	×	34.4	34.8	**34.6**	34.7	34.6	34.5
9.0	×	34.1	34.4	34.3	**34.2**	34.3	34.5	×	34.3	34.7	34.6	**34.6**	34.5	34.5
11.0	×	34.0	34.3	34.2	34.2	**34.3**	34.4	×	34.3	34.6	34.5	34.5	**34.5**	34.48
13.0	×	34.0	34.3	34.2	34.2	34.2	**34.4**	×	34.2	34.6	34.5	34.5	34.4	**34.4**

Table 4.7 The fluctuation of solar angle after RG evolution, at the EW scale is studied, against changing m_s, at constant SS scale. The Aj or Bj represent the set of initial entries at constant m_s as mentioned in Table 4.3. The diagonal entries marked in Bold texts reflect the output values of, θ_{12} within 3σ for which the initial entries of Aj or Bj are adjusted at constant m_s. On keeping a input data set (say, $A5$) fixed, if the m_s scale is varied, one sees that, against the radiative correction, the value of θ_{12}, at EW scale fluctuates, but the variations are a little and output values lie within 3σ range.

m_s in	$\theta_{13}/^\circ$ at EW													
TeV	$A1$	$A3$	$A5$	$A7$	$A9$	$A11$	$A13$	$B1$	$B3$	$B5$	$B7$	$B9$	$B11$	$B13$
1.0	**8.4**	8.6	8.6	8.6	8.6	8.6	8.6	**8.4**	8.5	8.4	8.4	8.4	8.4	8.4
3.0	8.4	**8.5**	8.5	8.5	8.5	8.5	8.5	8.3	**8.4**	8.4	8.3	8.4	8.4	8.4
5.0	×	8.4	**8.4**	8.5	8.50	8.50	8.5	×	8.4	**8.3**	8.3	8.3	8.3	8.3
7.0	×	8.4	8.4	**8.4**	8.4	8.4	8.4	×	8.3	8.3	**8.3**	8.3	8.3	8.3
9.0	×	8.4	8.4	8.4	**8.4**	8.4	8.4	×	8.3	8.3	8.3	**8.3**	8.3	8.3
11.0	×	8.4	8.4	8.4	8.4	**8.4**	8.4	×	8.3	8.3	8.3	8.3	**8.3**	8.3
13.0	×	8.4	8.4	8.4	8.4	8.4	**8.4**	×	8.3	8.3	8.3	8.3	8.3	**8.3**

Table 4.8 The fluctuation of the reactor angle after RG evolution, at the EW scale is investigated , against changing m_s, at constant SS scale. The Aj or Bj represent the set of initial entries at constant m_s as mentioned in Table 4.3. The diagonal entries marked in Bold texts represent the output values of, θ_{23} within 3σ for which the initial entries of Aj or Bj are adjusted at constant m_s. On keeping an input data set (say, $A5$) fixed, if the m_s scale is varied, one sees that, against the radiative correction, the value of θ_{23}, at EW scale fluctuates. The fluctuation is very feeble against the varying m_s. The irrelevant results in view of 3σ bound are omitted with '×' symbol.

m_s in	$m_1 \times 10^{-3}$ eV at EW scale for different sets of inputs													
TeV	$A1$	$A3$	$A5$	$A7$	$A9$	$A11$	$A13$	$B1$	$B3$	$B5$	$B7$	$B9$	$B11$	$B13$
1.0	10.3	9.43	9.35	8.83	8.66	8.53	8.40	10.2	9.46	9.04	8.83	8.67	8.55	8.44
3.0	9.63	8.82	8.56	8.26	8.10	7.98	7.85	9.62	8.85	8.45	8.06	8.11	8.00	7.89
5.0	×	8.53	8.17	7.99	7.83	7.71	7.59	×	8.56	8.17	7.99	7.84	7.73	7.63
7.0	×	8.34	7.99	7.81	7.65	7.54	7.42	×	8.36	7.99	7.81	7.66	7.56	7.46
9.0	×	8.19	7.84	7.67	7.52	7.40	7.29	×	8.21	7.85	7.67	7.53	7.42	7.33
11.0	×	8.07	7.73	7.56	7.41	7.30	7.18	×	8.10	7.73	7.56	7.42	7.31	7.22
13.0	×	7.97	7.63	7.46	7.31	7.20	7.09	×	7.99	7.63	7.46	7.32	7.22	7.11

Table 4.9 The fluctuations of m_1 after RG evolution, at the EW scale have been studied, against changing m_s, at constant SS scale. The Aj or Bj correspond to the set of initial entries at constant m_s as mentioned in Table 4.3. On keeping an input data set (say, $A5$) fixed, if the m_s scale is varied, one sees that, against the radiative correction, the value of m_1, at EW scale fluctuates. The irrelevant results in view of 3σ bound are omitted with '×' symbol.

m_s in TeV	$m_2 \times 10^{-2}$ eV at EW scale for different sets of inputs													
	$A1$	$A3$	$A5$	$A7$	$A9$	$A11$	$A13$	$B1$	$B3$	$B5$	$B7$	$B9$	$B11$	$B13$
1.0	1.34	1.41	1.47	1.44	1.44	1.45	1.45	13.4	1.42	1.43	1.44	1.45	1.46	1.46
3.0	1.05	1.23	1.28	1.29	1.30	1.31	1.31	10.5	1.24	1.27	1.27	1.30	1.31	1.32
5.0	×	1.15	1.19	1.21	1.23	1.24	1.24	×	1.15	1.19	1.22	1.23	1.24	1.25
7.0	×	1.08	1.14	1.16	1.18	1.19	1.20	×	1.09	1.14	1.17	1.19	1.20	1.21
9.0	×	1.03	1.09	1.13	1.15	1.16	1.17	×	1.04	1.09	1.13	1.15	1.16	1.18
11.0	×	0.99	1.06	1.10	1.12	1.13	1.14	×	0.99	1.07	1.10	1.12	1.14	1.15
13.0	×	0.95	1.03	1.07	1.09	1.11	1.12	×	0.95	1.04	1.07	1.10	1.11	1.12

Table 4.10 The fluctuations of m_2 after RG evolution, at the EW scale is studied, against changing m_s, at constant SS scale. The Aj or Bj correspond to the set of initial entries at constant m_s as mentioned in Table 4.3. On keeping an input data set (say, $A5$) fixed, if the m_s scale is varied, one sees that, against the radiative correction, the value of m_2, at EW scale fluctuates. The irrelevant results in view of 3σ bound are omitted with '$\times$' symbol.

m_s in TeV	$m_3 \times 10^{-2}$ eV at EW scale for different sets of inputs													
	$A1$	$A3$	$A5$	$A7$	$A9$	$A11$	$A13$	$B1$	$B3$	$B5$	$B7$	$B9$	$B11$	$B13$
1.0	5.12	5.24	5.43	5.27	5.31	5.36	5.36	5.09	5.17	5.20	5.23	5.25	5.27	5.30
3.0	4.99	5.11	5.19	5.14	5.18	5.23	5.23	5.00	5.08	5.10	5.10	5.15	5.18	5.20
5.0	×	5.05	5.07	5.08	5.12	5.17	5.17	×	5.03	5.05	5.09	5.10	5.13	5.15
7.0	×	5.01	5.03	5.04	5.08	5.12	5.12	×	4.99	5.02	5.05	5.07	5.09	5.12
9.0	×	4.98	5.00	5.00	5.04	5.09	5.09	×	4.96	4.99	5.02	5.04	5.07	5.09
11.0	×	4.95	4.97	4.98	5.02	5.06	5.06	×	4.94	4.97	5.00	5.02	5.04	5.07
13.0	×	4.93	4.95	4.95	4.99	5.04	5.04	×	4.92	4.95	4.98	5.00	5.02	5.04

Table 4.11 The fluctuations of m_3 after RG evolution, at the EW scale is studied, against changing m_s, at constant SS scale. The Aj or Bj correspond to the set of initial entries at constant m_s as mentioned in Table 4.3. On keeping an input data set (say, $A5$) fixed, if the m_s scale is varied, one sees that, against the radiative correction, the value of m_3, at EW scale fluctuates. The irrelevant results in view of 3σ bound are omitted with '$\times$' symbol.

Variation of m_s and SS scale	Effect of varying m_s and SS on the neutrino parameters						
	θ_{12}	θ_{13}	θ_{23}	Δm^2_{21}	Δm^2_{31}	δ	ψ_1
Increasing $m_s \rightarrow$	$-$	$-$	$-$	$-$	$-$	$-$	$+$
Decreasing $m_s \rightarrow$	$+$	$+$	$+$	$+$	$+$	$+$	$-$
Increasing SS $\rightarrow$	$+$	$-$	$+$	$-$	$-$	$+$	$-$
Decreasing SS $\rightarrow$	$-$	$+$	$-$	$+$	$+$	$-$	$+$

Table 4.12 Here we show the different effects each neutrino parameters receive due to the variation of m_s and SS. An increase in m_s cause a negative effect on all the EW scale neutrino parameters values, except for the Majorana phases (for decreasing m_s the finding is reverse). Whereas, variation in SS has unequal effects (positive effect on some parameters and negative effects on other parameters). The '$-$' sign indicates the negative effect whereas the '$+$' sign indicate the positive contribution due to varying m_s and SS.

4.5 Summary and Discussion

In this chapter, we have studied the radiative evolution of neutrino observational parameters for varying m_s scale following a top-down approach. We presume the hierarchy of the three neutrino masses to be of normal type. All the nine observational parameters related to neutrino oscillations are allowed to run down from the SS up to the electroweak scale using their respective RGEs (both MSSM and SM). We also use the RGEs of the three gauge couplings, third generation Yukawa couplings, and quartic Higgs coupling. All the neutrino parameters along with the other couplings undergo RG evolution and subsequently, get different RG corrections. The m_s, which appears to be a leading parameter is kept varying between 1 TeV to 13 TeV, and the effect of such a variation on the observational parameters at the EW scale is noted. Instead of adhering to a fixed SS scale, we allow the latter to change between 10^{10} GeV to 10^{15} GeV and have checked how the observational parameters vary. Besides, the work reveals that the self-complementarity relation among the mixing angles remains stable against the radiative evolution. Also, we have studied how certain parameters like neutrino mass ratios behave during this evolution.

The relevance of the SUSY is unavoidable in the context of particle physics, as it can answer to certain important theoretical issues like the hierarchy problem, the unification of gauge couplings, the existence of dark matter etc. But, unlike the Standard Model, the SUSY is still lacking the experimental evidences. Although the LHC experiment is running at 13 TeV, it has not yet witnessed any signature of SUSY. This may imply that the SUSY breaks at a certain higher energy scale which is not yet achieved by the LHC experiment, or even if it breaks at a low energy, the beam luminosity available in the LHC experiment is not sufficient to detect the same. Hence, there is still a hope that SUSY exists. The SUSY breaking scale, m_s, is an important parameter and influences the neutrino observational parameters. The origin of neutrino mass owes to the seesaw mechanism and the scale at which the latter occurred is also unknown. But theoretically one may predict that scale to

be lying within the range of 10^{10} to 10^{15} GeV. In our analysis, these two parameters, the m_s and the SS scale, partake a lot. Besides, the input data set (like, Aj or Bj) which are although model independent, plays an important role. Initially, the input parameters in the data sets are chosen such that against a fixed m_s and a fixed SS scale (10^{14} GeV), the neutrino observational parameters at the EW scale lie within the 3σ bound. It is mentioned that the initial entries in terms of the three mixing angles follow a self-complementarity relation.

At the EW scale, the three mixing angles, CP violating phases, and Δm^2_{31} try to maintain more or less stability with respect to the 3σ bound if the m_s scale is varied at a fixed SS scale. But the parameter Δm^2_{21}, is less stable at lower m_s, whereas the stability increases towards higher m_s. Similar stability is achievable for the three mixing angles, if the SS scale is varied. But for Δm^2_{31}, the stability is lost. One sees that if the stability of Δm^2_{21} is obtained towards higher m_s, ruling out of a certain SS scale is possible in the light of a 3σ bound of Δm^2_{21}. It is worth mentioning that a strong conclusion in view of the optimization of the SUSY breaking and SS scales can not be drawn by observing the plots [see Fig. 4.6- Fig. 4.7], because the the Δm^2_{21} at the EW scale is very much sensitive to the initial arbitrary model independent entries available in the data sets (Aj and Bj). Justifying these initial entries under certain model or framework goes beyond the scope of this thesis work. But through our analysis, one can at least visualize the interplay between the m_s and the SS scale and how these affects the final physical observables. Though in the present analysis, we limit ourselves not to invoke the model dependent ground of these data sets, yet we emphasize the certain traits that these numerals may carry. We see that the data set are characterized by the SC relation, $\theta_{13} + \theta_{12} \approx \theta_{23}$ and a mass ratio: $m_2/m_1 \sim 2$, which remains almost invariant against radiative evolution. Besides, we have observed the other mass ratios like m_3/m_1 or m_3/m_2, also tries to maintain a stability up to SUSY breaking scale, but after that they change. This study is motivated in the context of the quark sector, where the quark mass ratio $m_{down}/m_{strange}$ plays an important role in describing the quark mixing. Relations

among certain parameters and their stability during radiative evolution may bear the traits of a certain hidden symmetry present in the lepton sector and may serve as a key to some new models.

The present study is devoted to a simple visualization, concerning the interplay between the m_s and SS scale and its effect on the physical observables and certain phenomenological relations. The two Majorana phases are not yet been measured experimentally, and to simplify the analysis, we have considered both of them as equal. Again, we have restricted ourselves only to the normal hierarchy of neutrino masses. The consideration of a degenerate spectrum for all sparticles that we have adopted in our work is an idealized situation and is true if $m_s \gg m_t, m_Z$ [47, 172]. In principle, a general study can be made by minimizing the number of assumptions in order to get a more generalized result.

Chapter 5

Summary and Outlooks

5.1 Summary

In this thesis, we have studied some phenomenological aspects of neutrinos. More precisely, we have discussed the radiative properties of the various neutrino parameters. In order to do so, we first studied the radiative properties of the three gauge couplings, third generation three Yukawa couplings and the quartic Higgs coupling. All of these radiative studies are made possible through the Renormalization Group running technique. We use the bottom-up approach while studying the radiative properties of the couplings, whereas we used the top-down approach for the neutrino parameters. The RG method can relate physics at different energy scales by extrapolating the available data (e.g. EW scale data) to a different energy scale (e.g. the seesaw scale or the GUT scale), where our current technology cannot venture into.

The relevance of the SUSY is unavoidable in the context of high energy physics, as it can address various important theoretical issues like the hierarchy problem, the unification of gauge couplings, the existence of dark matter, stability of proton etc. In spite of these huge predictive power, SUSY is still lacking the experimental evidences. Moreover, the idea of SUSY breaking scale (m_s) is an important yet unknown parameter.

While studying the radiative nature of the couplings or the neutrino parameters we, instead of restricting ourselves to a fixed m_s, explored the possible effects of varying m_s on the various parameters concerned. We observed that, the couplings as well as the nine neutrino parameters are sensitive to a varying m_s scale. Further, the absence of a definite seesaw scale inspired us to vary the same (similar to m_s) and to study the possible consequences on the neutrino parameters values at the EW scale. By studying the numerical consistencies of the various parameters involved w.r.t the present oscillation data (see Table 1.3), we tried to narrow down the possible m_s and seesaw (SS) range. It is in this regard, the predictions presented in this thesis may have significant implications for future studies.

- In Chapter 2, we studied the radiative evolution of the three gauge couplings (electromagnetic, weak and strong) and the third generation three Yukawa couplings (top, bottom and tau) using the bottom-up approach against the varying SUSY breaking scale (m_s). In this study, we observed that both the gauge couplings and the Yukawa couplings received appreciable radiative corrections while running from the electrowewak scale up to the GUT scale. Moreover, the grand unification scale, which is expected to be $\sim 10^{16}$ GeV, varies with the variation of the m_s. The same case is also observed in the case of the Yukawa couplings unification scale but in the reverse trend. In short, the GUT unification scale decreases with the increase in m_s and tends to maintain a constant value, whereas the Yukawa couplings unification points increases with the increase in m_s and then tend to remain invariant. Further, the value of g_3^{DR} seems to place a bound on the upper limit of m_s for a particular choice of $\tan\beta$.

- In Chapter 3, we emphasized on how to modify the Bi-maximal mixing (BM) and the Tri-Bi-maximal mixing (TBM) patterns in order to account for the present neutrino oscillation data. We found that the matrices which can modify these two mixing schemes in consistent with the present oscillation data comes from the charged lepton correction. We also found that charged lepton mixing matrices U_{lL}'s in both cases

exhibit similar structures due to the $\mu - \tau$ symmetry. From numerical analysis it is also observed that the deviation matrices, U_{lL}^{BM} and U_{lL}^{TBM}, are close to the CKM matrix of the quark sector. This finding is in agreement with the general assumption in Grand Unified theory, that the charged lepton correction to neutrino mixing can be considered as CKM like.

- In Chapter 4, we studied the radiative properties of all the nine neutrino parameters in the top-down approach. It is observed that some of them undergoes appreciable radiative correction while some get mild quantum correction and other get very negligible correction. Here, we also studied how the variation of m_s affects the radiative evolution of the various neutrino parameters which in turn affect the low energy parameter values. In addition to varying m_s scale, we also studied the same for different values of the seesaw scale, starting from 10^{10} GeV - 10^{15} GeV. All the neutrino parameters are found to be sensitive to the variation of both m_s and seesaw scale. Inspired by the present neutrino oscillation date, we also emphasized on the possible existence of mixing angles self-complementarity relation among the three neutrino mixing angles at the seesaw scale. It is observed that this relation remains invariant under the radiative evolution with varying m_s and seesaw scale. Moreover, under the same conditions, we also studied the radiative stability of three neutrino mass ratios. It is observed that the three mass ratios behave in a similar pattern, they remain very much stable in the MSSM region and then changes slightly in the SM region. Of the three neutrino mass ratios, $m_2 : m_1$ is more immune to the radiative evolution. In short, this Chapter is devoted to a simple visualization, concerning the interplay between the m_s and SS scale and its effect on the physical observables and certain phenomenological relations.

While doing our works, we considered certain simplifying assumptions like the existence of a single degenerate sparticles spectrum thereby ignoring the possible threshold corrections. While using the top-down approach in the neutrino sector, we started the evolution process

from the seesaw scale. It could have been more general, if we started from either GUT scale or from Planck scale. By doing so, we may even include the possible effects from the gravity. More importantly, we have considered only one mass spectrum - the normal hierarchy. In these regards, our work can be further extended by the inclusion of a non-degenerate SUSY spectrum and proper threshold corrections with the RG evolution process starting from the GUT or Planck scale and for different neutrino mass spectrum.

5.2 Outlooks

Neutrino physics is becoming more and more exciting area of research due to its possible, multiple, connections with different areas of fundamental physics like the matter-antimatter asymmetry in our universe, dark matter, SUSY particle etc. The future development in neutrino physics are expected to be driven by new experiments. At present, several neutrino experimental facilities are running throughout the globe (see Table A.2) and several more advanced future programs are planned worldwide.

Deviation of the θ_{23} from the maximal mixing angle, as confirmed by recent experiment, may be a hint for the possibility of an underlying physics. Again, the recent experimental confirmation of the non-zero value of reactor angle [173–175] has boosted the eagerness of neutrino researchers to unravel the mysteries shrouding the phenomenon of CP-violation and neutrino mass hierarchy. The 1-3 mixing is the door to determining both the mysteries. It is very likely, that in the near future we will solve the neutrino mass hierarchy problem.

Even though CP symmetry is already violated in the SM, it is too small to account for the observed matter-antimatter asymmetry in the universe. CP violation may be related to the lepton asymmetry as well as baryon asymmetry [176]. The phenomenon seems to be deeply related to the origin of many unknown mysteries of the nature. The possibility of neutrinos having a relation with the dark matter will continue to be one of the exciting areas of research. Amongst the many proposed candidates of dark matter, sterile neutrino is one [177, 178].

Further studies on the possible connections may lead to the breakthrough both in particle physics and Cosmology. It can be expected that the next-generation neutrino experiments will provide us more detailed picture of this phenomena. Unless we are quite lucky, it will not be an easy task to establish the CP-violation, satisfactorily.

References

[1] P. F. de Salas, D. V. Forero, C. A. Ternes, M. Tortola, and J. W. F. Valle, Phys. Lett. **B782**, 633 (2018), arXiv:1708.01186 [hep-ph] .

[2] J. Beringer *et al.* (Particle Data Group), Phys. Rev. **D86**, 010001 (2012).

[3] C. Patrignani *et al.* (Particle Data Group), Chin. Phys. **C40**, 100001 (2016).

[4] G. Apollinari, O. Brüning, T. Nakamoto, and L. Rossi, CERN Yellow Report , 1 (2015), arXiv:1705.08830 [physics.acc-ph] .

[5] G. Aad *et al.* (ATLAS), Phys. Lett. **B716**, 1 (2012), arXiv:1207.7214 [hep-ex] .

[6] S. Chatrchyan *et al.* (CMS), Phys. Lett. **B716**, 30 (2012), arXiv:1207.7235 [hep-ex] .

[7] C. L. Cowan, F. Reines, F. B. Harrison, H. W. Kruse, and A. D. McGuire, Science **124**, 103 (1956).

[8] H. Bethe and R. Peierls, Nature **133**, 532 (1934).

[9] B. Pontecorvo, Sov. Phys. JETP **6**, 429 (1957), [Zh. Eksp. Teor. Fiz.33,549(1957)].

[10] B. Pontecorvo, Sov. Phys. JETP **7**, 172 (1958), [Zh. Eksp. Teor. Fiz.34,247(1957)].

[11] Z. Maki, M. Nakagawa, and S. Sakata, Prog. Theor. Phys. **28**, 870 (1962).

[12] S. P. Mikheev and A. Yu. Smirnov, Sov. J. Nucl. Phys. **42**, 913 (1985), [Yad. Fiz.42,1441(1985)].

[13] R. R. Volkas, *Progress in particle and nuclear physics. Vol. 48, Pt. 1: Neutrinos in astro, particle and nuclear physics. Proceedings, International School of Nuclear Physics, 23rd Course, Erice, Italy, September 18-26, 2001*, Prog. Part. Nucl. Phys. **48**, 161 (2002), [161(2001)], arXiv:hep-ph/0111326 [hep-ph] .

[14] C. Giunti and C. W. Kim, *Fundamentals of Neutrino Physics and Astrophysics* (2007).

[15] Z.-z. Xing and Y.-L. Zhou, Phys. Rev. **D88**, 033002 (2013), arXiv:1305.5718 [hep-ph] .

[16] M. Magg and C. Wetterich, Phys. Lett. **94B**, 61 (1980).

[17] G. Lazarides, Q. Shafi, and C. Wetterich, Nucl. Phys. **B181**, 287 (1981).

[18] R. Foot, H. Lew, X. G. He, and G. C. Joshi, Z. Phys. **C44**, 441 (1989).

[19] E. Ma, Phys. Rev. Lett. **81**, 1171 (1998), arXiv:hep-ph/9805219 [hep-ph] .

[20] B. Bajc and G. Senjanovic, JHEP **08**, 014 (2007), arXiv:hep-ph/0612029 [hep-ph] .

[21] V. Lucas and S. Raby, Phys. Rev. **D54**, 2261 (1996), arXiv:hep-ph/9601303 [hep-ph] .

[22] T. Blazek, M. Carena, S. Raby, and C. E. M. Wagner, Phys. Rev. **D56**, 6919 (1997), arXiv:hep-ph/9611217 [hep-ph] .

[23] G. Altarelli, F. Feruglio, and I. Masina, JHEP **11**, 040 (2000), arXiv:hep-ph/0007254 [hep-ph] .

[24] K. C. Wali, ed., *GRAND UNIFICATION. PROCEEDINGS, 8TH WORKSHOP, SYRACUSE, USA, APRIL 16-18, 1987*, WSP (WSP, Singapore, 1988).

[25] J. Ellis, J. L. Evans, A. Mustafayev, N. Nagata, and K. A. Olive, Eur. Phys. J. **C76**, 592 (2016), arXiv:1608.05370 [hep-ph] .

[26] A. Mütter, M. Ratz, and P. K. S. Vaudrevange, (2016), arXiv:1606.02303 [hep-ph] .

[27] T. Yanagida, *Proceedings: Workshop on the Unified Theories and the Baryon Number in the Universe: Tsukuba, Japan, February 13-14, 1979*, Conf. Proc. **C7902131**, 95 (1979).

[28] R. N. Mohapatra and G. Senjanovic, Phys. Rev. Lett. **44**, 912 (1980).

[29] K. S. Babu and C. Macesanu, Phys. Rev. **D72**, 115003 (2005), arXiv:hep-ph/0505200 [hep-ph] .

[30] H. S. Goh, R. N. Mohapatra, and S.-P. Ng, Phys. Rev. **D68**, 115008 (2003), arXiv:hep-ph/0308197 [hep-ph] .

[31] H. Georgi and S. L. Glashow, Phys. Rev. Lett. **32**, 438 (1974).

[32] S. Dimopoulos, S. Raby, and F. Wilczek, Phys. Rev. **D24**, 1681 (1981).

[33] M. B. Einhorn and D. R. T. Jones, Nucl. Phys. **B196**, 475 (1982).

[34] W. J. Marciano and G. Senjanovic, Phys. Rev. **D25**, 3092 (1982).

[35] K. Inoue, A. Kakuto, H. Komatsu, and S. Takeshita, Prog. Theor. Phys. **68**, 927 (1982), [Erratum: Prog. Theor. Phys.70,330(1983)].

[36] L. E. Ibanez and G. G. Ross, Phys. Lett. **110B**, 215 (1982).

[37] N. Sakai and T. Yanagida, Nucl. Phys. **B197**, 533 (1982).

[38] S. Weinberg, Phys. Rev. **D26**, 287 (1982).

[39] S. Dimopoulos, S. Raby, and F. Wilczek, Phys. Lett. **112B**, 133 (1982).

[40] J. R. Ellis, D. V. Nanopoulos, and S. Rudaz, Nucl. Phys. **B202**, 43 (1982).

[41] C. Regis *et al.* (Super-Kamiokande), Phys. Rev. **D86**, 012006 (2012), arXiv:1205.6538 [hep-ex] .

[42] H. Nishino *et al.* (Super-Kamiokande), Phys. Rev. **D85**, 112001 (2012), arXiv:1203.4030 [hep-ex] .

[43] M. Miura, *Proceedings, 35th International Conference on High energy physics (ICHEP 2010): Paris, France, July 22-28, 2010*, PoS **ICHEP2010**, 408 (2010).

[44] *Fundamental Physics at the Intensity Frontier* (2012) arXiv:1205.2671 [hep-ex] .

[45] N. Haba and T. Ota, Acta Phys. Polon. **B39**, 1901 (2008), arXiv:hep-ph/0608244 [hep-ph] .

[46] G. G. Ross and R. G. Roberts, Nucl. Phys. **B377**, 571 (1992).

[47] R. L. Arnowitt and P. Nath, Phys. Rev. Lett. **69**, 725 (1992).

[48] J. E. Bjorkman and D. R. T. Jones, Nucl. Phys. **B259**, 533 (1985).

[49] P. Langacker and N. Polonsky, Phys. Rev. **D47**, 4028 (1993), arXiv:hep-ph/9210235 [hep-ph] .

[50] V. D. Barger, M. S. Berger, and P. Ohmann, Phys. Rev. **D47**, 1093 (1993), arXiv:hep-ph/9209232 [hep-ph] .

[51] N. G. Deshpande and E. Keith, Phys. Rev. **D50**, 3513 (1994), arXiv:hep-ph/9402289 [hep-ph] .

[52] N. N. Singh and S. B. Singh, Eur. Phys. J. **C5**, 363 (1998).

[53] W. Siegel, Phys. Lett. **84B**, 193 (1979).

[54] H. Baer, J. Ferrandis, K. Melnikov, and X. Tata, Phys. Rev. **D66**, 074007 (2002), arXiv:hep-ph/0207126 [hep-ph] .

[55] I. Antoniadis, C. Kounnas, and K. Tamvakis, Phys. Lett. **119B**, 377 (1982).

[56] O. V. Tarasov, A. A. Vladimirov, and A. Yu. Zharkov, Phys. Lett. **93B**, 429 (1980).

[57] M. K. Parida and N. N. Singh, Phys. Rev. **D59**, 032002 (1999), arXiv:hep-ph/9710328 [hep-ph] .

[58] K. Inoue, A. Kakuto, H. Komatsu, and S. Takeshita, Prog. Theor. Phys. **67**, 1889 (1982).

[59] D. R. T. Jones and L. Mezincescu, Phys. Lett. **136B**, 242 (1984).

[60] B. Bajc, S. Lavignac, and T. Mede, *Proceedings, Workshop on Dark Matter, Neutrino Physics and Astrophysics CETUP* 2013: 7th International Conference on Interconnection between Particle Physics and Cosmology (PPC 2013): Lead/Deadwood, South Dakota, USA, July, 8-13, 2013*, AIP Conf. Proc. **1604**, 297 (2014), arXiv:1310.3093 [hep-ph] .

[61] B. Bajc, P. Fileviez Perez, and G. Senjanovic, Phys. Rev. **D66**, 075005 (2002), arXiv:hep-ph/0204311 [hep-ph] .

[62] F. P. An *et al.* (Daya Bay), Phys. Rev. Lett. **108**, 171803 (2012), arXiv:1203.1669 [hep-ex] .

[63] F. P. An *et al.* (Daya Bay), Phys. Rev. Lett. **112**, 061801 (2014), arXiv:1310.6732 [hep-ex] .

[64] J. K. Ahn *et al.* (RENO), Phys. Rev. Lett. **108**, 191802 (2012), arXiv:1204.0626 [hep-ex] .

[65] Y. Abe *et al.* (Double Chooz), Phys. Rev. Lett. **108**, 131801 (2012), arXiv:1112.6353 [hep-ex] .

[66] P. Adamson *et al.* (MINOS), Phys. Rev. Lett. **110**, 251801 (2013), arXiv:1304.6335 [hep-ex] .

[67] K. Abe *et al.* (T2K), Phys. Rev. Lett. **112**, 061802 (2014), arXiv:1311.4750 [hep-ex] .

[68] A. Renshaw (Super-Kamiokande), *Proceedings, 13th International Conference on Topics in Astroparticle and Underground Physics (TAUP 2013): Asilomar, California, September 8-13, 2013*, Phys. Procedia **61**, 345 (2015), arXiv:1403.4575 [hep-ex] .

[69] G. L. Fogli, E. Lisi, A. Marrone, D. Montanino, A. Palazzo, and A. M. Rotunno, Phys. Rev. **D86**, 013012 (2012), arXiv:1205.5254 [hep-ph] .

[70] D. V. Forero, M. Tortola, and J. W. F. Valle, Phys. Rev. **D86**, 073012 (2012), arXiv:1205.4018 [hep-ph] .

[71] D. V. Forero, M. Tortola, and J. W. F. Valle, Phys. Rev. **D90**, 093006 (2014), arXiv:1405.7540 [hep-ph] .

[72] V. D. Barger, S. Pakvasa, T. J. Weiler, and K. Whisnant, Phys. Lett. **B437**, 107 (1998), arXiv:hep-ph/9806387 [hep-ph] .

[73] P. F. Harrison, D. H. Perkins, and W. G. Scott, Phys. Lett. **B530**, 167 (2002), arXiv:hep-ph/0202074 [hep-ph] .

[74] C. S. Lam, Phys. Lett. **B507**, 214 (2001), arXiv:hep-ph/0104116 [hep-ph] .

[75] P. F. Harrison and W. G. Scott, Phys. Lett. **B547**, 219 (2002), arXiv:hep-ph/0210197 [hep-ph] .

[76] C. S. Lam, Phys. Rev. **D71**, 093001 (2005), arXiv:hep-ph/0503159 [hep-ph] .

[77] M. Jezabek and Y. Sumino, Phys. Lett. **B457**, 139 (1999), arXiv:hep-ph/9904382 [hep-ph] .

[78] Z.-z. Xing, Phys. Rev. **D64**, 093013 (2001), arXiv:hep-ph/0107005 [hep-ph] .

[79] Z.-z. Xing, Phys. Lett. **B533**, 85 (2002), arXiv:hep-ph/0204049 [hep-ph] .

[80] C. Giunti and M. Tanimoto, Phys. Rev. **D66**, 053013 (2002), arXiv:hep-ph/0207096 [hep-ph] .

[81] S. K. Kang and C. S. Kim, Phys. Rev. **D90**, 077301 (2014), arXiv:1406.5014 [hep-ph] .

[82] S. T. Petcov, Nucl. Phys. **B892**, 400 (2015), arXiv:1405.6006 [hep-ph] .

[83] J. Barry and W. Rodejohann, Phys. Rev. **D81**, 093002 (2010), [Erratum: Phys. Rev.D81,119901(2010)], arXiv:1003.2385 [hep-ph] .

[84] X.-G. He and A. Zee, Phys. Rev. **D84**, 053004 (2011), arXiv:1106.4359 [hep-ph] .

[85] S. Morisi, K. M. Patel, and E. Peinado, Phys. Rev. **D84**, 053002 (2011), arXiv:1107.0696 [hep-ph] .

[86] D. Aristizabal Sierra, I. de Medeiros Varzielas, and E. Houet, Phys. Rev. **D87**, 093009 (2013), arXiv:1302.6499 [hep-ph] .

[87] D. Aristizabal Sierra and I. de Medeiros Varzielas, JHEP **07**, 042 (2014), arXiv:1404.2529 [hep-ph] .

[88] S. F. King, Phys. Lett. **B659**, 244 (2008), arXiv:0710.0530 [hep-ph] .

[89] A. Romanino, Phys. Rev. **D70**, 013003 (2004), arXiv:hep-ph/0402258 [hep-ph] .

[90] K. A. Hochmuth, S. T. Petcov, and W. Rodejohann, Phys. Lett. **B654**, 177 (2007), arXiv:0706.2975 [hep-ph] .

[91] S. Boudjemaa and S. F. King, Phys. Rev. **D79**, 033001 (2009), arXiv:0808.2782 [hep-ph] .

[92] D. Marzocca, S. T. Petcov, A. Romanino, and M. C. Sevilla, JHEP **05**, 073 (2013), arXiv:1302.0423 [hep-ph] .

[93] D. Marzocca and A. Romanino, JHEP **11**, 159 (2014), arXiv:1409.3760 [hep-ph] .

[94] S. Dev, R. R. Gautam, and L. Singh, Phys. Rev. **D89**, 013006 (2014), arXiv:1309.4219 [hep-ph] .

[95] A. Rashed, Nucl. Phys. **B874**, 679 (2013), arXiv:1111.3072 [hep-ph] .

[96] S. Roy and N. N. Singh, Indian J. Phys. **88**, 513 (2014), arXiv:1211.7207 [hep-ph] .

[97] K. Siyeon, J. Korean Phys. Soc. **65**, 1347 (2014), arXiv:1208.2645 [hep-ph] .

[98] J. A. Acosta, A. Aranda, M. A. Buen-Abad, and A. D. Rojas, Phys. Lett. **B718**, 1413 (2013), arXiv:1207.6093 [hep-ph] .

[99] N. Cabibbo, *Meeting of the Italian School of Physics and Weak Interactions Bologna, Italy, April 26-28, 1984*, Phys. Rev. Lett. **10**, 531 (1963), [648(1963)].

[100] M. Kobayashi and T. Maskawa, Prog. Theor. Phys. **49**, 652 (1973).

[101] T. Ohlsson, Phys. Lett. **B622**, 159 (2005), arXiv:hep-ph/0506094 [hep-ph] .

[102] D. Marzocca, S. T. Petcov, A. Romanino, and M. Spinrath, JHEP **11**, 009 (2011), arXiv:1108.0614 [hep-ph] .

[103] S. Antusch and V. Maurer, Phys. Rev. **D84**, 117301 (2011), arXiv:1107.3728 [hep-ph] .

[104] S. Antusch, C. Gross, V. Maurer, and C. Sluka, Nucl. Phys. **B866**, 255 (2013), arXiv:1205.1051 [hep-ph] .

[105] M. Raidal, Phys. Rev. Lett. **93**, 161801 (2004), arXiv:hep-ph/0404046 [hep-ph] .

[106] H. Minakata and A. Yu. Smirnov, Phys. Rev. **D70**, 073009 (2004), arXiv:hep-ph/0405088 [hep-ph] .

[107] S. Antusch, S. F. King, and R. N. Mohapatra, Phys. Lett. **B618**, 150 (2005), arXiv:hep-ph/0504007 [hep-ph] .

[108] Y.-j. Zheng, Phys. Rev. **D81**, 073009 (2010), arXiv:1002.0919 [hep-ph] .

[109] S. F. King, Phys. Lett. **B718**, 136 (2012), arXiv:1205.0506 [hep-ph] .

[110] B. Hu, Phys. Rev. **D87**, 053011 (2013), arXiv:1212.4079 [hep-ph] .

[111] S. Roy, S. Morisi, N. N. Singh, and J. W. F. Valle, Phys. Lett. **B748**, 1 (2015), arXiv:1410.3658 [hep-ph] .

[112] P. H. Frampton, S. T. Petcov, and W. Rodejohann, Nucl. Phys. **B687**, 31 (2004), arXiv:hep-ph/0401206 [hep-ph] .

[113] F. Bazzocchi and L. Merlo, Fortsch. Phys. **61**, 571 (2013), arXiv:1205.5135 [hep-ph] .

[114] C. Duarah, A. Das, and N. N. Singh, Phys. Lett. **B718**, 147 (2012), arXiv:1207.5225 [hep-ph] .

[115] C. Duarah, A. Das, and N. N. Singh, Indian J. Phys. **87**, 1269 (2013).

[116] K. Nakamura *et al.* (Particle Data Group), J. Phys. **G37**, 075021 (2010).

[117] M. C. Gonzalez-Garcia, M. Maltoni, and T. Schwetz, Nucl. Phys. **B908**, 199 (2016), arXiv:1512.06856 [hep-ph] .

[118] D. V. Naumov, Phys. Part. Nucl. Lett. **8**, 717 (2011).

[119] M. C. Gonzalez-Garcia, *Proceedings, 36th International Conference on High Energy Physics (ICHEP2012): Melbourne, Australia, July 4-11, 2012*, PoS **ICHEP2012**, 005 (2013).

[120] M. Gerbino, M. Lattanzi, and A. Melchiorri, Phys. Rev. **D93**, 033001 (2016), arXiv:1507.08614 [hep-ph] .

[121] N. Palanque-Delabrouille *et al.*, JCAP **1502**, 045 (2015), arXiv:1410.7244 [astro-ph.CO] .

[122] Y. Huang and B.-Q. Ma, The Universe **2**, 65 (2014), 1407.4357 .

[123] A. Melfo, *Particles and fields, proceedings of the VI Latin American Symposium on High Energy Physics and the XII Mexican School of Particles and Fields, Puerto Vallarta, Mexico, 1-8 November 2006*, AIP Conf. Proc. **917**, 252 (2007), [252(2007)], arXiv:0705.4059 [hep-ph] .

[124] I. Dorsner and P. Fileviez Perez, Nucl. Phys. **B723**, 53 (2005), arXiv:hep-ph/0504276 [hep-ph] .

[125] E. Dudas, C. Petersson, and P. Tziveloglou, Nucl. Phys. **B870**, 353 (2013), arXiv:1211.5609 [hep-ph] .

[126] M. Dine, *Supersymmetry '96: Theoretical perspectives and experimental outlook. Proceedings, 4th International Conference, SUSY '96, College Park, USA, May 29-June 1, 1996*, Nucl. Phys. Proc. Suppl. **52A**, 201 (1997), [201(1996)], arXiv:hep-ph/9607294 [hep-ph] .

[127] B. Feldstein and T. T. Yanagida, Phys. Lett. **B720**, 166 (2013), arXiv:1210.7578 [hep-ph] .

[128] R. Aaij *et al.* (LHCb), Nature Phys. **11**, 743 (2015), arXiv:1504.01568 [hep-ex] .

[129] M. Kazana (CMS), *Proceedings, 22nd Cracow Epiphany Conference on the Physics in LHC Run 2: Cracow, Poland, January 7-9, 2016*, Acta Phys. Polon. **B47**, 1489 (2016).

[130] M. Bustamante, A. M. Gago, and J. Jones Perez, JHEP **05**, 133 (2011), arXiv:1012.2728 [hep-ph] .

[131] F. Cadiz and M. A. Díaz, Int. J. Mod. Phys. **A29**, 1450158 (2014), arXiv:1310.7437 [hep-ph] .

[132] B. Mukhopadhyaya, *Proceedings, Neutrino 2001 Meeting: Chennai, India, February, 2001*, Proc. Indian Natl. Sci. Acad. **A70**, 239 (2004), arXiv:hep-ph/0301278 [hep-ph] .

[133] *Search for heavy resonances decaying into a vector boson and a Higgs boson in hadronic final states with 2016 data*, Tech. Rep. CMS-PAS-B2G-17-002 (CERN, Geneva, 2017).

[134] M. Aaboud *et al.* (ATLAS), (2017), arXiv:1710.07235 [hep-ex] .

[135] A. V. Gladyshev and D. I. Kazakov, in *Proceedings, 2012 European School of High-Energy Physics (ESHEP 2012): La Pommeraye, Anjou, France, June 06-19, 2012* (2014) pp. 107–159, arXiv:1212.2548 [hep-ph] .

[136] S. Demidov, in *Proceedings, CMS Workshop: Perspectives on Physics and on CMS at Very High Luminosity, HL-LHC: Alushta, Crimea, Ukraine, May 28–31, 2012* (2013) pp. 162–168.

[137] Z. Ren and D.-X. Zhang, Eur. Phys. J. Plus **132**, 322 (2017), arXiv:1704.03959 [hep-ph] .

[138] C. Arbelaez, M. Hirsch, and L. Reichert, JHEP **02**, 112 (2012), arXiv:1112.4771 [hep-ph] .

[139] X. Zhang and B.-Q. Ma, Phys. Lett. **B710**, 630 (2012), arXiv:1202.4258 [hep-ph] .

[140] N. Haba, K. Kaneta, and R. Takahashi, EPL **101**, 11001 (2013), arXiv:1209.1522 [hep-ph] .

[141] H. Minakata, in *Eleventh International Workshop on Neutrino Telescopes, Venezia, February 22-25, 2005* (2005) pp. 83–97, arXiv:hep-ph/0505262 [hep-ph] .

[142] X. Zhang, Y.-j. Zheng, and B.-Q. Ma, Phys. Rev. **D85**, 097301 (2012), arXiv:1203.1563 [hep-ph] .

[143] N. Haba and R. Takahashi, JHEP **08**, 123 (2013), arXiv:1306.1375 [hep-ph] .

[144] R. Foot, A. Kobakhidze, K. McDonald, and R. Volkas, Phys. Rev. **D76**, 075014 (2007), arXiv:0706.1829 [hep-ph] .

[145] T. Tsuyuki, Phys. Rev. **D91**, 076004 (2015), arXiv:1501.07785 [hep-ph] .

[146] P. F. Harrison, R. Krishnan, and W. G. Scott, Phys. Rev. **D82**, 096004 (2010), arXiv:1007.3810 [hep-ph] .

[147] D. A. Demir, JHEP **11**, 003 (2005), arXiv:hep-ph/0408043 [hep-ph] .

[148] K. S. Singh and N. N. Singh, Adv. High Energy Phys. **2015**, 652029 (2015).

[149] V. D. Barger, M. S. Berger, and P. Ohmann, Phys. Rev. **D47**, 1093 (1993), arXiv:hep-ph/9209232 [hep-ph] .

[150] N. N. Singh and S. B. Singh, Eur. Phys. J. **C5**, 363 (1998).

[151] N. G. Deshpande and E. Keith, Phys. Rev. **D50**, 3513 (1994), arXiv:hep-ph/9402289 [hep-ph] .

[152] M. K. Parida and N. N. Singh, Phys. Rev. **D59**, 032002 (1999), arXiv:hep-ph/9710328 [hep-ph] .

[153] Y. Yamada, Z. Phys. **C60**, 83 (1993).

[154] S. Antusch, J. Kersten, M. Lindner, and M. Ratz, Nucl. Phys. **B674**, 401 (2003), arXiv:hep-ph/0305273 [hep-ph] .

[155] J. A. Casas, J. R. Espinosa, A. Ibarra, and I. Navarro, Nucl. Phys. **B573**, 652 (2000), arXiv:hep-ph/9910420 [hep-ph] .

[156] W. G. Hollik, Phys. Rev. **D91**, 033001 (2015), arXiv:1412.4585 [hep-ph] .

[157] P. H. Chankowski and Z. Pluciennik, Phys. Lett. **B316**, 312 (1993), arXiv:hep-ph/9306333 [hep-ph] .

[158] K. R. S. Balaji, R. N. Mohapatra, M. K. Parida, and E. A. Paschos, Phys. Rev. **D63**, 113002 (2001), arXiv:hep-ph/0011263 [hep-ph] .

[159] W. Chao and H. Zhang, Phys. Rev. **D75**, 033003 (2007), arXiv:hep-ph/0611323 [hep-ph] .

[160] N. Haba, K. Kaneta, R. Takahashi, and Y. Yamaguchi, Nucl. Phys. **B885**, 180 (2014), arXiv:1402.4126 [hep-ph] .

[161] A. Dighe, S. Goswami, and S. Ray, Phys. Rev. **D79**, 076006 (2009), arXiv:0810.5680 [hep-ph] .

[162] S. Gupta, S. K. Kang, and C. S. Kim, Nucl. Phys. **B893**, 89 (2015), arXiv:1406.7476 [hep-ph] .

[163] J. R. Ellis, A. Hektor, M. Kadastik, K. Kannike, and M. Raidal, Phys. Lett. **B631**, 32 (2005), arXiv:hep-ph/0506122 [hep-ph] .

[164] J. A. Casas, J. R. Espinosa, A. Ibarra, and I. Navarro, Nucl. Phys. **B569**, 82 (2000), arXiv:hep-ph/9905381 [hep-ph] .

[165] J. A. Casas, J. R. Espinosa, A. Ibarra, and I. Navarro, Nucl. Phys. **B573**, 652 (2000), arXiv:hep-ph/9910420 [hep-ph] .

[166] M.-C. Chen and K. T. Mahanthappa, Int. J. Mod. Phys. **A16**, 3923 (2001), arXiv:hep-ph/0102215 [hep-ph] .

[167] A. S. Joshipura, S. D. Rindani, and N. N. Singh, Nucl. Phys. **B660**, 362 (2003), arXiv:hep-ph/0211378 [hep-ph] .

[168] R. N. Mohapatra, M. K. Parida, and G. Rajasekaran, Phys. Rev. **D69**, 053007 (2004), arXiv:hep-ph/0301234 [hep-ph] .

[169] Y. Zhang, X. Zhang, and B.-Q. Ma, Phys. Rev. **D86**, 093019 (2012), arXiv:1211.3198 [hep-ph] .

[170] T. Araki, H. Ishida, H. Ishimori, T. Kobayashi, and A. Ogasahara, Phys. Rev. **D88**, 096002 (2013), arXiv:1309.4217 [hep-ph] .

[171] W. Wang, Int. J. Mod. Phys. **A29**, 1430040 (2014), arXiv:1407.6868 [hep-ph] .

[172] Y. Yamada, Z. Phys. **C60**, 83 (1993).

[173] Z. Y. Yu (Daya Bay), *Proceedings, 27th International Conference on Neutrino Physics and Astrophysics (Neutrino 2016): London, United Kingdom, July 4-9, 2016*, J. Phys. Conf. Ser. **888**, 012011 (2017).

[174] T. Lasserre (Double Chooz), *Proceedings, 14th International Conference on Topics in Astroparticle and Underground Physics (TAUP 2015): Torino, Italy, September 7-11, 2015*, J. Phys. Conf. Ser. **718**, 062034 (2016).

[175] M. Kaneda (Double Chooz), *Proceedings, 4th International Conference on New Frontiers in Physics (ICNFP 2015): Crete, Greece, August 23-30, 2015*, EPJ Web Conf. **126**, 04023 (2016).

[176] E. E. Jenkins and A. V. Manohar, Phys. Lett. **B668**, 210 (2008), arXiv:0807.4176 [hep-ph] .

[177] A. Kusenko, Phys. Rept. **481**, 1 (2009), arXiv:0906.2968 [hep-ph] .

[178] A. Merle, Int. J. Mod. Phys. **D22**, 1330020 (2013), arXiv:1302.2625 [hep-ph] .

[179] A. Suzuki (KamLAND), *Proceedings, Nobel Symposium 129: Neutrion Physics: Enkoeping, Sweden, August 19-24, 2004*, Phys. Scripta **T121**, 33 (2005).

[180] K. Eguchi *et al.* (KamLAND), Phys. Rev. Lett. **90**, 021802 (2003), arXiv:hep-ex/0212021 [hep-ex] .

[181] M. Apollonio *et al.* (CHOOZ), Eur. Phys. J. **C27**, 331 (2003), arXiv:hep-ex/0301017 [hep-ex] .

[182] P. Adamson *et al.* (MINOS), Phys. Rev. Lett. **108**, 191801 (2012), arXiv:1202.2772 [hep-ex] .

[183] D. G. Michael *et al.* (MINOS), Nucl. Instrum. Meth. **A596**, 190 (2008), arXiv:0805.3170 [physics.ins-det] .

[184] A. Aguilar-Arevalo *et al.* (LSND), Phys. Rev. **D64**, 112007 (2001), arXiv:hep-ex/0104049 [hep-ex] .

Appendix A

A.1 A short note on some selected neutrino experiments

Neutrinos interact only through the weak interaction in two different ways viz.

(i) Neutral-current interaction, involving Z-boson. Here, the neutrino leaves the interacting medium/detector after transferring a fraction of its energy/momentum to a target particle. If the target is a light charged particle, it can be accelerated to a relativistic speed resulting to a Cherenkov radiation, which can be observed directly. In this interaction, the incoming neutrino does not leave any flavor information behind. All three neutrino flavors can participate in this interaction regardless of their energy.

(ii) Charged current interaction, involving $W^{\pm}$ bosons. Here, the incoming neutrino transforms into its partner charged lepton (electron, muon, or tau). However, if the neutrino does not have enough energy to create its heavier partner, the charged current interaction is unavailable to it. Because the interaction involves the exchange of a charged boson, the target particle also changes its character (e.g., neutron to proton). Solar and reactor neutrinos have enough energy to create electrons. Most accelerator-based neutrino beams can also create muons, and a few can create taus.

All the neutrino detectors are based on these two interactions. A single neutrino experiment cannot explore all the neutrino parameters, since a particular neutrino experiment is

sensitive only to some specific neutrino parameters. It is in this regard, we need a comprehensive analysis of all the available data from different experiments, finally leading to the global data of neutrinos as given in Table 1.3.

A.2 Classification of neutrino experiments

The phenomenon of neutrino oscillation clearly demands a non-zero neutrino mass. But, a clear-cut experiment for measuring the absolute neutrino masses is still missing. Determining the absolute neutrino mass scale is of utmost importance in other branches of physics like astrophysics and cosmology, as they are directly related to the evolution of the universe. In spite of their vanishingly small masses, neutrinos may contribute significantly to the total mass density of the universe (with 336 neutrinos per cm^3). Neutrinos left after the big bang are nearly a billion times more abundant than atoms.

Numbers of neutrino experimental facilities are operating worldwide (see Table A.2). A simple classification of the different available neutrino experimental facilities are shown in Fig. A.1.

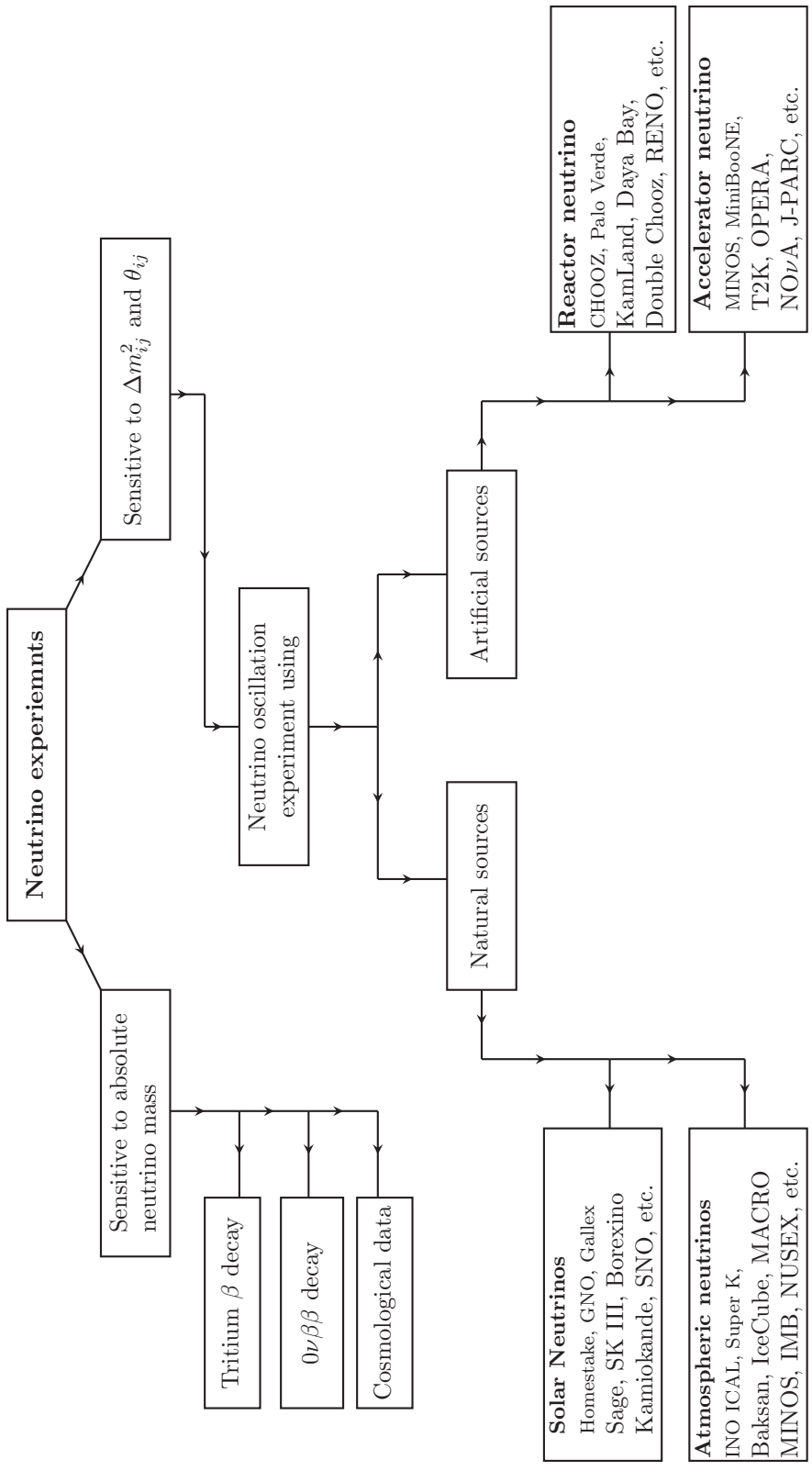

Fig. A.1 Classification of different types of neutrino experiments worldwide based on their sensitivity to various neutrino parameters and on the different neutrino sources.

A.2.1 Absolute neutrino mass determination experiments

At present there are three possible ways to determine the absolute neutrino mass scale (see Fig. A.1).

(i) **Kinematic test:** This method provides a model independent way of determining the neutrino mass (ν_e), entirely based on the kinematics or energy and momentum conservation of a single β decay process (without any further assumptions). The electron and the anti-neutrino emitted in the beta decay share 18.6 keV of energy between them. Here, the anti-neutrino is not observed directly but the charged decay products are precisely measured. Using the energy and momentum conservation the neutrino mass can be obtained. Usually the "average electron neutrino mass squared" $m^2(\nu_e)$ is determined or constrained (at present they are too closed to be resolved experimentally):

$$m^2(\nu_e) = \sum_i |U_{ei}^2| m^2(\nu_i) \tag{A.1}$$

KATRIN (Karlsruhe Tritium Neutrino Experiment) is one such experiment which uses the β decay of tritium to measure the mass of emitted neutrino. It is specially designed to produce a very accurate spectrum of electrons with energies very close to the total energy (mentioned above) thereby resulting to a very low energy neutrino. If the neutrino is massless, there would be no lower bound to the energy the neutrino can carry, so the electron energy spectrum should extend all the way to the 18.6 keV limit. On the other hand, if the neutrino is massive, then it must always carry away at least the amount of energy equivalent to its mass by $E = mc^2$, and the electron spectrum should drop off before the total energy limit and have a different shape. What KATRIN is interested, is in the process where the electron takes almost all the energy (leaving nearly zero for the neutrino). However, such events are very rare, occurring roughly once in a trillion decays.

A limit on $m_{\nu e}$ implies an upper limit on the minimum value of $m_{\nu_{min}}$ of all m_{ν_i} independent of the mixing parameters U_{ei}: $m_{\nu_{min}} \leq m_{\nu_e}$, i.e., the lightest neutrino cannot be heavier than m_{ν_e}.

(ii) **Neutrinoless double beta decay**: This is another possible aspect for determining the absolute value of neutrino mass. It was first considered by Wolfgang Furry in 1939,

$$(A,Z) \rightarrow (A,Z+2) + e_1^- + e_2^- \tag{A.2}$$

This decay process is forbidden in Standard Model electroweak theory as it violates lepton number by two units. The process of (A.2) is mediated by the exchange of a light neutrino, which must be a Majorana particle. The Q value of this decay is much smaller than the nuclear masses and the nuclear recoil energy can be neglected. The electron energy is simply a peak at $T_{e1} + T_{e2} = Q$. Thus, the experimental observables are number or upper limits of signal counts or equivalent half live times $T_{1/2}$. The decay rate is proportional to the square of the effective Majorana mass m_{ee} :

$$T_{\frac{1}{2}}^{0\nu-1} = G^{0\nu} \, |M^{0\nu}|^2 \, m_{ee}^2, \tag{A.3}$$

where $G^{0\nu}$ denotes the exact calculable phase space factor and $M^{0\nu}$ is the nuclear matrix element (which must be theoretically calculated). If the nuclear matrix elements are known, than the Majorana mass m_{ee} can be deduced by

$$m_{ee} = |\sum_i U_{ei}^2 m_i|^2, \tag{A.4}$$

where the sum is over the light Majorana neutrinos ($m_{\nu_i} < 10 MeV$) only. Due to the presence of a complex Majorana phase (which can be either 0 or π if the neutrinos are CP eigenstates), cancellation can occur such that m_{ee} can be smaller than any of the

m_{ν_i}. The experimental observation of $0\nu\beta\beta$ as well as accurate determination of m_{ee} would establish the Majorana nature of neutrinos and would contribute towards the determination of absolute neutrino masses.

Many different isotopes and techniques are used to search of $0\nu\beta\beta$. Nuclei that allow the $2\nu\beta\beta$ are also a possible candidate for $0\nu\beta\beta$. Some potential candidates are ^{100}Mo, ^{82}Se, ^{48}K, ^{76}Ge, ^{116}Cd, ^{136}Xe.

(iii) **Cosmological or Astrophysical** observations provide another, quite different, source of information on the neutrino masses. This model dependent technique provides the most stringent upper bound on the combined neutrino masses, using the idea of cosmological structure formation. The neutrino density Ω_ν is one important parameter (out of 11 parameters) for the standard cosmological model and is related to the neutrino mass and their number (massive neutrinos) by

$$\Omega_\nu = \frac{\rho_\nu}{\rho_c} = \frac{\sum m_\nu}{93.2eVh^2}, \tag{A.5}$$

where h is the Hubble parameter (in unit of 100Km/s/Mpc), ρ_ν is the neutrino energy density and ρ_c is the critical density of the Universe. This direct relation between Ω_ν and the $\sum m_\nu$ follows from the fact that the present neutrino abundance is determined by the cross section for weak interactions, that fixes the neutrino decoupling temperature $T_d = 1$ MeV.

Different cosmological observations that put constraint on the sum of the neutrino masses are Planck Data, ΛCDM, Large Scale Structure formation (LSS), Baryon Acoustic Oscillation data (BAO), Sloan Digital Sky Survey (SDSS) observation etc.

A.2.2 Neutrino experiments using natural sources

The neutrino parameters that are sensitive to the phenomenon of neutrino oscillation are the three mixing angles (θ_{ij}), two mass squared differences (Δm_{ij}), and the Dirac CP phase (δ). Some selected neutrino oscillation experiments using natural neutrino sources are

(i) **Homestake Chlorine detector**: The Chlorine experiment of Ray Davis and John N. Bahcall [1] is one of the pioneering experiments in the field of neutrino physics. It lead to the successful determination of the solar neutrino for the first time leading to the Solar Neutrino problem. The detector was based on a concept first proposed by Bruno Pontecorvo in 1946, in which neutrinos interact with chlorine atoms leading to an isotope of argon atom with a threshold energy of 0.814 MeV

$$\nu_e + {}^{37}Cl \rightarrow e^- + {}^{37}Ar. \tag{A.6}$$

It is a very rare reaction and sensitive only to the highest energy neutrinos. In fact, one atom of argon is produced each week in a tank containing 371 tons of the dry-cleaning fluid (perchlorethylene). They exposed the tank, containing the chemical, for about a month and then extracted the few resulting argon atoms using helium gas and cold trap method, which were then transferred to a low background counter where any decays were recorded over a period of several months. The argon atoms produced decayed back to chlorine atoms after a half life of 35 days. The first results were announced in 1968.

(ii) **Gallium experiment (Gallex, GNO, SAGE)**: Unlike the chlorine based experiments which are sensitive only to the high energy neutrinos, gallium bases experiments target to study the low energy neutrinos and to verify the hypothesis of neutrino oscillation. The main motivation of the gallium experiments was to disentangle MSW neutrino oscillation scenario causing the Solar Neutrino Problem. Like the ^{37}Cl detector, the

gallium detectors are sensitive only to electron type neutrino

$$\nu_e + {}^{71}Ga \rightarrow e^- + {}^{71}Ge. \tag{A.7}$$

The energy threshold of the reaction is 0.223 MeV thereby allowing the interactions of pp, ^7Be, ^8B, and pep neutrinos. SAGE used a liquid metal target containing 50 tons of gallium, whereas GALLEX/GNO used 30 tons of natural gallium in an aqueous acid solution. The ^{71}Ge decay with a half life of 16.5 days. Auger electrons and X-rays are produced during the decay with a typical L-peak and K-peak energy distribution. All the experiments found about half of the expected rate inconsistent with the SSM predictions.

(iii) **KamiokaNDE, Super Kamiokande (SK)**: The Kamiokande experiment, which became operational in July 6, 1983, was specially designed for detecting the proton decay signal. Unfortunately, no proton decay signal was observed, instead it first set a limit on the lifetime of proton. Afterward, KamiokaNDE was upgraded to **KamiokaNDE-II** which started taking data in 1987. KamiokaNDE-II provide the first hint that Sun is a source of neutrinos. Later on, it observed the deficit in the solar neutrino flux which was in conflict with both the Standard Solar Model and the Davis' experiment resulting to the solar neutrino problem. KamiokaNDE-II still fails to observe the proton decay signal and again sets a lower-bound on the half-life of the proton. Studies on atmospheric neutrinos were also a part of the KamiokaNDE-II and it also announced the observation of deficit in atmospheric neutrino. Both KamiokaNDE and KamiokaNDE-II are water Cherenkov detectors.

Water Cerenkov detector gave the first experimental confirmation (1987) of the chlorine based neutrino experiment regarding the deficit of solar neutrinos. The main advantage of the KamiokaNDE detector is the real-time nature of the neutrino interactions viewed

in the active water volume (2,140 tons of ultra-pure light water) by 948 photomultiplier tubes (PMT). Light water detectors are mainly sensitive to ν_e , but also to ν_μ and ν_τ (with a reduced cross section $\sigma(\nu_{\mu,\tau} + e^- \rightarrow \nu_{\mu,\tau} + e^-) \simeq 0.15 \times \sigma(\nu_e + e^- \rightarrow \nu_e + e^-)$).

Super Kamiokande (SK) was designed to test the neutrino oscillation hypothesis for both solar and atmospheric neutrinos. It allows one to do an in depth analysis of both the solar and atmospheric neutrinos oscillations. SK is a huge cylinder of 41.4 m in height and 39.3 m in diameter containing 50,000 tons of ultra-pure light water and viewed by 11,146 PMT. It operates at an energy threshold of 5 MeV thereby permitting the study of the ^8B neutrinos. Similar to the Kamiokande, SK also uses the Cerenkov radiation emitted by the resulting electrons. Both kamiokande and SK can determine the direction of the incoming neutrinos, by using the Cerenkov photons collected by the PMT, and by reconstructing the direction of flight of the incident neutrinos from the scattering reaction $\nu_x + e^- \rightarrow \nu_x + e^-$. The particular advantage of the real time nature of SK is that we can study in detail the time and shape variation of the ES energy spectrum (zenith angle spectrum). In 1998, Super-K found the first strong evidence of neutrino oscillation from the observation where ν_μ changed to ν_τ[40]. SK also set limits on proton lifetime (5.9×10^{33} yr) and other rare decays and neutrino properties.

(iv) **Sudbury Neutrino Observatory (SNO)**: Unlike the Kamiokande and SK, SNO uses 1,000 tons of **heavy water** as the detecting medium. An additional 7,000 tons of ultra-pure light water is used for supporting and shielding. There are 9,456 PMT all mounted on a geodesic structure 18 m in diameter waiting for the Cerenkov radiations. SNO clearly demonstrated that solar electron neutrinos from ^8B decay in the solar core change into other active neutrino flavors in transit to Earth. This experiment provided revolutionary insight into the properties of neutrinos and the core of the sun. The advantage of using heavy water (instead of light water) is that it allows the flux of all

the three types of neutrinos to be measured and it also provides a very accurate measure of the initial solar flux for comparison with solar models. Plans are currently underway to upgrade the SNO detector for the new SNO+ experiment.

Using heavy water, SNO was able to calculate two different reactions on deuteron (d) as shown below:

$$\nu_e + d \rightarrow p + p + e^- \quad \text{(CC reaction sensitive only to } \nu_e\text{)} \tag{A.8}$$

$$\nu_\alpha + d \rightarrow n + p + \nu_\alpha \quad \text{(NC reaction equally sensitive to all flavors),} \tag{A.9}$$

where $\alpha = e,\ \mu,\ \tau$.

A significant deficit in the ^8B neutrino flux measured by the CC reaction over that measured by the NC reaction would directly prove that ν_e from Sun were changing into one of the other two flavors (without reference to solar models). The NC reaction provided a measurement of the total flux of ^8B solar neutrinos independent of neutrino flavor change. The CC reaction was detected by observing the Cherenkov light. The NC reaction was detected in three different phases of the project. Moreover, the SNO detector could observe neutrinos of all flavors via the elastic scattering (ES) of electrons by neutrinos: $\nu_\alpha + e^- \rightarrow \nu_\alpha + e^-$.

(v) **IceCube:** Set up at the cold, dry, and stable atmosphere of Antarctica, South Pole, the IceCube Neutrino Observatory was, specially, designed to detect ultra-high energy cosmic neutrinos. It extends the range of energy at which neutrinos have been observed. It has recorded the evidence of neutrino oscillation traveling through the Earth and its atmosphere. It is also designed to measure the so called neutrino mass hierarchy.

It has more than 5000 optical sensors which are distributed in an of array over a cubic kilometer of the ice. The last three years of IceCube data yielded a similar precision to that of Super-Kamiokande data (taken over 15 Years). It uses the glacier ice as the

target material and its large observational volume produces larger event statistics in shorter times. Like the Super-Kamiokande, IceCube also uses the same atmospheric neutrinos, but at different energies. Neutrinos are not directly detected in IceCube but through the resulting Cherenkov radiation in the ice. The energetic muon produced by the interaction of neutrinos with protons and neutrons travels a significant distance before it decays.

At present, the scientists are planning an upgrade of the IceCube detector called PINGU (Precision IceCube Next Generation Upgrade). The new upgraded version will have a much higher density of optical modules in the whole central region.

(vi) **INO:** It is a proposed underground laboratory. Its main aim is to make precision measurements of the neutrino parameters related to the phenomenon of neutrino oscillations and also to determine the neutrino mass order. This is possible because INO detectors will have the ability to differentiate the positive and negative muons. INO has many long term plans. In its different phases of operation it may be using the natural neutrino sources and also from the accelerators.

INO can also be used as a far-detector of a long-base-line (6000 to 11500 km) neutrino experiment. It may be using the neutrino beam from various neutrino factories like from Japan, Europe or USA. These are the propose future neutrino facilities that will be directed towards different parts of Earth.

Recently, the government of India has given the environmental clearance for the construction which was delaying the project for more than a decade.

A.2.3 Reactor neutrino experiments

Reactor based neutrino experiments have been playing an indispensable role for both discovery and precision measurement in the history of neutrino physics. Since its first inception

in the 1950s, the detector technology has advanced immensely. On the basis of earlier experiments (like Palo Verde, CHOOZ, and Monte Carlo), modern neutrino experiments Daya Bay, Double Chooz, and RENO were designed with unprecedented precision. They all measured the smallest mixing angle θ_{13} by observing the oscillation at a baseline of $\sim$ 1 km. These new generation reactor experiments have significantly reduced uncertainties associated with the measurement of θ_{13} by using two identically performing detectors at near and far locations from reactor(s). Earlier version of reactor experiments had a single detector located at about 1 km or less from reactor(s).

The reactor neutrino experiments has the advantage that the measurements are not disturbed by degeneracies, correlations between different oscillation parameters, and the matter affect (prevented by short baseline). The reactor neutrino experiments are based on the disappearance of electron anti-neutrinos produced in reactor cores. Nuclear reactors provide an intense beam of $\overline{\nu}_e$ (with an average energy of 2 MeV) from the β-decay of the fuel elements like ^{235}U, ^{238}U, ^{239}Pu, ^{241}Pu etc

$$\overline{\nu}_e + p \rightarrow e^+ + n. \tag{A.10}$$

For measuring the vale of θ_{13}, the detectors are placed at such a distance ($\sim$1 km) which maximize the disappearance probability at the scale of Δm^2_{32}.

The reactor neutrino experiments have a similar detector mechanism. They all consist of concentric cylinder filled with different liquids. The innermost portion is filled with gadolinium doped liquid scintillator (GLS) and γ-catchers. The e^+ carry almost all of the $\overline{\nu}_e$ energy and get deposited in the scintillator which can then be correlated with the $\overline{\nu}_e$ energy. The neutrino signature is identified by the delayed coincidence of the prompt positron signal and the Gd signal (from the neutron capture). The neutron capture signal delay by about 200 μs in liquid scintillator and is reduced to about 30 μs in gadolinium loaded liquid scintillator.

(i) **Kamioka Liquid scintillator AntiNeutrino Detector (KamLAND)**: It is a monolithic long baseline liquid scintillator detector, proposed by A. Suzuki [179]. It is filled with 1,000 ton of ultra-pure liquid scintillator. It is installed after dismantling the old Kamiokande detector. The multiple numbers of commercial reactors distributed at 130-220 km around Kamioka provide an effective baseline of 180 km from KamLAND and gives a superior sensitivity toward determining the neutrino mass. KamLAND started data taking in January 2002 and published its first result in January 2003 where they reported the result on reactor neutrino disappearance with 99.95% C.L. significance [180] consistent with the expectation from the solar neutrino result (assuming CPT). The statistical significance of the disappearance experiment was further strengthened in 2005 and 2008 and observed the clear pattern of oscillation. In case of the 2 flavor neutrino oscillation, KamLAND successfully pinned down the solar neutrino problem to large mixing angle solution. The KamLAND experiment also observed geo-neutrinos for the first time in consistent with geo-scientific expectation within the experimental accuracy.

(ii) **Daya Bay**: It is located at the southern coast of China, 55 km to the northeast of Hong Kong and 45 km to the east of Shenzhen. It was first proposed in 2003 with the aim of determining θ_{13}. Its construction began on 2007 and started data taking (with the full configuration) on 19 October 2012, which is still running reliably. It consists of three underground experimental halls connected with horizontal tunnels and a total of eight antineutrino detectors are installed in the three halls. Each of the antineutrino detectors has three concentric cylinders. The innermost cylinder is filled with clear gadolinium-doped liquid scintillator (20 tones). The middle cylinder is filled with undoped liquid scintillator (20 tones) while the outermost cylinder contain mineral oil (37 tones).

Daya Bay experiment has an excellent capability for high precision measurements of reactor anti-neutrinos. Current precision on $\sin^2\theta_{13}$ and $|\Delta m^2_{ee}|$ are 6% and 4.5%, respectively. The Daya Bay experiment is expected to operate until 2020; by then, the precision is expected to be $\sim 3\%$ for both $\sin^2\theta_{13}$ and $|\Delta m^2_{ee}|$.

(iii) **Chooz and Double Chooz**: CHOOZ experiment is a long baseline reactor neutrino experiment located in France. It used a 5 ton target located in an underground laboratory and at a distance of about 1 km from the two pressurized water reactor. It had an average value of $\frac{L}{E} \sim 300$ ($L \sim 1$ km, $E \sim 3$ MeV). It was designed to detect reactor antineutrino via. the inverse β-decay reaction as in (A.10). It showed no evidence for neutrino oscillations in the $\overline{\nu}_e$ disappearance mode for the mass region Δm^2_{32} ,where muon neutrinos oscillate intensively. The first best limit on θ_{13} was established by the CHOOZ experiment [181].

Double Chooz is a short baseline reactor neutrino experiment. It is the upgraded version of the earlier Chooz experiment. Among the reactor neutrino experiments, the Double Chooz Collaboration was the first one to present an indication of non-zero value of θ_{13}. The no oscillation hypothesis was excluded at the 94.6% C.L. Like the other reactor based neutrino experiment, the Double Chooz experiment measures the $\overline{\nu}_e$ from the a nearby nuclear reactor (Chooz power station). Double Chooz uses two detectors with the identical structure, one near the oscillation maximum (1.05 km) and the other closer to the reactors (400 m) where the oscillation is still small. By comparing the data from the near and the far detectors, the systematic uncertainties of reactor neutrino flux, neutrino detection efficiency and detector mass, can be largely suppressed. The two detectors are located close to the iso-flux line, which enable the cancellation of the neutrino flux uncertainty caused by possible property differences between the two reactors..

(iv) **RENO:** It was proposed in 2005, started construction in 2007, and data-taking with both the near and far detectors began in August, 2011. Like all the other reactor neutrino experiments, RENO measured the value of θ_{13} by the disappearance of electron antineutrinos (as in A.10).

Using the extensive data taken in 1,500 live days RENO has successfully reduced the uncertainties of both the $\sin^2 2\theta_{13}$ and $|\Delta m^2_{ee}|$ measurements to 9% and 7%, respectively. By including the data from the next 2-3 years, RENO has a plan for further reducing the uncertainties of $\sin^2 2\theta_{13}$ and $|\Delta m^2_{ee}|$ to 6% and $4-5\%$, respectively.

RENO provides a detailed picture of neutrino transformation among the three neutrino flavors thereby shedding light on the possibility of search for CP violation in the leptonic sector. The large value of θ_{13} will strongly promote the upcoming neutrino experiments to emphasize on the CP violation effects and determine the neutrino mass hierarchy.

A.2.4 Accelerator based neutrino experiments - Long baseline

Unlike the reactor based neutrino experiments, accelerator based neutrino experiments are long baseline in nature. In the three flavored neutrino model there is a close relationship among the disappearance and appearance modes of oscillation study, which trace back to their origin in the PMNS matrix. Following reference [36], it is possible to write the disappearance possibility for muon neutrinos in vacuum, as

The earth between the beam creation point and the detector location, forms an essential part of any long-baseline experiment. This creates both problems and opportunities - problems because of the introduction of degeneracies between matter effects and CP violation, and opportunities because of the possibilities to exploit the differences between neutrino and antineutrino interactions, and from the two mass hierarchies. Some selected accelerator based neutrino experiments are

(i) **Main injector neutrino oscillation search (MINOS):** MINOS was designed for the precision measurements of the parameters governing the atmospheric oscillation regime, in addition it has also contributed an important role in the measurement of θ_{13} and will, in the future, make sensitive searches for the existence of sterile neutrinos. MINOS specific design has the ability to identify both ν_μ and $\overline{\nu_\mu}$ interactions separately. Such features have allowed MINOS to make the first direct precision tests that neutrinos and antineutrinos obey the same oscillation parameters in the atmospheric regime [182, 66].

MINOS are interested in three types of interactions (i) CC interaction of ν_μ

$$\nu_\mu(\overline{\nu}_\mu) + x \rightarrow \mu^{-(+)} + x', \tag{A.11}$$

where x' is a cascade of hadrons producing a diffused shower. The resulting muon trace a curve path in the magnetic field and depending on the direction of curvature the incoming neutrino can be identified (either ν_μ or $\overline{\nu}_\mu$). (ii) All active neutrino flavors undergo NC interactions through the process $\nu + x \rightarrow \nu + x'$. Only the hadronic cascade is observed, producing a diffuse shower of energy deposits. (iii) Finally, ν_e undergo CC interactions through the process $\nu_e + x \rightarrow e^- + x$. The electron gives rise to an electromagnetic shower producing a denser energy.

MINOS uses the world's most powerful neutrino beam, the NuMI beam (based at Fermilab in Chicago), to achieve its goals. NuMI facility provides an intense muon neutrino beam of few GeV in energy. Two steel-scintillator calorimeters detectors [183] are installed in the MINOS experiment. The Near Detector (also smaller and having a mass of 0.98 kton) is installed at the Fermilab, 1.04 km from the target. It measures the energy spectra of the neutrinos before oscillation. The Far Detector is installed at the Soudan Underground Laboratory in northern Minnesota, 705 m underground and 735 km away from the target. It has a mass of 5.4 kton, it again measures the

neutrino energy spectra, observing both the appearance and disappearance phenomena of neutrinos due to oscillation. This two-detector are arranged in such a way that it reduces the systematic uncertainties to an unprecedented level.

(ii) **NOνA:** The NOνA experiment is a long-baseline accelerator-based neutrino oscillation experiment. It is optimized for exploring (mostly) the appearance of ν_e in the oscillation of $\nu_\mu \rightarrow \nu_e$. Like the MINOS experiment, NOνA also uses the well defined NuMI beam of ν_μ, which has been upgraded to 700 KW (from 300 KW). Using its two detectors, NOνA measures the ν_e appearance and ν_μ disappearance between its onsite near detector and the far detector. The near detector (1 km away) contains 0.3 kt liquid scintillator to measure the unoscillated neutrino beam and to estimate background at the far detector. The far detector contains 14 kt liquid scintillator and is located at Ash River, Minnesota 810 km from target. These two detectors are located 14.6 mrad off-axis and has the advantage that it can enhance the $\nu_\mu \rightarrow \nu_e$ in the far detector while reducing the background ν_e from high energy unoscillated neutrino beam and neutral current.

The ν_e appearance analysis at NOνA aims to resolve the neutrino mass hierarchy problem and to constrain the CP-violating phase. Such analyses are made possible at NOνA due to it exceptional long baseline, which enhanced the matter effect up to 30% thereby enhancing the sensitivity to neutrino mass hierarchy determination. The first measurement of ν_e appearance in NOνA based on its first year's data was announced in 2015, providing solid evidence of ν_e oscillation and some hints on mass-hierarchy and CP.

(iii) **Tokai to Kamioka (T2K):** It is a long-baseline accelerator neutrino oscillation experiment located at Japan. The main goals of the T2K experiment are (a) discovery of $\nu_\mu \rightarrow \nu_e$ and to extend the search of $\sin^2 2\theta_{13} \simeq 2sin^2 2\theta_{\mu e} > 0.008$, (b) investigation of CP symmetry conservation/violation in the neutrino sector, (c) neutrino-nucleus cross-

section measurements, and (d) searching for sterile neutrino from the ν_μ disappearance by detecting the neutral current events.

The intense T2K neutrino beam is produced in the J-PARC accelerator complex at Tokai, by impinging the accelerated protons (30 GeV) on a graphite target. This produces mainly the pions ($\sim 90\%$) and kaons ($\sim 10\%$). These positive (negative) pions then decay to produce $\overline{\mu}$ (μ) and ν_μ ($\overline{\nu}_\mu$). T2K housed three detectors, two near detectors (INGRID and ND280) and a far detector (Super-Kamiokande). The beam after traveling a distance of 280 m goes through INGRID and ND280, where they measured the beam parameters before oscillation and the neutrino cross-section too. The far detector distance (250 km) corresponds to the first oscillation maximum. A comparative studies of the beam characteristic between the near and far detectors makes it possible to determine the oscillation parameters.

The leading measurement of the θ_{23} value is provided by T2K. It is also the first to observe ν_e appearance, with a significance of 7.3σ. These findings made it possible to determine the θ_{13} and to provide the first hint of a non-zero value of the δ CP phase. At present, T2K is collecting data using $\overline{\nu}_\mu$ beam, for the δ CP and antineutrino cross-section measurements. It has also yielded several neutrino cross-section measurements at neutrino energies $\sim$1 GeV.

(iv) **MiniBooNE:** The booster neutrino experiment, at Fermilab, was designed to test the evidence for neutrino oscillations ($\nu_\mu \rightarrow \nu_e$) in the ($\sin^2 2\theta$, Δm^2) parameter space region where the LSND experiment, at Los Alamos [184], reported a signal. The LSND experiment observed more $\overline{\nu}_e$ candidate events than expected from background. If the excess is interpreted as being due to $\overline{\nu}_\tau \rightarrow \overline{\nu}_e$ oscillations, then the most favored oscillation region is a band in Δm^2 stretching from ~ 0.2 eV^2 to $\sim$2 eV^2 . The MiniBooNE experiment was designed to search for $\nu_\mu \rightarrow \nu_e$ and $\overline{\nu}_\tau \rightarrow \overline{\nu}_e$ oscillations with approximately the same $\frac{L}{E} \simeq 1$ value as LSND, where L is the neutrino travel

distance from the source to the detector in meters and E is the neutrino energy in MeV. Whereas the LSND neutrino beam travelled a distance of 30 m with a typical energy of 30 MeV, the MiniBooNE neutrino beam traveled 500 m and had a typical energy of 500 MeV. With neutrino energies an order of magnitude higher, the MiniBooNE backgrounds and systematic errors are completely different from those of LSND. MiniBooNE, therefore, constitutes an independent check of the LSND evidence for neutrino oscillations at the ~ 1 eV^2 mass scale.

For a deep analysis of the $\nu_\mu \rightarrow \nu_e$ and $\overline{\nu}_\tau \rightarrow \overline{\nu}_e$ reactions, MiniBooNE required a (i) target mass of ~ 1 kton in order to generate $\sim$1000 neutrino oscillation events for 10^{21} protons on target, (ii) detector with excellent discrimination between ν_μ and ν_e induced events, (iii) completely active volume with no dead regions, (iv) detector having a 4π veto to reject cosmic ray events, neutrino interactions that occur outside the detector, and neutrino events with tracks that escape the fiducial volume. Liquid Cherenkov detectors have all these requirements.

Timeline	**Contributors and their contributions**
1920-27	Charles D. Ellis (along with J. Chadwick and colleagues) established the continuous nature of β decay spectrum.
1930	W. Pauli postulated the idea of ν to account for β decay and named it neutron.
1932	James chadwick discovered a heavy neutral particle and named it neutron but couldn't account for the Pauli's neutron.
1934	Ernico Fermi coined the term neutrino resolving the naming problem and wrote down the correct theory for beta decay, incorporating ν.
1956	First discovery of $\overline{\nu}_e$ by Clyde Cowan, Frederick Reines, F. B. Harrison, H. W. Kruse, and A. D. McGuire.
1957	ν found to be left handed by Goldhaber, Grodzins and Sunyar.
1957	B. Pontecorvo first suggested a practical method for investigating ν oscillations.
1960	Leon M. Lederman, Melvin Schwartz and Jack Steinberger showed the possibility of more than one type of ν leading to the 1988 Nobel Prize.
1962	Z. Maki, M. Nakagawa and Sakata introduced ν flavor mixing and oscillations.
1962	ν_μ discovered by L. Lederman, M. Schwartz, J. Steinberger and colleagues at BNL and confirmed the difference from ν_e.
1965	First natural neutrino independently observed by Reines and colleagues (SA), and by G. Menon and colleagues in India, setting first astrophysical limits.
1968	R. Davis and colleagues get first radiochemical solar ν results in the Homestake Mine in North Dakota, leading to solar ν problem.
1976	Discovery of tau lepton at the SLAC, implying the possibility of ν_τ.
1985	The "atmospheric ν anomaly" observed by IMB and Kamiokande.
1988	Lederman, Schwartz and Steinberger awarded the Physics Nobel Prize for the discovery of the ν_μ.
1989	The LEP and the SLC at SLAC (Stanford) determine that there are only 3 light ν species ($\nu_e,\ \nu_\mu,\ \nu_\tau$).
1995	Nobel Prize to Clyde Cowan and Frederick Reines.
1998	Super-Kamiokande team reports oscillations in atmospheric ν and, thus, ν mass.
2000	The DONUT Collaboration announces the first direct observation of the ν_τ collaboration at Fermilab .
2001-02	SNO observed neutral currents and charged currents showing that ν oscillations are the cause of the solar ν problem.
2002	KamLAND observes ν oscillations consistent with the solar ν puzzle using man-made ν.
2005	KamLAND published the best estimate of Δm^2_{21}.
2006	the MINOS experiment measured the Δm^2_{32}.
2009	Lensing data of a galaxy cluster predicted a ν mass of about 1.5 eV.
2010	May 31, OPERA observed the first ν_τ candidate event in a ν_μ beam, providing further evidence for mass.
2010	July, the 3-D MegaZ DR7 galaxy measured a limit of the combined mass of the three 3 ν varieties to be < 0.28eV.
2013	Daya Bay confirms that θ_{13} is non-zero.
2015	Nobel Prize in Physics for the discovery of neutrino oscillation in 1998 and 2001.

Table A.1 List of some important milestone in the history of neutrino physics.

Names	Current status	Location	Purpose
	Not operational		
HOMESTAKE–CHLORINE	closed (1967-1998)	USA	neutrino oscillation
SNO	closed (1999-2006)	Ontario, Canada	Detection of solar ν through heavy water
	In operation		
Super kamiokande	operational (1986)	Japan	search for proton decay using high energy ν, study of solar, atmospheric neutrino and, supernova in Milky Way galaxy
BOREXINO	Operational (1993)	Italy	measurement of individual ν fluxes from SUN for comparison with SSM prediction.
KamLAND	Operational (2002)	Japan	search for $\overline{\nu}_e$ oscillation from nuclear reactor
MiniBooNE	Operational (2002)	US	testing m_i through ν oscillations.
IceCube	Operational (2006)	Antarctica	search for DM and TeV range ν source from astrophysical phenomena
OPERA	Operational (2008)	Italy and CERN	detection of $\nu_\mu \rightarrow \nu_\tau$ oscillation
Double Chooz	operational (2011)	France	Measurement of θ_{13}
NOνA	Operational (2011)	US	observation $\nu_\mu \rightarrow \nu_e$ oscillation
RENO	Operational (2011)	South Korea	Measurement of θ_{13}
T2K	Operational (2011)	Japan	measurement of $\nu_\mu \rightarrow \nu_e$ and θ_{13}
DAYA BAY	Operational (2011)	China	Measurement of θ_{13}
	Future program		
ANNIE		USA	to measure the neutron yield of atmospheric ν interactions in Gd-doped water.
ARIANNA		Antarctica	detection of coherent radio Cherenkov from particle shower due to ν with energies $> 10^{17}$eV.
LAGUNA		CERN, ...	study of proton decay, galactic supernova, solar and terrestrial neutrino, matter-antimatter asymmetry
LBNE/DUNE		USA	to study matter-antimatter asymmetry, proton decay and black hole formation.
UNO		USA	to study physics far beyond the reach of SuperK and search for nucleon decay etc.
INO		India	Precision measurement of oscillation parameters

Table A.2 List of some neutrino experimental facilities around the world including already closed one and future projects.

List of Publications

1. K. S. Singh and N. N. Singh, Adv. High Energy Phys. **2015**, 652029 (2015).

2. C. Duarah, K. S. Singh, and N. N. Singh, in *Proceedings, National Conference on Current Issues in Cosmology, Astrophysics and High Energy Physics (CICAHEP): Dibrugarh, India, November 2-5, 2015*, Dibrugarh Univ. (Dibrugarh Univ., Dibrugarh, India, 2016) pp. 204–209, arXiv:1503.07672 [hep-ph].

3. K. S. Singh, S. Roy, and N. N. Singh, Phys. Rev. **D97**, 055038 (2018).